The Messenger

No. 125 – September 2006

The Galactic Centre: The Flare Activity of SgrA* and High-Resolution Explorations of Dusty Stars[1]

Andreas Eckart[1]
Rainer Schödel[1]
Leonhard Meyer[1]
Koraljka Mužić[1]
Jörg-Uwe Pott[1]
Jihane Moultaka[1]
Christian Straubmeier[1]
Michal Dovciak[2]
Vladimir Karas[2]
Reinhard Genzel[3,4]
Thomas Ott[3]
Sascha Trippe[3]
Francisco Najarro[5]
Mark Morris[6]
Fred Baganoff[7]

[1] I. Physikalisches Institut, University of Cologne, Germany
[2] Astronomical Institute, Academy of Sciences, Prague, Czech Republic
[3] Max-Planck-Institut für Extraterrestrische Physik, Garching, Germany
[4] Physics Department, University of California at Berkeley, USA
[5] Instituto de Estructura de la Materia, Consejo Superior de Investigaciones Científicas, Madrid, Spain
[6] Department of Physics and Astronomy, UCLA, Los Angeles, USA
[7] Kavli Institute for Astrophysics and Space Research, Massachusetts Institute of Technology, Cambridge, USA

We summarise the most recent efforts to investigate the properties of the Galactic Centre making extensive use of the instrumental capabilities of the Paranal observatory.

The Galactic Centre is one of the most exciting targets in the sky. At a distance of ~ 8 kpc it is about one hundred times closer than the second nearest nucleus of a similar galaxy such as M31 and therefore the closest Galactic Nucleus that we can study. As has been proven convincingly by the analysis of stellar dynamics the central stellar cluster harbours a $(3.7 \pm 0.3) \times 10^6\ M_\odot$ black hole at the position of the compact radio source Sagittarius A* (SgrA*). SgrA* represents the largest Schwarzschild radius projected on the sky and provides us with unique information to understand the physics and possibly the evolution of these objects (see also Eckart, Schödel and Straubmeier 2005 and references therein).

Compelling evidence for a massive black hole at the position of Sgr A* is also provided by the observation of variable emission from that position both in the X-ray and the near-infrared domain. Here NACO observations provided the infrared data for the first simultaneous NIR/X-ray flare detections. Repeated measurements have shown that to within less than 10 minutes the brighter X-ray flares occur simultaneously to the NIR flare events. Recent near-infrared polarimetric observations with NACO at the VLT UT4 (Yepun) have revealed that some of the one to two hour flares from SgrA* show a surprising fine structure in the form of polarised sub-flares that have a width of only about 7–10 minutes and are spaced by about 18 ± 3 minutes from peak to peak. These features can successfully be interpreted as emission from hot spots that are on relativistic orbits around the central black hole.

In the near future infrared interferometry with the VLT – which is already possible for the bright and dusty stars at the Galactic Centre – will allow us to determine the emission mechanism and to model the accretion flow onto the Milky Way's central black hole.

Polarised sub-flares from SgrA*

Using the NACO adaptive optics (AO) instrument at the ESO VLT in 2004 and 2005 we have obtained new polarisation data of the variable NIR emission of SgrA* (Eckart et al. 2006a; see also Yusef-Zadeh et al. 2006a). The new data reveal that some of the typically 100 minute long infrared flares are modulated by highly polarised sub-flares with durations of only about 10 minutes (Figure 1 left). These polarised sub-flares have been observed in both years and have an overall degree

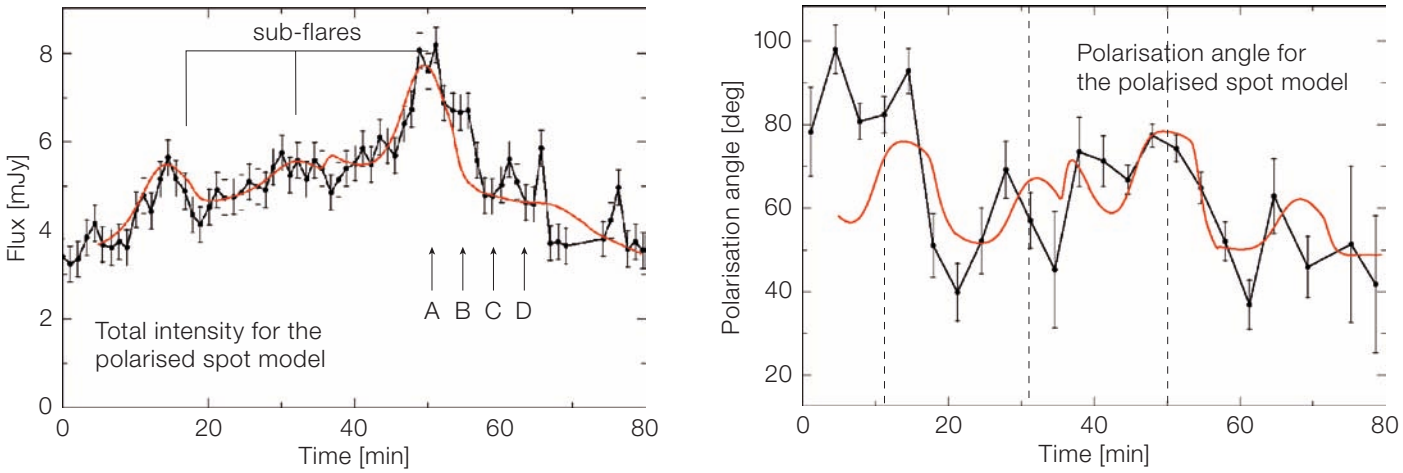

[1] Based on observations with CHANDRA and ESO VLT observations 271.B-5019, 073.B-0249, 75.B-0093, 075.B-0113, 076.B-0863, and 077.B-0028.

Figure 1: Comparison between model results of an orbiting spot model (red lines) for July 2005 and the measured total flux density (left) and polarisation angle (right). The vertical dashed lines indicate the times at which sub-flares occurred. For details see Eckart et al. 2006b. The model calculations show the compatibility of the orbiting spot model with the NIR polarisation data.

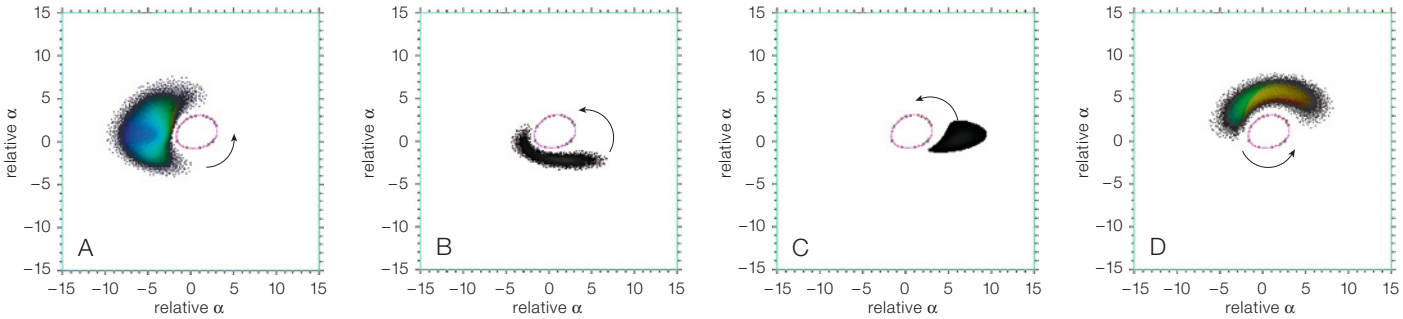

Figure 2: Apparent images of an orbiting hot spot as seen from the observer. The images have been calculated for a case of $i = 60°$, $a = 1$ for a spot at a distance of four gravitational radii (R_g) from the SgrA* black hole (Dovciak, Karas and Yaqoob 2004). This model compares well to best χ^2 fits to the recent polarisation data. (Meyer et al. 2006, submitted to A&A). Colours indicate the energy shift, the blackest structures correspond to the faintest spot images. The labels A to D correspond to the appearance of the spot model at the times labelled for a single flare in Figure 1. Lables are given in R_g at the location of SgrA*.

of polarisation of the order of 20 %. In 2005 the main underlying flare was long enough to observe a minimum of three consecutive sub-flares that are consistent with a quasi-periodicity of 18 ± 3 minutes similar to the value of 17 ± 2 minutes found in previous NACO observations (Genzel et al. 2003; see also Gillessen et al. 2005). A similar periodicity has recently also been reported for a bright X-ray flare (Bélanger et al. 2006). The rapid variation of polarised emission is most likely indicative of synchrotron radiation by relativistic electrons. The intrinsic polarisation of the sub-flares could therefore be up to 60 %.

A preferred model that is used to explain the quasi-periodic polarised flux density variabilities is that of a faint temporal disc as part of which a hot spot is orbiting the central black hole (Figure 2). Details of the exact modelling we used are given in Dovciak, Karas and Yaqoob (2004). In this model the temporal variations are explained due to a relativistic apparent flux density increase and decrease when the spot is approaching and receding from the observer. At the same time formation of partial Einstein rings due to gravitational lensing decreases the overall polarisation of the hot spot. All these effects are a function of the spot properties as well as the spin parameter of the black hole and the spin orientation with respect to the spot orbit. Another model parameter is the orientation of the magnetic field. A toroidal B-field will result in a rotating apparent E-field vector. As an alternative the B-field arrangement of the spot may be such that the apparent E-field is perpendicular to the disc. The minimum spin parameter of $a \sim 0.5$ is given by the observed quasi-periodicity. If the spot is at the last stable orbit its period will be about 3 minutes for a prograde orbit around a black hole with maximum spin ($a = 1$) and close to 30 minutes for a stationary non-rotating black hole ($a = 0$). The χ^2 fits show the consistency between the model and the data. (Figure 1). We find a tendency for high inclinations, spot radii larger than the last stable orbit and spin parameters larger than $a = 0.5$ (Meyer et al. submitted to A&A).

As an unexpected surprise the position angle of the mean E-field vector on the sky during the sub-flare has a similar value of about 60 ± 30 degrees for the two flares in 2004 and 2005. This suggests a preferred orientation of the overall black hole/disc arrangement with respect to the observer. Observations of further polarised flare events are needed to determine how stable the orientation of the polarisation vector is. Given that we have not included other possibly important facts that can have an influence on the observed light curve, like tilts and warps of the accretion disc, there is a surprisingly good agreement between the data and the highly idealised model. Future simultaneous observations covering the near-infrared, radio millimetre and sub-millimetre domain should provide a clear discrimination against explanations involving jets. However, near the last stable orbit a short jet with a length of only a few Schwarzschild radii (of the order of or larger than the width of the jet base, i.e., nozzle) emerging from a disc may likely look almost indistinguishable from a case involving a pure disc or orbiting spots. Here new NACO polarisation observations to be taken in the upcoming years as well as planned future simultaneous radio/NIR/X-ray observing runs will be needed to confine the models.

Simultaneous observations of flares in the NIR and X-ray domain

Following the first successful experiment between the VLT and the Chandra satellite during which simultaneous X-ray and near-infrared flare emission has been detected (Eckart et al. 2004) new simultaneous NIR/sub-millimetre/X-ray observations of the SgrA* counterpart were recently presented by Eckart et al. 2006b (Figure 3). In addition to NACO, the Chandra X-ray Observatory as well as the Submillimeter Array on Mauna Kea, Hawaii, and the Very Large Array in New Mexico were involved. For a total of four near-IR flares we found an upper limit for a time lag between the X-ray and NIR flare of ≤ 10 minutes – mainly given by the required binning width of the X-ray data. The NIR/X-ray flares from SgrA* can be explained with a synchrotron self-Compton (SSC) model involving up-scattered submillimetre photons from a compact source component. Inverse Compton scattering of the THz-peaked flare spectrum by the relativistic electrons then accounts for the X-ray emis-

Figure 3: The 6–7 July VLT/Chandra observations as described by Eckart et al. 2006a. The X-ray and NIR light curves plotted with a common time axis. For the labelled times we show 1.3″ × 1.2″ *K*-band images of the Galactic Centre region with SgrA* in its bright and dim state.

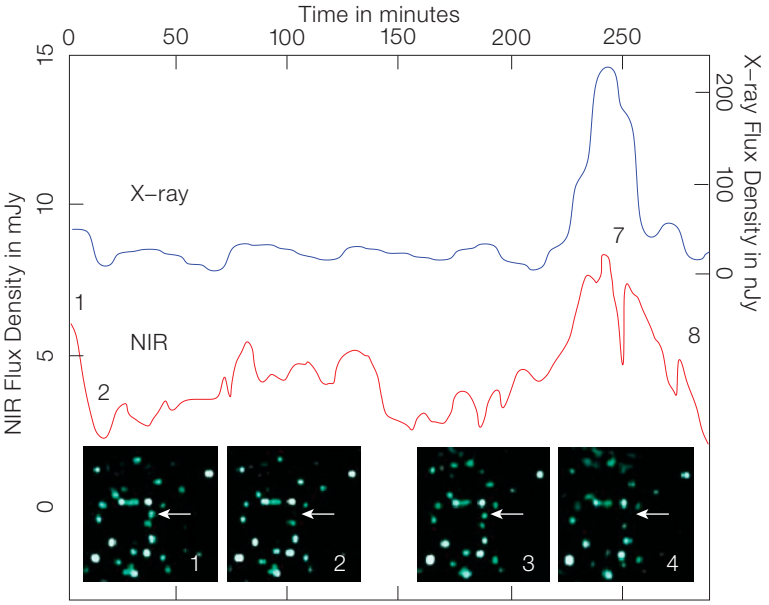

sion. This model is in full agreement with the relativistic orbiting spot model described above. In addition – as a consequence of the possible IR turnover of the synchrotron spectrum (see Eckart et al. 2006b) – the flare rates at longer IR wavelengths may be higher than those at shorter NIR wavelengths. The excess flux densities detected in the radio and submillimetre may be linked with the NIR flare activity via cooling through adiabatic expansion of a synchrotron component (see also Marrone et al. 2006, Mauerhan et al. 2005). A similar behaviour was recently found in dual wavelength radio data by Yusef-Zadeh et al. (2006b).

The NIR *K*-band is the ideal wavelength band to study the flare emission from SgrA*. In combination with adaptive optics systems it provides the highest angular resolution and the lowest amount of contamination by dust emission. Future progress will mainly depend on further successful simultaneous observing campaigns – especially between the NIR and submm(mm)-domain, since until now there was only a few hour overlap between the NIR/X-ray data and the VLA and SMA data. Extensive simultaneous data are not available so far. Further polarisation data from the NIR to the radio as well as (sub-)mm-VLBI and NIR interferometric experiments are also highly desirable to study the details of the accretion process in SgrA*.

VLTI and the Galactic Centre: MIDI and AMBER results

In the future a particularly strong emphasis will also be put on measurements of the Galactic Centre using infrared interferometers like the Very Large Telescope Interferometer (VLTI), as well as comparisons to properties of other low-luminosity galactic nuclei. Infrared interferometry has already started with the observations of the luminous dust-enshrouded star IRS 3 using MIDI at the VLTI (Pott et al. 2005, 2006). In 2005 we obtained data on the UT3–UT4 (62 m) and UT1–UT4 (130 m) baselines. In Figure 4 we plot measured visibilities together with a two-component model with a FWHM size of 20 mas (160 AU) for an inner and 50 mas (400 AU) for an outer component. The wavelength dependent flux density ratios of the two components can be used to estimate blackbody temperatures. We find 920 ± 100 K and 510 ± 50 K for the hotter inner and the cooler outer components, respectively. This agrees well with the interpretation that IRS 3 is a luminous compact object in an intensive dust-forming phase. In fact sources like IRS 3 may contribute substantially to the dust content in the overall Galactic Centre region. While most of the other MIR bright GC sources like IRS 1W, 2, 8,

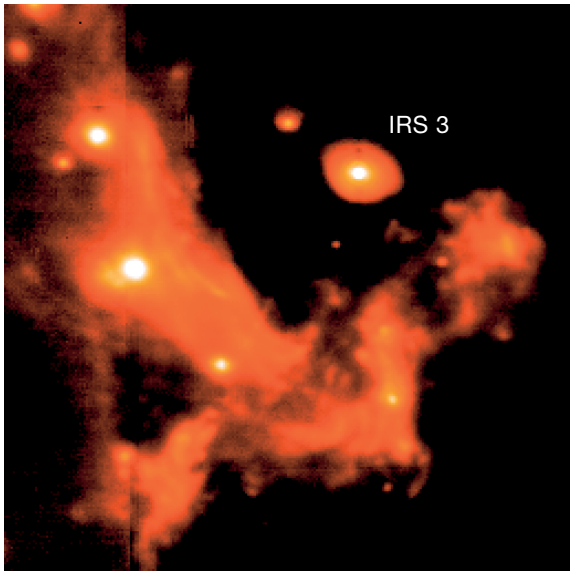

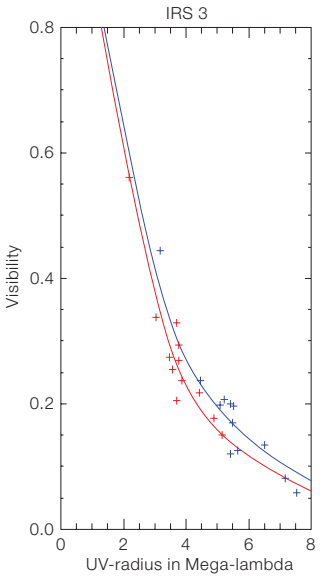

Figure 4: **Left:** A 20″ × 20″ VISIR image of the Galactic Centre at a wavelength of 8.6 μm taken in June 2006. SgrA* is located at the centre of the image. IRS 3 is labelled. **Right:** Visibilities of IRS 3 as obtained by MIDI at the ESO VLTI facility on the UT2–UT3 baseline in 2004 and the UT3-UT4 baseline in 2005 at a wavelength of 8.2 μm (blue) and 12 μm (red) (Pott et al. 2005 and 2006). We also show a possible two-component Gaussian model with given model size and flux density ratios (compact versus extended). Two Gaussian intensity profiles give a slightly better fit than uniform discs.

Figure 5: *M*-band spectra of the IRS 2S and IRS 3 Galactic Centre sources. The CO gas- and solid-phase absorptions are indicated, too. Telluric lines longward of 4.75-μm wavelength have been blanked.

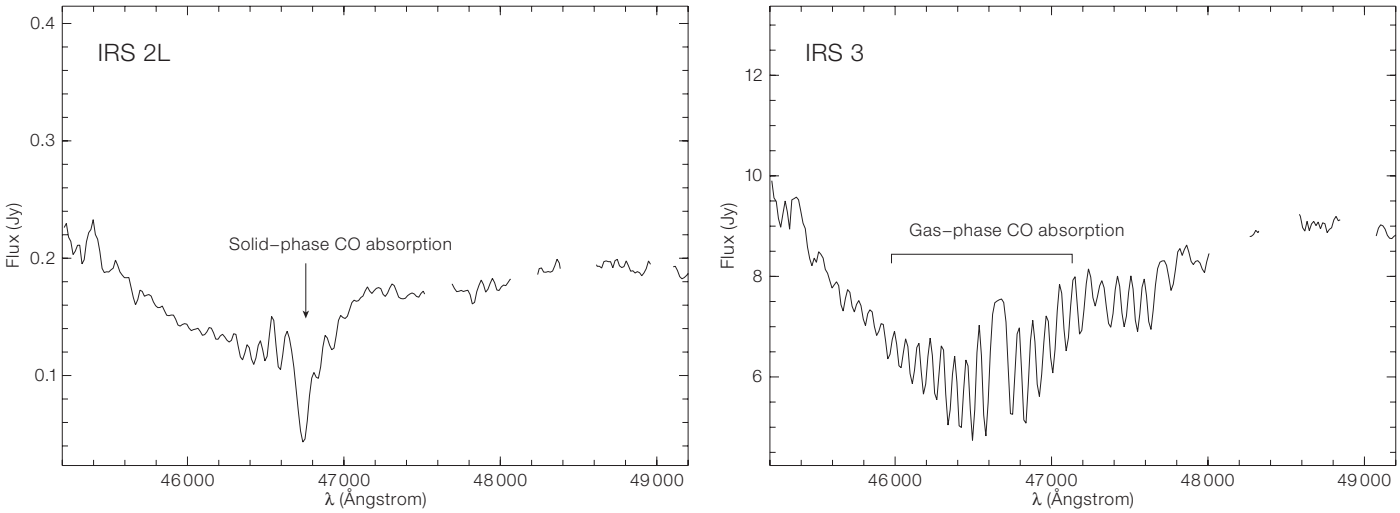

9, 10, 13W are more extended and remain currently undetected by MIDI we recently succeeded in obtaining fringes on the compact supergiant IRS 7 in the *N*-band with MIDI on UT2–UT3 (47 m) and in the *K*-band with AMBER on UT1–UT3 (102 m) and UT3–UT4 (62 m). The compactness of the supergiant IRS 7 is of special importance since it can serve as a fringe tracker in future experiments at longer NIR/MIR wavelengths. AMBER observations will be especially suited to study apparent and physical binaries in the Galactic Centre (1 mas ~ 8 AU). A thorough analysis of the diffuse emission and the dust enshrouded sources at the Galactic Centre is essential to parameterise the ISM in the central parsec. Here ISAAC and VISIR have recently contributed in the thermal infrared.

The Galactic Centre in the thermal infrared: recent ISAAC and VISIR observations

During the past few years we have also carried out extensive observations of the central parsec of our Galaxy in the thermal infrared (Moultaka et al. 2004, 2005, Viehmann et al. 2005, 2006). Spectroscopic observations with ISAAC allowed us to build the first *L*-band data-cube of the central region corrected for foreground extinction. This led to the discovery of three Wolf-Rayet stars, all of which show a prominent 3.09 μm HeII line without showing the HeII line at 2.189 μm in emission. The presence of hot, HeII line emitting stars is indicative of ongoing star formation within the central cluster. The data-cube also allows us to study the distribution of water ice and hydrocarbon absorption features in the central parsec. Through recent ISAAC *M*-band spectroscopic observations of a number of bright sources in the central parsec a detailed study of the CO gas- and solid-phase distribution is possible and in progress (Moultaka et al. in prep.; Figure 5). NACO NIR photometry was also combined with VISIR *N*- and *Q*-band MIR photometry obtained in May 2004 (see also Lagage et al. 2004). For an unprecedentedly large number of over 60 compact sources – most of which are giants and/or young stars enshrouded in the Galactic Centre gas and dust – the observed spectra cover the *H*- to *Q*-band, i.e., 1.6 μm–19.5 μm wavelength. The combined data indicate that a significant portion of the absorption features can be associated with the individual sources and therefore most probably occur in the local Galactic Centre medium close to or even within the dust shells around the objects. Detailed Brα and Pfγ emission line maps also demonstrate that the physical conditions of the more extended Galactic Centre ISM are not uniformly the same in the observed region of the minispiral, especially at the edges of the minicavity. We can clearly distinguish between luminous Northern Arm bow shock sources, lower luminosity bow shock sources, hot stars, and cool stars. For the first time a high angular resolution distribution of *L*-band water ice and hydrocarbon absorption features was determined. A significant contribution to these features also appears to be closely associated with the individual sources at the Galactic Centre.

Acknowledgements

This work was supported in part by the Deutsche Forschungsgemeinschaft (DFG) via grant SFB 494. We are grateful to all members of the NAOS/CONICA and the ESO Paranal team. Jörg-Uwe Pott was partially subsidised by an ESO studentship grant. The X-ray work was supported by NASA through Chandra award G05-6093X.

References

Bélanger G. et al. 2006, astro-ph/0604337
Dovciak M., Karas V. and Yaqoob T. 2004, ApJS 153, 205
Eckart A. et al. 2004, A&A 427, 1
Eckart A., Schödel R. and Straubmeier C. 2005, "The black hole at the centre of the Milky Way", London: Imperial College Press, ISBN 1-86094-567-8
Eckart A. et al. 2006a, A&A, in press
Eckart A. et al. 2006b, A&A 450, 535
Gillessen S. et al. 2005, The Messenger 120, 26
Lagage P. O. et al. 2004, The Messenger 117, 12
Marrone D. P. et al. 2006, ApJ 640, 308
Mauerhan J. C. et al. 2005, ApJ 623, L25
Moultaka J. et al. 2005, A&A 443, 163
Moultaka J. et al. 2004, A&A 425, 529
Pott J.-U. et al. 2006, Proc. of the ESO workshop: "The power of optical/IR interferometry: recent scientific results and second-generation VLTI instrumentation", astro-ph/0505513
Pott J.-U. et al. 2005, The Messenger 119, 43
Viehmann T. et al. 2005, A&A 433, 117
Viehmann T. et al. 2006, ApJ 642, 861
Yusef-Zadeh F. et al. 2006a, ApJ 644, 198
Yusef-Zadeh F. et al. 2006b, ApJ, in press, astro-ph/0603685

New Abundances for Old Stars – Atomic Diffusion at Work in NGC 6397

Andreas Korn[1]
Frank Grundahl[2]
Olivier Richard[3]
Paul Barklem[1]
Lyudmila Mashonkina[4]
Remo Collet[1]
Nikolai Piskunov[1]
Bengt Gustafsson[1]

[1] Uppsala Astronomical Observatory, Sweden
[2] Århus University, Denmark
[3] University of Montpellier II, France
[4] Institute of Astronomy, Moscow, Russia

A homogeneous spectroscopic analysis of unevolved and evolved stars in the metal-poor globular cluster NGC 6397 with FLAMES-UVES reveals systematic trends of stellar surface abundances that are likely caused by atomic diffusion. This finding helps to understand, among other issues, why the lithium abundances of old halo stars are significantly lower than the abundance found to be produced shortly after the Big Bang.

When Joseph Chamberlain and Lawrence Aller in 1951 announced the discovery of stars significantly more metal-poor than the Sun, a new field of astronomical research was born: the observational study of nucleogenesis (or cosmochemistry) which attempts to answer the question of where the chemical elements come from and how their build-up proceeds with time. Today, while many details remain unsettled, we have a general understanding of how the cosmos developed chemically, from a mixture of hydrogen, helium and traces of lithium a few minutes after the Big Bang to stars as metal-rich as the Sun and beyond. The majority of this knowledge has been gathered by studying starlight by means of quantitative spectroscopy. Solar-type stars (here defined to be stars of spectral types F, G and K) have always played a central role in cosmochemical studies, primarily for two reasons: they have rich photospheric spectra (allowing a great variety of elements to be studied) and are long-lived (allowing all phases of Galactic chemical evolution to be investigated).

The art of deriving chemical abundances from spectra is to relate the observed line strengths of a certain element to its abundance in the stellar atmosphere these lines originate in. This is achieved by capturing the essence of the matter-light interaction in a theoretical model. To make this problem computationally feasible, a number of assumptions about the physics of stellar atmospheres are introduced: the atmosphere is assumed to be well represented by a one-dimensional and static temperature and pressure structure in local thermodynamic equilibrium (LTE), convection is treated according to the mixing-length recipe, rotation, mass loss and magnetic fields are disregarded all together. All these are traditional assumptions, to mention only the most obvious ones. Some of these have in the meantime been abandoned, but many analyses still rest on them and are adorned with the flattering title 'classical analysis'. One less explicit assumption often made when interpreting the abundance results concerns the chemical abundances themselves: they are assumed to be representative of the material the star originally formed out of. This means in particular that there are no physical processes which alter photospheric abundances with time.

It comes with the profession of a theorist to question the (sometimes bold) approximations made by more observationally inclined astrophysicists. Lawrence Aller, Evry Schatzmann and others addressed the problem of atomic diffusion already in the 1960s. Later, when a common abundance of lithium was found among warm halo stars by Monique and François Spite (1982; the so-called Spite plateau) and interpreted as a relic of the Big Bang, Georges Michaud and colleagues presented models of stellar evolution with atomic diffusion that "change the lithium abundance by at least a factor of about two in solar-type stars". Larger effects were predicted for Population II stars. In other words, this study showed that lithium and other elements slowly settle into the star under the force of gravity. In particular for old stars the assumption of the constancy of photospheric abundances seemed questionable.

Models with atomic diffusion were subsequently shown to be very successful in reproducing the abundances of hot, chemically peculiar (CP) stars. The significance of diffusion for solar-type stars has, however, been seriously questioned: predicted effects from early models were quite large and failed to, e.g., meet the observational constraint of a flat and thin Spite plateau of lithium (Ryan et al. 1999). This problem has been alleviated in recent years by including additional effects like radiative levitation and turbulent mixing which counterbalance gravitational settling.

Putting diffusion in solar-type stars to the test

Globular clusters of the Galactic halo are primary testbeds for stellar evolution theory in general and for effects of atomic diffusion in particular. Stars in globular clusters have the same age and initial composition (with certain exceptions). To test the atomic-diffusion hypothesis, one thus compares photospheric abundances of stars at the main-sequence turnoff (where the effects of diffusion are largest) to the abundances of red giants (where the original heavy-element abundances are essentially restored due to the large radial extent of the outer convection zone). What sounds like a straightforward measurement in theory is challenging in practice: at a magnitude of 16.5^{m}, turnoff stars in one of the most nearby globular clusters (NGC 6397, see Figures 1 and 2) are too faint to analyse on 4-m-class telescopes at high resolution and high signal-to-noise (S/N) ratio. It took the VLT and the efficient spectrograph UVES to analyse these stars for the first time.

When UVES became available in the late 1990s, there were two teams that focussed their efforts on NGC 6397. Raffaele Gratton and co-workers wanted to further constrain the nature of the anti-correlations of certain elements commonly found among giants by looking for them in unevolved stars. Frédéric Thévenin and colleagues investigated the connection between globular clusters and halo field stars as regards alpha-capture elements. Two different metallicities were advocated for the cluster by these two groups, $\log \varepsilon(\mathrm{Fe}) = \log (N_{\mathrm{Fe}}/N_{\mathrm{H}}) + 12 = 5.50 \pm 0.01$ (five stars; Gratton et al. 2001) and $\log \varepsilon(\mathrm{Fe}) = 5.23 \pm 0.01$

Figure 1: The nearby metal-poor globular cluster NGC 6397 as seen by the Wide-Field Imager on the ESO/MPI 2.2-m. Its distance modulus is $(m - M) \approx 12.4^{m}$.

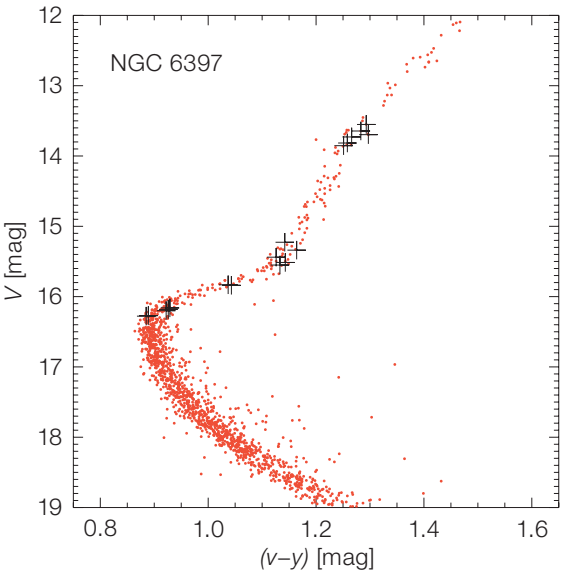

Figure 2: Colour-magnitude diagram of NGC 6397 with the FLAMES-UVES targets marked by the crosses. According to literature values, the metallicity of this cluster is just below 1/100th solar ([Fe/H] ≈ –2.1). The data were acquired with the Danish 1.54-m telescope on La Silla.

(seven stars, assuming LTE, Thévenin et al. 2001), where the error given is the standard deviation of the mean. Obviously, these results are quite incompatible with one another. Gratton et al. backed up their high metallicity scale by analysing three stars at the base of the red-giant branch (RGB) which gave log $\varepsilon(\mathrm{Fe})_{\mathrm{LTE}} = 5.47 \pm 0.03$ suggesting the good agreement between the two groups of stars to be "a constraint on the impact of diffusion". But what if Thévenin et al. were right with their turnoff-star metallicity?

We started to investigate this issue in mid-2003 and uncovered potential systematic effects in the temperature determination of the Gratton et al. analysis which could produce the apparent abundance differences between the two analyses and mimic the good agreement between the turnoff and base-RGB stars. The problems found concern the imperfect removal of blaze residuals in the UVES pipeline spectra that Gratton et al. used to set constraints on the effective temperatures of the stars from the Balmer line Hα (cf. Korn 2002). With the help of sophisticated echelle-data reduction routines developed by Nikolai Piskunov and Jeff Valenti, we could show that the systematic corrections are non-negligible amounting to –250 K. We subsequently applied for observing time with FLAMES-UVES to investigate this issue further. Fibre-fed spectrographs are less prone to the above-mentioned problems and this multi-object facility seemed ideally suited for this research.

The proposal was accepted, but was moved to Visitor Mode, as we had requested the 'old' (now 'B') high-resolution settings for GIRAFFE. The visit to Paranal in June of 2004 was fruitless: high winds and thick clouds did not allow us to collect more than 20 % of the necessary data. We continued the analysis of the archival data and in a talk at the ESO-Arcetri workshop on "Chemical Abundances and Mixing in Stars" in September 2004 concluded that "gravitational settling of iron of up to 0.1 dex at [Fe/H] ≈ –2 seems possible".

A second chance with FLAMES

The successful reapplication for observing time in Period 75 gave us a second chance, this time in Service Mode. We observed a variety of stars in NGC 6397, from the turnoff to the red-giant branch. In every observing block, two UVES fibres were given to two stars in the middle of the subgiant branch (SGB), one fibre monitored the sky background. Five turnoff stars were observed for a total of 12 hours, while the six RGB stars only required 1.5 h to reach a S/N of 100. With a total integration time of 18 h, the two SGB stars have the highest S/N. The 130 fibres to GIRAFFE were filled with stars along the SGB. After receiving the data, the analysis could begin, first with a look to the effective temperatures of the turnoff stars. Already at this early stage, we learned that our preliminary analysis essentially pointed in the right direction.

The fully spectroscopic analysis of the 18 FLAMES-UVES targets took a few months. Meaningful results were only obtained once we had properly accounted for the sky background (via the sky fibre) and the fibre-to-fibre throughput correction. By November 2005 the spectroscopic results were ready and we asked Olivier Richard to compute diffusion models including radiative accelerations and turbulent mixing for comparison with our derived abundances. It is mainly

the overall size of metal diffusion (in terms of iron) and the behaviour of calcium which set limits on the unknown strength of turbulent mixing (see Figure 3). The analysis is based on traditional 1D models (see above), but for iron and calcium detailed (non-LTE) line formation was used. We also investigated the impact of using hydrodynamic model atmospheres and found very similar results for weak lines.

The main challenge lies in determining a realistic effective-temperature *difference* between the turnoff and the RGB stars. This is because most spectral lines originate from neutral species which react most strongly to the temperature. Besides, the surface-gravity difference is well constrained by the apparent-magnitude difference of stars at a given distance.

For the spectroscopic analysis, we rely on Hα which gives an effective-temperature difference between turnoff and RGB stars of 1124 K (see Table 1). This number is in excellent agreement with the photometric estimate based on the Strömgren index (*v*–*y*) which indicates 1108 K. The surface-gravity differences agree equally well, the (logarithmic) spectroscopic value being 0.05 dex smaller than the photometric one. This good agreement between two independent techniques gave us confidence that we could determine relative abundance *differences* with high accuracy.

The diffusion signature

We uncovered systematic trends of abundances with evolutionary phase. The best determined abundance is that of iron for which the analysis rests on 20–40 lines of FeI and FeII. The abundance difference between turnoff and RGB stars is found to be (0.16 ± 0.05) dex which is significant at the 3σ level. Other elements were also investigated (calcium and titanium). The trends for these elements are found to be shallower than for iron which is a specific prediction of the diffusion model with turbulent mixing (see Figures 4 and 5).

This is the first time that metal diffusion in old stars is constrained by means of observations. Via the diffusion model,

Figure 3: Theoretical predictions for a 0.77 $M_\odot$, [Fe/H] = –2 star (located at the turnoff after 13.5 Gyr) as a function of age using different input physics: with atomic diffusion only (dashed magenta), with atomic diffusion and radiative levitation (red), with atomic diffusion and turbulent mixing, but without radiative levitation (dashed green), with atomic diffusion, turbulent mixing and radiative levitation (blue). The dashed horizontal line indicates the original abundance. The panels for Ca and Fe clearly show the importance of radiative levitation for heavy elements. The blue model describes our observations of calcium and iron best.

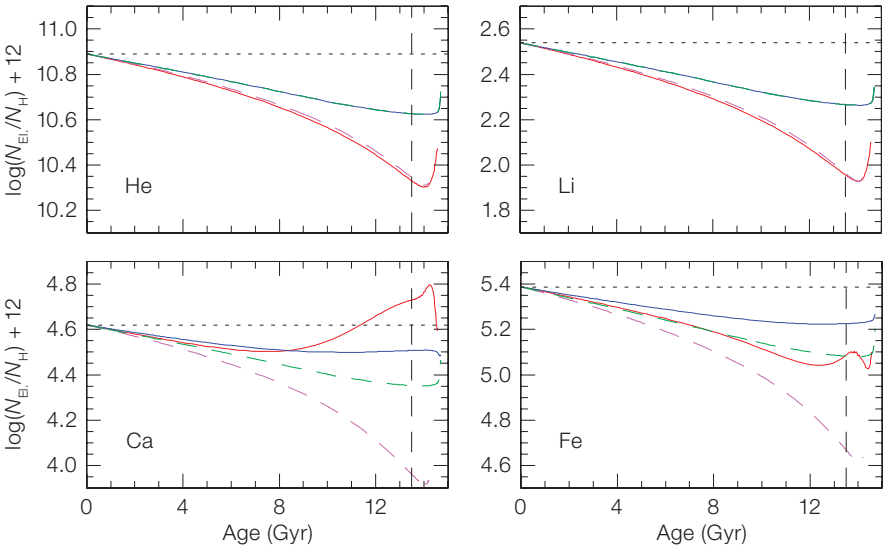

Table 1: Mean stellar parameters of the FLAMES-UVES stars. Typical errors on T_{eff} and log *g* are 150 K and 0.15, respectively. The errors in log ε(Fe) are the combined values of the line-to-line scatter of FeI and FeII for the individual stars propagated into the mean value for the group.

Stars	#	T_{eff} [K]	log (*g* [cm/s])	log ε(Fe)
Turnoff	5	6254	3.89	5.23 ± 0.04
Subgiant	2	5805	3.58	5.27 ± 0.05
base-RGB	5	5456	3.37	5.33 ± 0.03
RGB	6	5130	2.56	5.39 ± 0.02

Figure 4: Abundance variations for a 0.77 $M_\odot$, [Fe/H] = –2 star after 13.5 Gyr. As in Figure 3, the model describing our observations is the blue one. Among the heavy elements ($Z \geq 20$), the abundance change is minimal for calcium and titanium, while it is largest for iron and nickel. Lighter elements show even larger variations (e.g. magnesium and aluminium), but are subject to anticorrelations in globular clusters (Gratton et al. 2001). Of all elements, helium and lithium are affected the most.

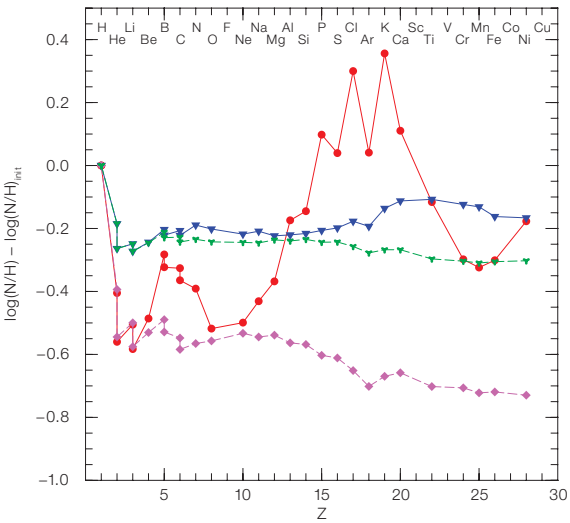

0.77 $M_\odot$ Dif. without g_{rad} + T6.0 — 13.49 Gyr, T_{eff} = 6358 K, log *g* = 4.19
0.77 $M_\odot$ Dif. without g_{rad} — 13.49 Gyr, T_{eff} = 6325 K, log *g* = 4.18
0.77 $M_\odot$ Dif. + T6.0 — 13.50 Gyr, T_{eff} = 6356 K, log *g* = 4.19
0.77 $M_\odot$ Dif. — 13.50 Gyr, T_{eff} = 6317 K, log *g* = 4.18

Figure 5: Observed trends of abundance with effective temperature for calcium, iron and lithium. The blue line represents the prediction from the diffusion model with turbulent mixing at an age of 13.5 Gyr (see Figure 3) with the dashed line indicating the original abundance. Measurements for individual stars are marked by crosses, group averages by bullets. For calcium, measurements were made on the group-averaged spectra to increase the S/N.

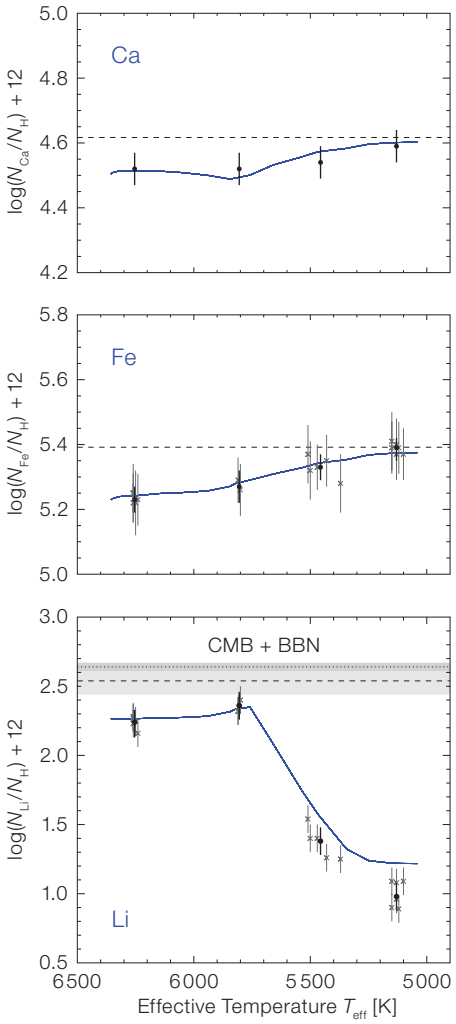

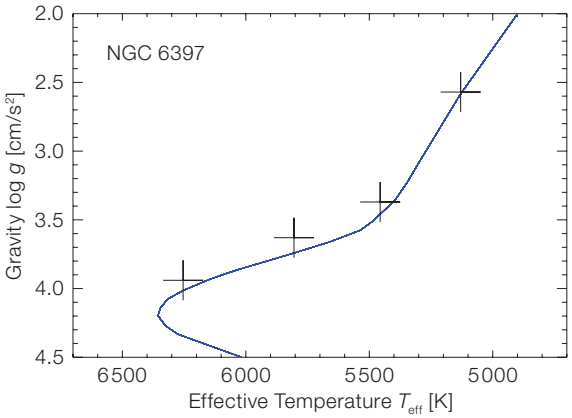

Figure 6: Kiel diagram showing the mean positions of the stars relative to a 13.5 Gyr isochrone constructed from the diffusion model with turbulent mixing. Unlike in Table 1, helium diffusion has been considered as a structural effect in the spectroscopic analysis which results in higher gravities (by +0.05 dex) for the turnoff and SGB stars (see Korn et al. 2006 for details).

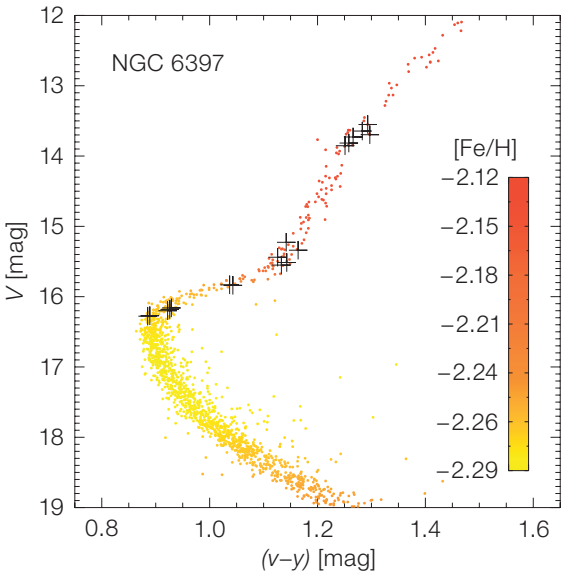

Figure 7: Colour-magnitude diagram of NGC 6397 with the FLAMES-UVES targets marked by the crosses. The colour-coding represents abundance trends in iron taken from the diffusion model with turbulent mixing calibrated on the measured abundance trends. All stars were once born with an initial iron abundance around [Fe/H] = −2.12, but unevolved stars now display lower abundances in their atmospheres.

this also constrains helium diffusion. Comparison with a 13.5 Gyr isochrone constructed from the diffusion model with turbulent mixing shows that the spectroscopic stellar parameters meet the cosmological age constraint (see Figure 6). Residual discrepancies are small, but may point towards a somewhat younger age for NGC 6397. As can be seen in Figure 3, the absolute age assumed has only a minor impact on the results.

While helium diffusion is nowadays considered a standard ingredient in stellar-evolution theory, this is not the case for metal diffusion. The latter has, however, a smaller impact on stellar evolution of metal-poor stars and we therefore expect only moderate changes to isochrone ages of globular clusters in general (nonetheless, globular clusters are now more intriguing objects than ever, see Figure 7). When it comes to unevolved field stars, the situation is different: the high ages for halo field stars that are reported in the literature are systematically overestimated by underestimated metallicities. Together with helium diffusion, the removal of this bias will likely bring down field-star isochrone ages by several billion years.

The diffusion of lithium and its cosmological implications

The recent upward revision of the baryonic matter content (Ω_b) of the Universe by experiments like WMAP (see Spergel et al. 2006 for the most recent results) has led to revised abundances of deuterium, helium and lithium produced in Big-Bang nucleosynthesis (BBN). More lithium than previously thought is found to be produced in BBN (log $\varepsilon(\mathrm{Li})_{\mathrm{BBN}} = 2.64 \pm 0.03$, "CMB + BBN" in Figure 5). This has led to a distressing difference of about a factor of two or more with respect to the common abundance measured in stars on the Spite plateau. We now find that, once atomic diffusion is accounted for, the stellar abundances (log $\varepsilon(\mathrm{Li}) = 2.54 \pm 0.10$) are in good agreement with the primordial lithium abundance (Figure 5). Note that we even seem to see the effects of atomic diffusion in the behaviour of lithium in the turnoff and SGB stars: the measured upturn towards the SGB stars (before dilution sets in) is a specific prediction of the diffusion model.

With this work, the existence of the Spite plateau is more fascinating than ever: it is essentially of cosmological origin, but is *uniformly* lowered by physical processes in the stars. This theoretical idea has been

around for decades, yet it never really caught on with the observers. Only recently, with the latest diffusion models making such a uniform lowering plausible and the WMAP results constraining the primordial lithium abundance, has the idea gained credence. Atomic diffusion may thus resolve the cosmological lithium discrepancy (Korn et al. 2006), but we caution that other effects (the absolute temperature scale of Population II stars and the related issue of a trend of lithium with metallicity, the chemical evolution of lithium in the early Galaxy, see Asplund et al. 2006 for a recent review) may also play a significant role.

This work highlights three methodological points: the possibilities of the new generation of multi-object spectrometers at the largest telescopes, the virtue of a homogeneous and consistent analysis of all relevant criteria (spectroscopic as well as photometric) and the benefits of developing physical models to a higher degree of self-consistency. The empirical result that atomic diffusion affects atmospheric chemical abundances of old unevolved stars and that models can account for its effects is significant and has a number of consequences, some of which were discussed above. For the time being, turbulent mixing is introduced in an ad-hoc manner, without specifying the physics behind it. Likewise, we neglect the spectral effects of the thermal inhomogeneities and the 3D nature of convection in our traditional 1D analysis. Thus, a lot remains to be done before the quality of current observational data is adequately matched by physical models of stars, so that we can fully read the fingerprints of chemical elements in stellar spectra.

References

Asplund M. et al. 2006, ApJ 644, 229
Gratton R. G. et al. 2001, A&A 369, 87
Korn A. J. 2002, in: Scientific Drivers for ESO Future VLT/VLTI Instrumentation, ed. by Bergeron J. and Monnet G. (Springer, Heidelberg), 199
Korn A. J. et al. 2006, Nature 442, 657
Michaud G., Fontaine G. and Beaudet G. 1984, ApJ 282, 206
Piskunov N. E. and Valenti J. A. 2002, A&A 385, 1095
Richard O., Michaud G. and Richer J. 2005, ApJ 619, 538
Ryan S. G., Norris J. E. and Beers T. C. 1999, ApJ 523, 654
Schatzmann E. 1969, A&A 3, 331
Spergel D. N. et al. 2006, ApJ, in press
Spite M. and Spite F. 1982, Nature 297, 483
Thévenin F. et al. 2001, A&A 373, 905

VLT Image of Globular Cluster 47 Tuc

47 Tucanae is an impressive globular cluster that is visible with the unaided eye from the southern hemisphere. It appears as big on the sky as the full moon.

The colour image of 47 Tucanae presented here was taken with FORS1 on ESO's Very Large Telescope in 2001. The image covers only the densest, very central part of the cluster. The red giants, stars that have used up all the hydrogen in their core and have increased in size, are especially easy to pick out.

47 Tuc is so dense that stars are less than a tenth of a light year apart, which is about the size of the Solar System. By comparison, the closest star to our Sun, Proxima Centauri, is four light years away. This high density can cause interactions; these dynamic processes are the origin of many exotic objects, to be found in the cluster.

Thus, 47 Tuc contains at least twenty millisecond pulsars (neutron stars). The Hubble Space Telescope recently also looked at 47 Tuc to study planets orbiting very close to their parent stars. These observations showed that such 'hot Jupiters' must be much less common in 47 Tucanae than around stars in the Sun's neighbourhood. This may tell us either that the dense cluster environment is unhealthy for even such close planets, or that planet formation is a different matter today than it was very early in our Galaxy's history.

(Based on ESO Press Photo 20/06)

ESO PR Photo 20/06 is based on data obtained with FORS1 on Kueyen, UT2 of the Very Large Telescope. The image, seven arcmin wide, covers the central core of the 30 arcmin large globular cluster. The observations were taken in three different filters: *U*, *R*, and a narrow-band filter centred around 485 nm, for a total exposure time of less than five minutes. The data were extracted from the ESO Science Archive and processed by Rubina Kotak (ESO) and the final image processing was done by Henri Boffin (ESO). North is up and East is to the left.

The SINS Survey: Rotation Curves and Dynamical Evolution of Distant Galaxies with SINFONI

Natascha M. Förster Schreiber[1]
Reinhard Genzel[1,2]
Frank Eisenhauer[1]
Matthew D. Lehnert[1]
Linda J. Tacconi[1]
Nicole Nesvadba[1]
Nicolas Bouché[1]
Richard Davies[1]
Dieter Lutz[1]
Aprajita Verma[1]
Andrea Cimatti[3,4]
Dawn K. Erb[5]
Alice E. Shapley[6]
Charles C. Steidel[7]
Emanuele Daddi[8]
Alvio Renzini[9]
Xu Kong[10]
Nobuo Arimoto[11]
Marco Mignoli[12]
Roberto Abuter[1]
Stefan Gillessen[1]
Amiel Sternberg[13]
Andrea Gilbert[14]

[1] Max-Planck-Institut für Extraterrestrische Physik (MPE), Garching, Germany
[2] Department of Physics, University of California, Berkeley, California, USA
[3] Istituto Nazionale di Astrofisica, Osservatorio Astrofisico di Arcetri, Firenze, Italy
[4] Visiting at MPE with the support of the Alexander von Humbolt Foundation through a Bessel Prize Award
[5] Harvard-Smithsonian Center for Astrophysics, Cambridge, Massachusetts, USA
[6] Department of Astrophysical Sciences, Princeton University, Princeton, New Jersey, USA
[7] California Institute of Technology, Pasadena, California, USA
[8] National Optical Astronomy Observatory, Tucson, Arizona, USA
[9] ESO
[10] Center for Astrophysics, University of Science and Technology of China, Heifei, China
[11] National Astronomical Observatory, Tokyo, Japan
[12] Istituto Nazionale di Astrofisica, Osservatorio Astronomico di Bologna, Bologna, Italy
[13] School of Physics and Astronomy, Tel Aviv University, Tel Aviv, Israel
[14] IGPP, Lawrence Livermore National Laboratory, Livermore, California, USA

It has become clear in recent years that about half of the stellar mass in galaxies was put in place by redshift z ~ 1, when the Universe was 40 % of its current age. However, the details of how the mass was assembled and what physical processes were involved at early stages of galaxy evolution remain unclear. Progress has been hampered by the lack of detailed spatially-resolved studies of galaxies beyond *z* ~ 1. This has now become possible with SINFONI, the adaptive optics-assisted near-infrared integral field spectrometer at the VLT. Here we report on our SINFONI observations of massive star-forming galaxies at *z* ~ 2–3. The data enabled us to investigate their morphologies and kinematics on typical spatial scales of 4–5 kpc. The most surprising outcome is that a majority of these galaxies appear to be large, rotating, and often gas-rich discs. Even more compelling evidence is provided by the exceptionally detailed SINFONI data of a *z* ~ 2 galaxy observed with adaptive optics, resulting in a spatial resolution of 1.2 kpc, and of a highly magnified *z* ~ 3 galaxy for which the gravitational lensing of a foreground galaxy cluster acts as a microscope, revealing the dynamics on scales as small as 200 pc.

Our understanding of the formation and evolution of galaxies has improved dramatically over the past two decades. This has been driven by the advent of large ground-based telescopes and space-based facilities equipped with sensitive instruments, leading to a veritable explosion of multiwavelength surveys accumulating ever larger samples of galaxies over an ever increasing range of redshifts. We now have a robust outline of the global evolution of the stellar mass and luminosity density, star-formation history, and nuclear activity over cosmic time. In parallel, theoretical models and semi-analytical simulations have matured and provide a global framework for galaxy formation in the cold dark-matter paradigm: galaxies form as baryonic gas cools at the centre of collapsing dark-matter halos while mergers of halos and galaxies lead to the hierarchical build-up of galaxy mass.

Much of our current knowledge about high-redshift galaxies, however, rests on relatively crude broad-band photometric information, rarely on integrated spectra probing their rest-frame UV emission, even less frequently their rest-frame optical light. As a result, very little is known about the dynamical and detailed physical properties of high-redshift galaxies. The description of galaxy formation in models and simulations remains uncertain because the complex physics of the baryonic processes driving the growth of galaxies lacks observational constraints.

Clearly, the next step is now to understand *how* galaxies were built up. When and how fast did galaxies of different masses assemble? What was the relative importance of mergers versus smooth infall in the accretion of mass? What were the physical processes involved and their interplay? What is the connection between bulge and disc formation?
A promising way to address these issues observationally is from detailed spatially-resolved studies of individual galaxies. Until only recently, galaxies in the crucial redshift range *z* ~ 1–4 were virtually inaccessible to such studies: they are faint, their projected angular sizes are small, and important spectral diagnostic features that are emitted in the rest-frame optical are redshifted into the near-infrared bands, between 1 and 2.5 µm. SINFONI (Eisenhauer et al. 2003; Bonnet et al. 2004), mounted on Yepun (UT4) at the VLT, has now changed the situation. SINFONI consists of a cryogenic near-infrared integral field spectrometer, SPIFFI, that obtains simultaneously the entire *J*, *H*, *K*, or *H*+*K* band spectrum of each spatial pixel within the field of view. SPIFFI is coupled to a curvature-sensing adaptive-optics (AO) module, MACAO, that currently enables diffraction-limited observations with a natural guide star, and with a laser guide star when PARSEC becomes available.

The SINS survey

Given the new opportunities afforded by SINFONI, we have undertaken a large and coherent observational programme of near-infrared integral field spectros-

copy of high-redshift galaxies, the 'SINS' survey. This will provide new insight on the dynamics, sizes, morphologies, masses, gas-phase metallicities and ionisation state of galaxies at early stages of their evolution. Ultimately, SINS aims at elucidating the evolution of star formation, angular momentum, mass growth/assembly, and metal enrichment as a function of cosmic time, baryonic mass, and dark-matter halo mass. The integral field capabilities of SINFONI have substantial advantages over the classical long-slit spectroscopy: measurements do not suffer from the biases and uncertainties due to the fixed orientation and possible misalignments of slits relative to the targets, and the kinematics can be directly related to morphological features and spatial variations in physical properties. This is essential for reliable structural and dynamical studies of high-redshift sources that are often complex and whose morphologies can dramatically vary depending on the wavelength of study.

Our work focuses on the crucial redshift range $z \sim 1$–4, where the peak of major mergers, QSO, and (dust-enshrouded) star-formation activity occurred, and where probably a substantial fraction of massive elliptical galaxies and bulges of spiral galaxies were assembled. In what follows, we concentrate on the dynamics and morphologies derived from the Hα line emission of galaxies at $z \sim 2$, and the [OIII]λ5007 line emission of one galaxy at $z \sim 3$.

First convincing evidence for rotating discs at $z \sim 2$

Our largest sample to date consists of 14 star-forming 'BM/BX' galaxies at $z \sim 2$ (Förster Schreiber et al. 2006). BM/BX galaxies are selected on the basis of their optical (rest-frame UV) colours (e.g., Adelberger et al. 2004). We chose our targets primarily from the sample with near-infrared long-slit spectroscopy presented by Erb et al. (2006). The optical and near-infrared colours and magnitudes of the 14 objects span nearly the full range observed for the general BM/BX population. The SINFONI observations were carried out under typical seeing conditions of ~ 0.5″–0.6″, giving a spatial resolution of 4–5 kpc at the redshift of the sources.

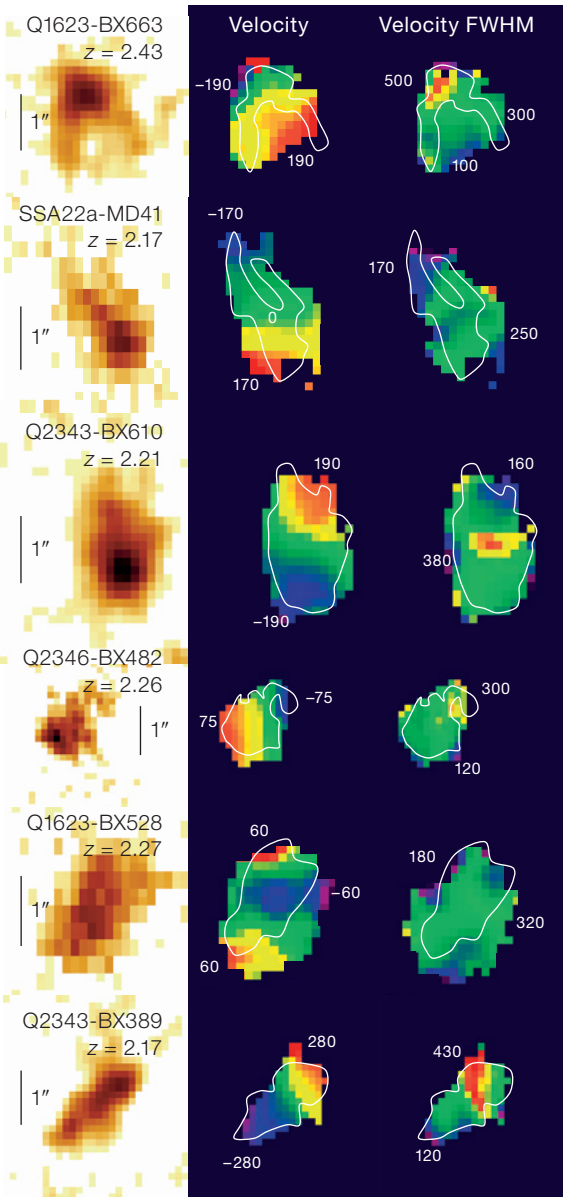

Figure 1: Two-dimensional Hα morphologies and kinematics from SINFONI of six of our $z \sim 2$ BM/BX galaxies. Each row shows the spatial distribution of the velocity-integrated emission (left), the velocity field (middle), and the FWHM velocity width (right). The angular scale of 1″, corresponding to ≈ 8.3 kpc at the redshifts of the sources, is shown for each galaxy. The velocities (relative to the systemic velocity) and velocity FWHM increase from purple to red, and the range in km s^{-1} is given for each map; the white contour outlines the Hα morphology. All velocity fields exhibit the smooth gradient expected for rotating discs, except for Q1623-BX528 where the reversal in velocities possibly indicates a counter-rotating merger (Förster Schreiber et al. 2006).

The immediate result from the observations is that the Hα emission for the majority of the sources is spatially resolved, extending over ~ 10–20 kpc in several of them. The Hα morphology of the larger systems tends to be irregular and clumpy. The most surprising outcome, however, was the discovery in several galaxies of convincing evidence for rotation in a disc. We expected that most of the larger systems would exhibit irregular and chaotic gas kinematics, but found instead the opposite.

Figure 1 shows the Hα line maps and kinematics for the six largest BM/BX galaxies in our sample. The velocity fields appear smooth and ordered, and all but one show a monotonic variation and steepest gradient along the morphological major axis, as expected for rotating discs. Smooth kinematic structure despite a clumpy and asymmetric morphology is reminiscent of the Hα velocity fields of many local star-forming disc galaxies. Moreover, for three sources in particular, the velocity gradient along the major axis flattens at radii ~ 10 kpc, tracing the rotation curve out to the flat part that is characteristic of disc galaxies

(Figure 2). Their observed velocity dispersion peaks close to the geometric/kinematic centre, another property of rotating discs. Quantitatively, the kinematics of these three galaxies can be very well fit with dynamical models of rotating discs.

Implications for the evolution of high-redshift galaxies

Our SINFONI data provide new ways of exploring the dynamical properties and evolution of distant galaxies. In the framework of rotating discs, we derive for our BM/BX sample an average maximum circular velocity (i.e., where the rotation curve of a disc galaxy turns over) of 180 ± 90 km s^{-1}, and dynamical masses from ~ 5 × 10^9 $M_\odot$ to as large as ~ 2.5 × 10^{11} $M_\odot$. The specific angular momentum of the sample is ~ 900 km s^{-1} kpc, up to 1000–2000 km s^{-1} kpc for a few objects. Interestingly, these values are similar to the specific angular momenta of local late-type spiral galaxies.

A potentially interesting probe of the dynamical evolution of high-redshift galaxies is the ratio of the circular velocity to the local velocity dispersion, v_c/σ. Characteristic values are ~ 0.1–1 for local ellipticals and ~ 10–50 for local discs of spirals. From the kinematic modelling of our best resolved BM/BX galaxies, we infer v_c/σ ~ 2–4. This implies that their discs are dynamically hot and geometrically thick, probably very gas-rich and unstable to global star formation and fragmentation.

The properties revealed by SINFONI for several of our BM/BX sources are not unlike those seen in some simulations of the evolution of gas-rich galactic discs (e.g., Immeli et al. 2004), in which the clumpy fragmenting discs are unstable and the star-forming clumps sink towards the gravitational centre by dynamical friction against a diffuse underlying gas disc to form a central bulge on ~ 1 Gyr time-scales. This could provide a mechanism whereby some of the BM/BX objects in our sample later evolve into galaxies with a massive spheroidal component like those observed in the present-day Universe.

A z ~ 3 Lyman-break galaxy under the microscope: rotation on fine spatial scales

In another remarkable SINS target, a star-forming Lyman-break galaxy at z = 3.2, the small-scale dynamics revealed by our SINFONI data add strong support for disc rotation at high redshift (Nesvadba et al. 2006). For this source, the 1E0657-56 'arc and core', the linear resolution in terms of physical scale is boosted by a factor of ~ 20 due to strong gravitational lensing by the foreground galaxy cluster 1E0657-56. The angular resolution of the data is ≈ 0.5″, corresponding in the source plane to about 200 pc over the well-sampled inner ~ 2.5 kpc. The velocity curve (Figure 3), even on such small scales, is very similar to those observed in nearby rotating disc galaxies. Remarkably, the dynamical mass surface density in the central few kpc is comparable to that of bulges in local galaxies. This may suggest that a significant amount of mass could already be in place on small physical scales at $z \gtrsim 3$, which in turn would favour 'inside-out' scenarios of galaxy formation.

SINFONI AO observations: detailed anatomy of a z = 2.38 star-forming galaxy

Very recently (March/April 2006), we obtained a spectacular data set for a massive z = 2.38 star-forming galaxy. The results appeared in the 17 August issue of Nature (Genzel et al. 2006). This galaxy, BzK-15504, was selected by the 'star-forming BzK' colour criteria (Daddi et al. 2004) as part of a wide-field optical/near-infrared imaging survey (Kong et al. 2006). We benefitted from a lucky combination of a suitable AO star near the source and excellent atmospheric conditions during the SINFONI observations. This resulted in a deep 6-hour on-source integration and a spatial resolution of ≈ 0.15″, or 1.2 kpc at the redshift of the galaxy. This provides the most detailed view of the Hα morphology and kinematics for a z ~ 2 system to date.

The Hα emission of BzK-15504 has many characteristics in common with that of several of our BM/BX objects but revealed with three times better spatial resolution, and there are interesting differences too (Figure 4). The morphology is clumpy and embedded in a more diffuse low-surface brightness component that extends over nearly 2″ (16 kpc) but it is overall fairly symmetic along the major

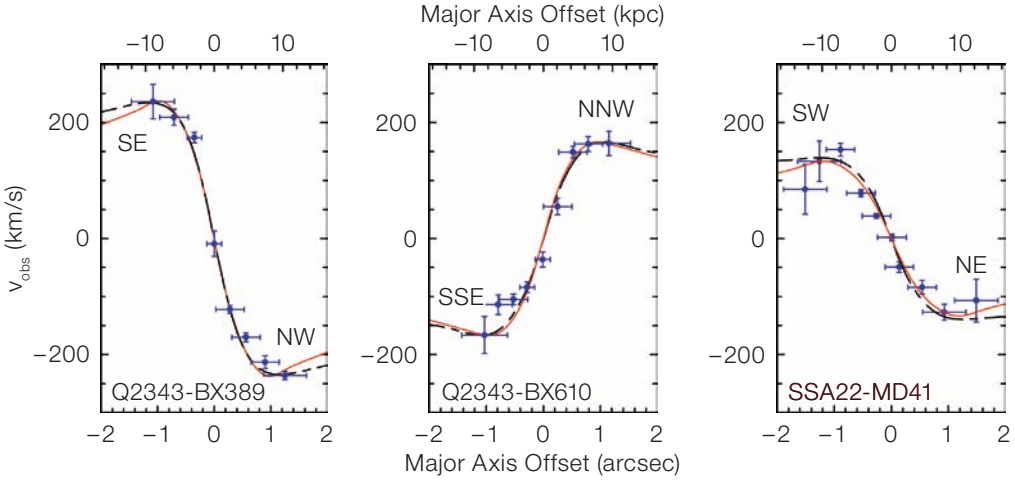

Figure 2: Rotation curves of three z ~ 2 BM/BX galaxies, derived from Hα observations with SINFONI. The blue data points show the velocities (relative to the systemic velocity) as a function of position along the kinematic major axis of each galaxy. The SINFONI data trace well the rotation curves out to their flat part. The rotation curves of the disc models that best fit the observed Hα kinematics of each galaxy are overplotted: the black dashed line for an exponential disc with central hole and the red solid line for a ring-like distribution (Förster Schreiber et al. 2006).

axis and centered on the continuum peak. The kinematics in the outer parts show a smooth velocity field and the rotation curve flattens at radii ~ 8–10 kpc, compelling evidence for a rotating disc. In the inner few kpc, the twist of the isovelocity contours relative to the larger-scale pattern suggests radial flows that could be related to inflow of material towards the nuclear regions, and/or to an outflow possibly due to an AGN present in this galaxy. The AGN, however, clearly does not dominate the global Hα line emission and kinematics. There are no obvious signs for a major merger. BzK-15504 appears to be a large, massive (dynamical mass of ~ 10^{11} $M_{\odot}$ within 10 kpc), gas-rich clumpy disc possibly in the process of channeling gas towards a central growing bulge and fueling an AGN.

Outlook

Our SINFONI results unveil the morphologies and kinematics of high redshift galaxies in unprecedented detail. As we pursue our SINS survey and exploit fully the rich SINFONI data sets, we can look forward to substantial progress in our understanding of galaxy formation and evolution. In this respect, SINFONI is paving the way for the science to come from similar instruments now becoming available worldwide – and in the future when KMOS at the VLT as well as facilities such as the Extremely Large Telescope and the James Webb Space Telescope will enable us to conduct these kinds of observations routinely.

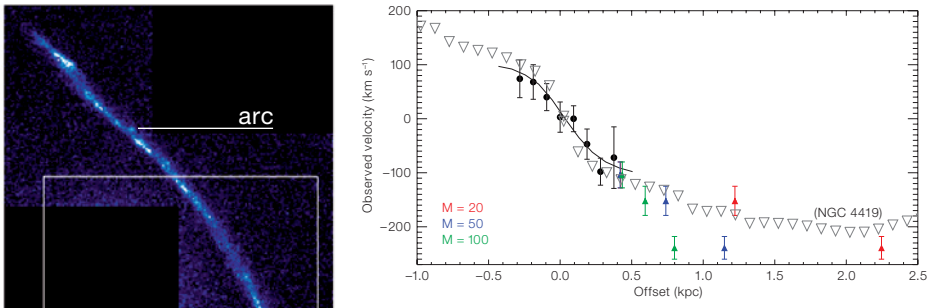

Figure 3: Left: The 1E0657-56 'arc and core,' a highly magnified $z = 3.2$ star-forming Lyman-break galaxy behind the galaxy cluster 1E0657-56, as seen in the optical with the ACS camera on-board the Hubble Space Telescope through the F814W filter. The box indicates the SINFONI field of view (~ 8″ × 8″). The high surface brightness region at the bottom right is the core while the arc curves to the upper left (north-east). **Right:** The velocity curve of the core (black dots) on scales of 200 pc derived from the SINFONI observations of the [OIII]λ5007 emission line is compared to the rotation curve of the nearby disc galaxy NGC 4419 (upside-down grey triangles). The coloured triangles indicate the velocity curve of the arc under the assumption of various magnifications: 20, 50, and 100 for red, blue, and green, respectively (Nesvadba et al. 2006).

References

Adelberger K. L. et al. 2004, ApJ 607, 226
Bonnet H. et al. 2004, The Messenger 117, 17
Daddi E. et al. 2004, ApJ 617, 746
Eisenhauer F. et al. 2003, Proc. SPIE 4841, 1548
Erb D. K. et al. 2006, ApJ 646, 107
Förster Schreiber N. M. et al. 2006, ApJ 645, 1062
Genzel R. et al. 2006, Nature 442, 786
Immeli A. et al. 2004, ApJ 611, 20
Kong X. et al. 2006, ApJ 638, 72
Nesvadba N. et al. 2006, ApJ, in press, astro-ph/0606527

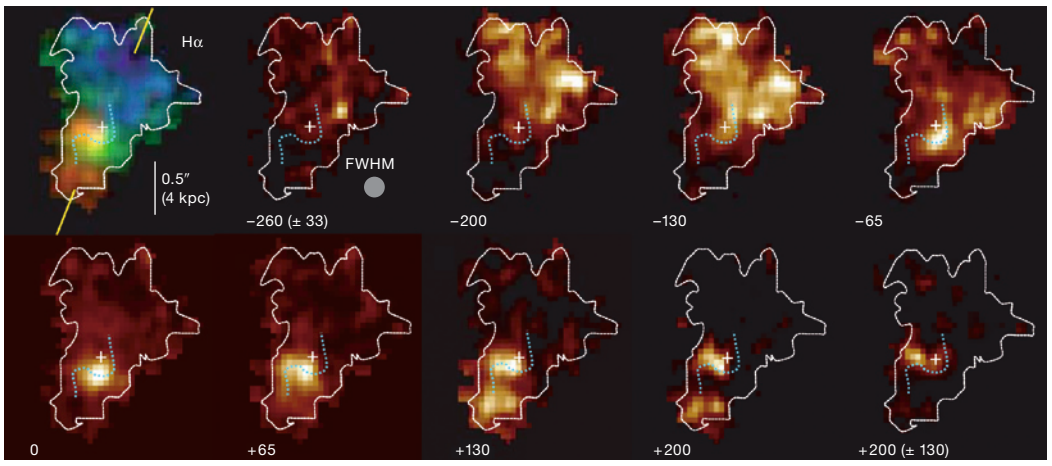

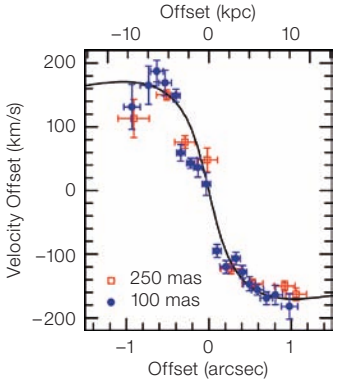

Figure 4: Left: Maps of the Hα line emission of the $z = 2.38$ star-forming galaxy BzK-15504. The SINFONI data, taken in adaptive optics mode, have an angular resolution with FWHM ≈ 0.15″, or 1.2 kpc at $z = 2.38$ (indicated by the grey-filled circle). The top left panel is a RGB composite of 'blue' (−320 to −100 km s^{-1}), 'green' (−100 to +130 km s^{-1}) and 'red' velocity emission (+130 to +320 km s^{-1}). The two yellow lines mark the orientation of the major axis of the disc. The other panels show channel maps integrated in velocity over 65 km s^{-1} wide intervals with increasing central velocity (given in km s^{-1} below each map), except for the map at the bottom right panel, which is integrated over 260 km s^{-1} and centred at +400 km s^{-1}. All velocities are relative to the systemic velocity. The vertical bar indicates the angular scale of 0.5″ and the white cross marks the position of the continuum peak. The dotted, thin white curve outlines the shape of the integrated Hα emission. The dotted, light blue S-shape traces the radial flow of gas into the central bulge region. **Right:** Rotation curve of BzK-15504 extracted from the high-resolution (0.15″) SINFONI data set (taken with the 100 mas pixel scale; blue filled circles), and from additional 0.45″ resolution SINFONI observations (taken with the largest 250 mas pixel scale; red open squares). The black solid line shows the rotation curve of the best-fitting exponential disc model to the kinematics data (Genzel et al. 2006).

The Evolution of Galaxies in the FORS Deep and GOODS-S Fields

Niv Drory[1,3]
Ralf Bender[2,3]
Georg Feulner[2,3,5]
Armin Gabasch[2,3]
Ulrich Hopp[2,3]
Stefan Noll[3]
Maurilio Pannella[3]
Roberto P. Saglia[3]
Mara Salvato[3,4]

[1] University of Texas at Austin, USA
[2] Universitäts-Sternwarte München, Germany
[3] Max-Planck-Institut für Extraterrestrische Physik, Garching, Germany
[4] Caltech, Pasadena, California, USA
[5] Currently: Potsdam-Institut für Klimafolgenforschung, Germany

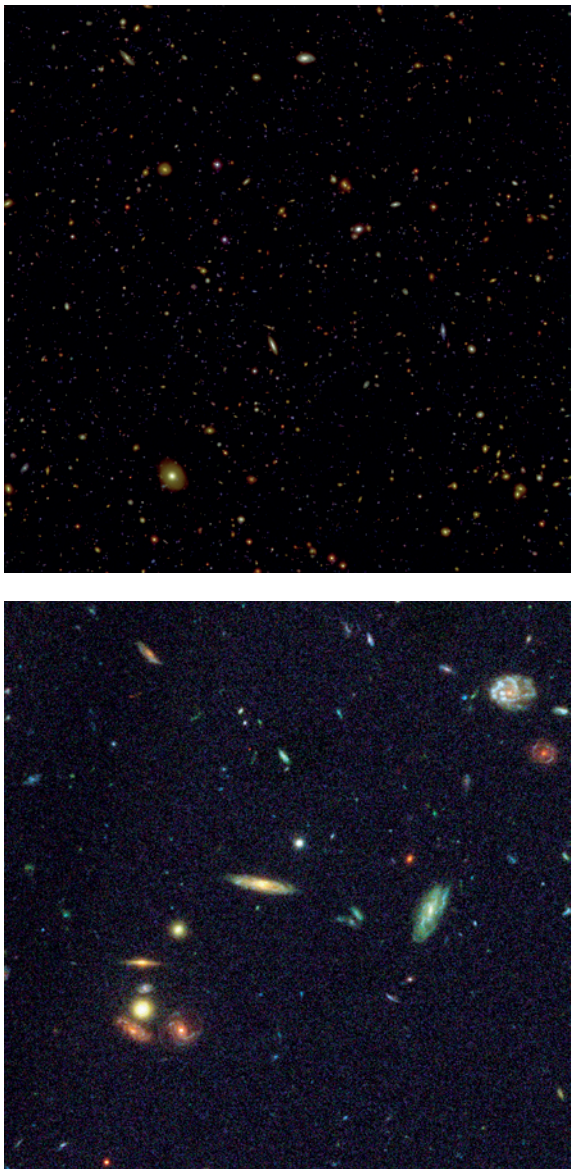

Figure 1: Composite *BRI* image of the 6 × 6 arcminute-sized FORS Deep Field (top panel) and a 1 × 1 arcminute cutout from the HST/ACS *BVz* data in the GOODS-S region (bottom panel).

Deep multicolour surveys obtained with ESO telescopes provide new insights into the evolution of galaxies from 1 Gyr after the Big Bang to the present epoch. With the broad wavelength coverage (*U* to *K*) of the FORS Deep Field and the GOODS-S field, we can derive accurate photometric redshifts for about 8000 galaxies between $z = 0$ and $z = 6$. Modelling their spectral energy distributions yields galaxy stellar masses and star-formation rates as a function of cosmic time. Interestingly, massive galaxies ($M > 10^{11}\ M_{\odot}$) seem to be present even at the highest redshift and do not disappear faster with redshift than lower-mass galaxies. Star-formation activity moves from bright to faint objects with decreasing redshift (downsizing).

The advent of 10-m-class telescopes provided the opportunity to routinely measure the evolution of galaxies as a function of redshift directly, instead of having to infer or extrapolate their evolution from information about its endpoint only, the present-day galaxy population. Large telescopes make it possible to survey huge volumes photometrically and spectroscopically to great depth and therefore obtain representative samples of galaxies spanning a large fraction of the Universe's age.

Among the parameters that have been found to evolve are stellar populations, morphology, structure, star-formation rates, and stellar and total mass. Total and stellar mass, and their change with time, are of particular importance because mass assembly is intricately linked to gravitationally driven hierarchical structure formation, which is thought to provide the wider context in which galaxy formation and evolution is to be understood. While total (baryonic and dark) mass is still very hard to measure at $z > 0$, stellar mass and star-formation rates are much more accessible to observations.

Our group is using surveys conducted with ESO facilities to study the assembly history of mass in galaxies and the history of star formation in the Universe. Results from two of these surveys having multicolour photometry and rich follow-up spectroscopy are highlighted in this article: The FORS Deep Field (FDF; Heidt et al. 2003; Noll et al. 2004) and the Great Observatories Origins Deep Survey (GOODS; Giavalisco et al. 2004) South region (for more information of the FDF see The Messenger 116, 18).

The *I*-band selected FDF photometric catalogue covering the UBgRIzJKs bands in 40 arcmin^2 is published in Heidt et al. 2003. This catalogue lists 5 557 galaxies down to $I \sim 26.8$. This sample is discussed in detail in Gabasch et al. 2004a.

Distances to all the galaxies are estimated using photometric redshift techniques, whereby the redshift is deduced by comparing each object's photometry to a library of likely galactic spectral energy distributions at various distances. These photometric redshifts for the FDF are calibrated against 362 spectroscopic redshifts up to $z \sim 5$ (Noll et al. 2004) and provide distances to an accuracy of $\Delta z/(z_{spec}+1) \leq 0.03$ with only ~ 1 % outliers (Gabasch et al. 2004a).

Our *K*-band selected catalogue for the GOODS-S/CDFS field is based on the publicly available 8 2.5 × 2.5 arcmin^2 *J*, *H*, *Ks* ISAAC images (as of version 1.1), taken at the ESO/VLT with excellent image quality (seeing in the range 0.40″–0.50″). The *U* and *I* images are from ESO GOODS/EIS public survey, while the *B*, *V*, and *R* images are taken from the Garching-Bonn Deep Survey. The catalogues are discussed and made available to the public by Salvato et al. 2006.

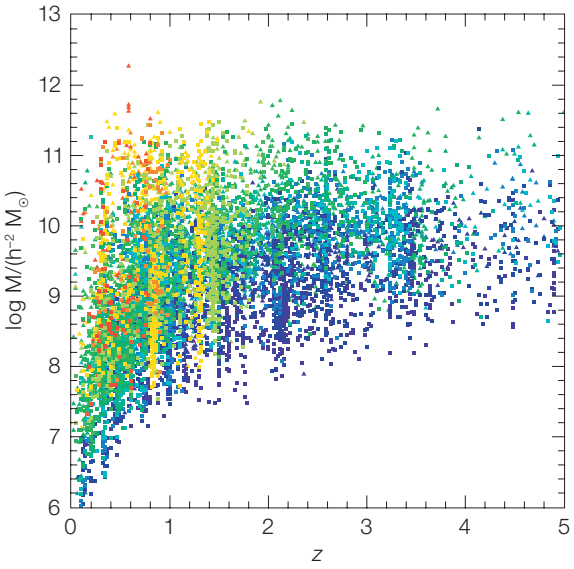

Figure 2: Stellar mass of galaxies derived from fitting stellar population models to multicolor photometry plotted against redshift (squares: FDF; triangles: GOODS). Colour encodes the effective age of the stellar population: young populations (age < 1 Gyr) are shown in blue and old population (age > 5 Gyr in red).

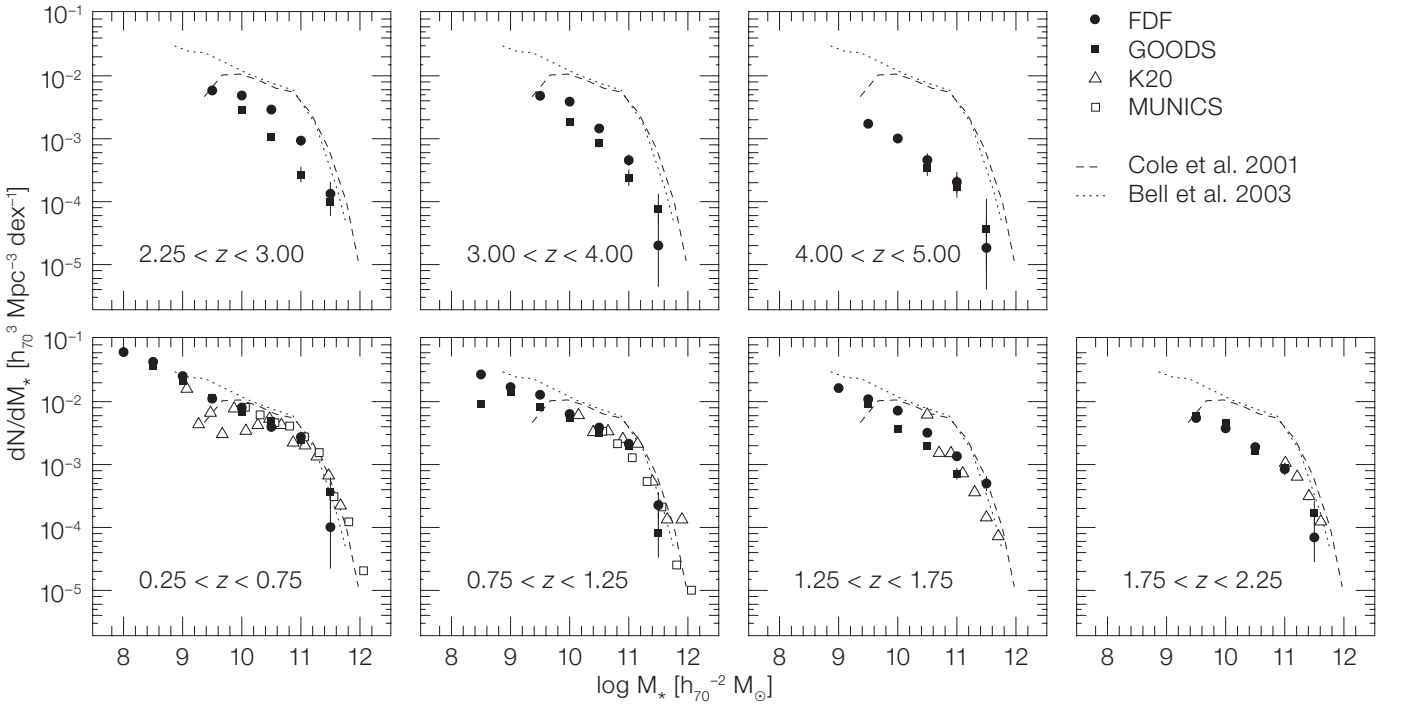

Figure 3: The stellar mass function as a function of redshift. The local mass function of is shown for comparison (dotted and dashed line). Results from the MUNICS survey (Drory et al. 2004) and the K20 survey (Fontana et al. 2004) at $z < 2$ are also shown.

In this article we will focus on the evolution of the stellar mass function (Drory et al. 2005) and the specific star-formation rates (star-formation rate per unit stellar mass; Feulner et al. 2005) of galaxies in the redshift range $0 < z < 5$. Moreover, we will study the morphological evolution up to $z \sim 1$ using HST/ACS data (Pannella et al. 2006). These observables taken together provide a valuable data set to study the mass assembly of galaxies, probing both mass and its change over time.

The stellar mass function

We derive stellar masses (the mass locked up in stars) by comparing each galaxy's multi-color photometry to a grid of stellar population synthesis models covering a wide range in parameters, such as redshift, star-formation histories, dust extinction, and starburst fractions (see Drory et al. 2004 for details).

In Figure 2 we show the distribution of galaxies in the mass versus redshift plane for the FDF (squares) and GOODS-S (triangles). In addition, we code the age of each galaxy (using the best-fitting model) in colours ranging from blue for young (age < 1 Gyr) to red for old stellar populations (age > 5 Gyr). A striking feature of Figure 2 is that the most massive galaxies harbour the oldest stellar populations at all redshifts.

Figure 3 shows the mass function (the number density of galaxies per unit log mass interval) in seven redshift bins from $z = 0.25$ to $z = 5$. For comparison, we also show the local mass function and the mass functions to $z \sim 1.2$ of MUNICS (Drory et al., 2004) and to $z \sim 2$ by the K20 survey (Fontana et al. 2004).

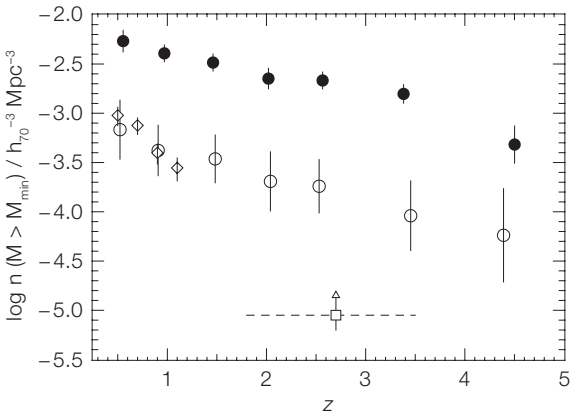

● M > 10^{10} h_{70}^{-2} $M_\odot$ (FDF + GOODS-S)
○ M > 10^{11} h_{70}^{-2} $M_\odot$ (FDF + GOODS-S)
◇ M > 10^{11} h_{70}^{-2} $M_\odot$ (MUNICS)
□ M > 10^{11} h_{70}^{-2} $M_\odot$ (Sub-mm; Tecza et al. 2004)

Figure 4: The number density of galaxies with stellar masses M > 10^{10} $M_\odot$ and M > 10^{11} $M_\odot$. Results from the MUNICS survey as well as results from Sub-mm studies are also shown.

In our lowest redshift bin, $z \sim 0.5$, the mass function follows the local mass function very well. The depth of the FDF ($I \sim 26.8$) allows us to extend the faint end of the mass function down to 10^8 $M_\odot$, a decade lower in mass than before, with no change of slope. Furthermore, the faint end slope is consistent with the local value of $\alpha \sim 1.1$ at least to $z \sim 1.5$. Our mass function also agrees very well with the MUNICS and K20 results at $z < 2$.

The mass function seems to evolve in a regular way at least up to $z \sim 2$ with the normalisation decreasing by 50 % to $z = 1$ and by 70 % to $z = 2$, with the largest change occurring at masses of M > 10^{10} $M_\odot$. These likely progenitors of today's $L > L^*$ galaxies are found in much smaller numbers above $z \sim 2$. However, we note that massive galaxies with M > 10^{11} $M_\odot$ are present even to the largest redshifts we probe (albeit in much smaller numbers). Beyond $z \sim 2$ the evolution becomes more rapid.

In Figure 4 we compare the number density evolution of massive galaxies (M > 10^{11} $M_\odot$) with that of less massive systems (M > 10^{10} $M_\odot$), combining our two survey fields. We find that high-mass galaxies evolve similarly to lower mass galaxies, and do not disappear faster with redshift.

We find that the stellar mass density at $z = 1$ is 50 % of the local value. At $z = 2$, 25 % of the local mass density is assembled, and at $z = 3$ and $z = 5$ we find that at least 15 % and 5 % of the mass in stars is in place, respectively.

The specific star-formation rate

The stellar mass content of galaxies evolves in two ways: by star formation within the galaxy, and by merging with other galaxies driven by hierarchical structure formation. Ultimately, the goal is to distinguish these two contributions to the mass build-up process. This cannot be done from measurements of the mass function alone; measurements of the star-formation rates are necessary.

We determine the star-formation rate for each galaxy in our sample from its rest-frame UV luminosity (see Gabasch et al. 2004b). Star-formation rates determined in this way suffer from problems of dust extinction. Heavily dust-enshrouded objects might escape detection completely, or, objects might be detected, but their star-formation rate (and stellar mass) might be underestimated. We try to correct for the second effect by including dust attenuation in our model fitting. However, an advantage is that in our sample, each detected galaxy has both a stellar mass and a star-formation rate measurement. In principle both of the above sources of uncertainty could be overcome with observations in the thermal infrared (albeit not without some problems of their own). Such data from the Spitzer Space Telescope are becoming available now and will be used in future papers.

In Figure 5 we show the specific star-formation rate as a function of stellar mass and age for six different redshift bins covering the range $0.4 < z < 5.0$. The upper cut-off of the specific star-formation rate runs essentially parallel to lines of constant star-formation rate and shifts to higher star-formation rates with increasing redshift. This was already noted in earlier work. This trend seems to continue to the highest redshifts probed by our sample: While at $z \sim 0.6$ we find $SFR_{max} \simeq 5$ $M_\odot$ yr^{-1}, galaxies reach as much as $SFR_{max} > 100$ $M_\odot$ yr^{-1} at $z \sim 4$. Note that this upper envelope is partly due to a selection effect: Heavily dust-obscured star bursts cannot be detected in our sample, and hence the large star-formation rates in massive galaxies at high redshift are to be regarded as lower limits. The lack of galaxies with low specific star-formation rates is due to the flux limit of the sample.

It is helpful to visualise schematically different ways to double a galaxy's mass as shown in the lower right-hand panel of Figure 5.

Quiescently star-forming galaxies: A galaxy doubling its stellar mass by quiescent star formation at 0.5 $M_\odot$ yr^{-1} moves along a line of constant star-formation rate towards the lower right part of the diagram. Note that galaxies below the doubling

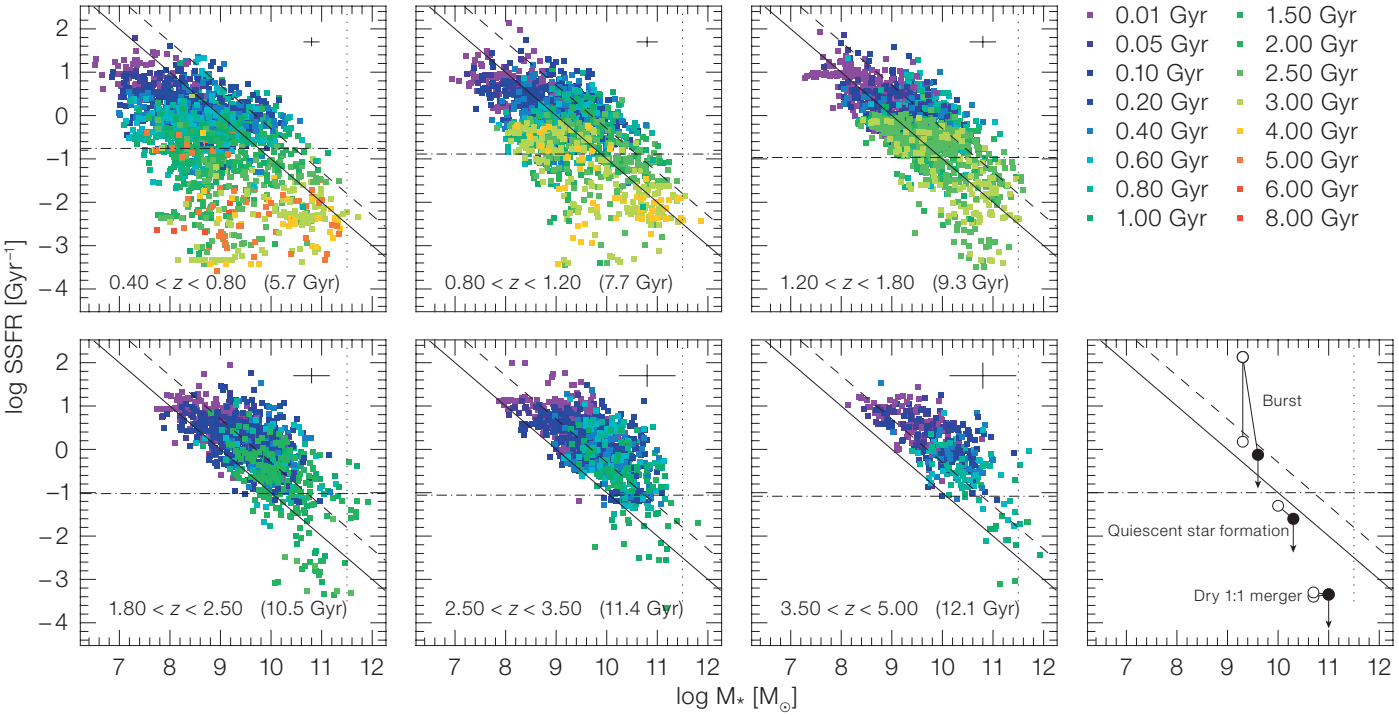

Figure 5: The specific star-formation rate as a function of stellar mass and redshift. The solid and dashed lines correspond to star-formation rates of 1 $M_\odot$ yr^{-1} and 5 $M_\odot$ yr^{-1}, respectively. Objects are coloured according to the age of their stellar population. The dot-dashed line is the specific star-formation rate required to double a galaxy's mass between each redshift epoch and today (assuming constant star-formation rate); the corresponding lookback time is indicated in each panel. **Lower right-hand panel:** Examples for evolutionary paths yielding a doubling of a galaxy's mass, through quiescent star formation, through a burst of star formation superimposed on quiescent star formation, and through a dry equal-mass merger.

line in Figure 5 do not have enough time to double their mass until the present epoch, assuming that their star-formation rate remains constant.

Starbursts: In contrast to a quiescent galaxy, a starburst can increase its mass in a shorter time interval, provided it has enough gas to consume. Bursts of star formation may be triggered by gas inflow or galaxy interactions, and quickly move a galaxy to high specific star-formation rates, where it stays for a brief period of time before it fades back. Given the typical dusty nature of starburst galaxies, they might escape detection in optical surveys during this stage, or their star-formation rates may be underestimated. However, since these bursts are typically brief, the galaxies spend most of their time with the quiescent galaxies.

Dry mergers: Two galaxies undergoing a dry merger (i.e. a merger without interaction-induced star formation) basically move to the right in the diagram. We illustrate this with equal stellar mass mergers; the stellar mass clearly doubles, while the final specific star-formation rate is the average of the two initial specific star-formation rates or below.

Note that the 'true' endpoint of the galaxies' evolution will in all three cases likely be lower than shown, since all three processes diminish the limited gas supply. This is indicated by the downward pointing arrows.

In the light of these evolutionary possibilities it is obvious that the only two ways to form massive galaxies with old stellar populations is by highly efficient early star formation in massive halos, or by dry merging of less massive galaxies harbouring old stars. Both scenarios can, in principle, be distinguished by analysing the redshift dependence of the specific star-formation rate in the most massive galaxies.

It is therefore interesting to ask when galaxies of a particular mass form most of their stars. The answer is presented in Figure 6, where we show the average specific star-formation rate as a function of redshift for galaxies in three mass intervals. At redshifts $z < 2$, the most massive galaxies with $\log M_\star/M_\odot \in [10.5, 11.5]$ are in a quiescent state with specific star-formation rates not contributing significantly to their growth in stellar mass. However, at redshifts $z > 2$, the picture changes dramatically: The specific star-formation rate for massive galaxies increases rapidly by a factor of ~ 10 until we reach their formation epoch at $z > 2$. Galaxies of lower mass seem to be forming a larger portion of their stars progressively later.

Evolution by morphology

High-resolution HST-based imaging is available in both the FDF and GOODS-S (see Figure 1). We use these images to derive quantitative morphology allowing us to discriminate between disc-dominated and bulge-dominated galaxies by their surface brightness profiles up to $z \sim 1$. In Pannella et al. 2006 we compare the evolution of the mass function of disc galaxies to that of bulge dominated galaxies. We find that the mass at which disc galaxies dominate the total mass function decreases with cosmic time, i.e., that since $z \sim 1$, mass has shifted from disc-dominated systems to bulge-dominated systems. Based on a comparison of the specific star-formation rates in disc-dominated and bulge-dominated galaxies, we conclude that merging events, and not star formation, play the key role in this process.

Figure 6: Average specific star-formation rates for galaxies with stellar masses of log $M_*/M_\odot \in$ [8.5, 9.5] (blue), [9.5, 10.5] (green) and [10.5, 11.5] (red) and star-formation rates larger than 1 $M_\odot$ yr^{-1} as a function of *z* for FDF (open squares), GOODS-S (open diamonds) and the combined sample (filled circles). The error bar represents the error of the mean. The solid line indicates the doubling line of Figure 5 which can be used to discriminate quiescent and star-forming galaxies.

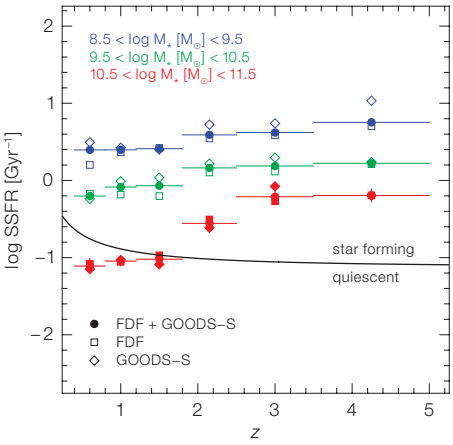

Such samples allow us to view the assembly of galaxies in principle for the first time. Also, theoretical models of galaxy formation can use these data to compare wide ranges of observables to their predictions.

Future surveys will provide yet better constraints on the current set of observables and will add further observables for each galaxy, until a complete picture of the star-formation and merging history of galaxies can be obtained.

References

Drory N. et al. 2004, ApJ 608, 742
Drory N., Bender R. and Hopp U. 2004, ApJ 616, L103
Drory N. et al. 2005, ApJ 619, L131
Feulner G. et al. 2005, ApJ 633, L9
Fontana A. et al. 2004, A&A 424, 23
Gabasch A. et al. 2004a, A&A 421, 41
Gabasch A. et al. 2004b, ApJ 616, L83
Giavalisco M. et al. 2004, ApJ 600, L93
Heidt J. et al. 2003, A&A 398, 49
Noll S. et al. 2004, A&A 418, 885
Pannella M. et al. 2006, ApJ 639, L1
Salvato M. et al. 2006, A&A, submitted

A Supernova in an Interacting Pair of Galaxies

MCG-01-39-003 (bottom right) is a peculiar spiral galaxy, apparently interacting with its neighbour, the spiral galaxy NGC 5917 (upper right). Both galaxies are located at similar distances, about 87 million light years away, towards the constellation of Libra.

Last year, a star exploded in the vicinity of the hook. The supernova, noted SN 2005cf as it was the 84th found that year, was discovered by astronomers Pugh and Li with the robotic KAIT telescope on 28 May. It appeared to be projected on top of a bridge of matter connecting MCG-01-39-003 with NGC 5917. Further analysis with the Whipple Observatory 1.5-m Telescope showed this supernova to be of the Ia type and that the material was ejected with velocities up to 15 000 km/s. Immediately after the discovery, the European Supernova Collaboration (ESC), led by Wolfgang Hillebrandt (MPA-Garching, Germany) started an extensive observing campaign on this object, using a large number of telescopes around the world. The ESC includes ten institutions across Europe (Stockholm, MPA, Barcelona, CNRS, ESO, ICSTM, ING, IoA, Padua, Oxford).

There have been several indications about the fact that galaxy encounters and/or galaxy activity phenomena may produce enhanced star formation. As a consequence, the number of supernovae in this kind of system is expected to be larger with respect to isolated galaxies. Normally, this scenario should favour mainly the explosion of young, massive stars. Nevertheless, recent studies have shown that such phenomena could increase the number of stars that eventually explode as Type Ia supernovae.

The supernova was followed by the ESC team during its whole evolution, from about ten days before the object reached its peak luminosity until more than a year after the explosion. As the SN becomes fainter and fainter, larger and larger telescopes are needed. One year after the explosion, the object is indeed about 700 times fainter than at maximum.

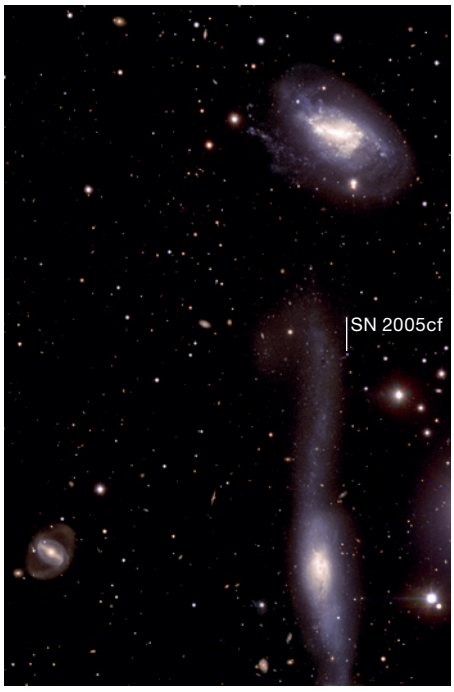

The supernova was observed with the VLT equipped with FORS1 by ESO astronomer Ferdinando Patat, who is also member of the team led by Massimo Turatto (INAF-Padua, Italy), and at a later stage by the Paranal Science Team, with the aim of studying the very late phases of the supernova. These late stages are very important to probe the inner parts of the ejected material, in order to better understand the explosion mechanism and the elements produced during the explosion. The deep FORS1 images reveal a beautiful tidal structure in the form of a hook, with a wealth of details that probably include regions of star formation triggered by the close encounter between the two galaxies.

(Based on ESO Press Photo 22/06)

ESO PR Photo 22/06 is a composite image based on data acquired with the FORS1 multi-mode instrument in April and May 2006 for the European Supernova Collaboration. The observations were made in four different filters (*B*, *V*, *R*, and *I*) that were combined to make a colour image. The field of view covers 5.6 × 8.3 arcmin. North is up and East is to the left. The observations were done by Ferdinando Patat and the Paranal Science team (ESO), and the final processing was done by Olivia Blanchemain, Henri Boffin and Hans Hermann Heyer (ESO).

Searching for the First Galaxies through Gravitational Lenses

Daniel Schaerer[1,2]
Roser Pelló[2]
Johan Richard[2,5]
Eiichi Egami[3]
Angela Hempel[1]
Jean-François Le Borgne[2]
Jean-Paul Kneib[4,5]
Michael Wise[6]
Frédéric Boone[7]
Françoise Combes[7]

[1] Geneva Observatory, Sauverny, Switzerland
[2] Observatoire Midi-Pyrénées, Laboratoire d'Astrophysique, Toulouse, France
[3] Steward Observatory, University of Arizona, Tucson, Arizona, USA
[4] OAMP, Laboratoire d'Astrophysique de Marseille, Marseille, France
[5] Caltech Astronomy, Pasadena, California, USA,
[6] Astronomical Institute Anton Pannekoek, Amsterdam, the Netherlands
[7] LERMA, Observatoire de Paris, France

Observing the first galaxies formed during the reionisation epoch, i.e. approximately within the first billion years after the Big Bang, remains one of the challenges of contemporary astrophysics. Several efforts are being undertaken to search for such remote objects. Combining the near-IR imaging power of the VLT and the natural effect of strong gravitational lensing our pilot programme has allowed us to identify several galaxy candidates at redshift $6 \lesssim z \lesssim 10$. The properties of these objects and the resulting constraints on the star-formation rate density at high redshift are discussed. Finally we present the status of follow-up observations (ISAAC spectroscopy, HST and Spitzer imaging) and discuss future developments.

Like the explorers of seas and continents in the past centuries, astronomers keep pushing the observational frontiers of the Universe with their telescopes thereby tracing back the history of stars and galaxies since their birth. Just a few years ago, in 2002, the most distant galaxy known was a faint unconspicuous object called HCM 6A at redshift $z = 6.56$ discovered thanks to the natural effect of gravitation lensing provided by a foreground cluster of galaxies, which magnifies the light of this distant background object (Hu et al. 2002). A few quasars at similar distances had also been discovered, pushing our 'observational horizon' already back in time to a little less than one billion years after the Big Bang, close to the end of cosmic reionisation. However, evidence from cosmic microwave background polarisation measurements and other arguments indicate that star formation in galaxies must have occurred even earlier.

Since the early nineties, the so-called Lyman break or 'dropout' technique had established itself as a simple and successful method to identify distant galaxies through the use of broadband photometry. Furthermore, sensitive infrared instruments were now available on the large ground-based telescopes, able in principle to detect protogalaxies out to even higher redshifts. Given these advances, we started a few years ago a pilot project with the aim of finding star-forming galaxies at redshifts beyond 6–6.5 using lensing clusters as gravitational telescopes, a well-established technique nowadays. This project is mainly based on ISAAC and FORS2 data plus additional observations obtained at CFHT and HST.

Observations

Focussing on two well-known gravitational lensing clusters, Abell 1835 and AC114, we obtained deep near-IR images in the *SZ*, *J*, *H*, and *Ks* bands with ISAAC and an additional *z*-band image with FORS2. These deep images, reaching e.g. a 1 σ depth of 26.1 in H_{AB}, were then used to search for objects which are detected at least in two near-IR bands, which show a blue near-IR colour, and which are undetected (i.e. 'drop-outs') in all optical bands. These criteria are optimised to select high-redshift ($z > 6$) objects with intrinsically blue UV-restframe spectra, i.e. very distant starburst galaxies, and to avoid contamination from intrinsically faint and red cool stars. Different combinations of colour-colour plots allow a crude classification into several redshift bins. An example of such a diagram, showing the expected location of $z \sim 8$–11 galaxies and of candidates found behind Abell 1835 is shown in Figure 1. A complete report is given in Richard et al. (2006).

High-*z* galaxy candidates and the cosmic star formation density during reionisation

In spring 2003 the analysis of the candidates behind Abell 1835 yielded an intriguing, strongly lensed object whose spectral energy distribution was compatible with that of a galaxy at $z \sim 9$–11. During our first spectroscopic follow-up run with ISAAC in summer 2003 we were able to secure *J*-band long-slit spectroscopy centred at this position under excellent seeing conditions. Interestingly, careful data reduction revealed at this location the presence of a single faint emission line detected at ~ 4–8 σ (depending on the integration aperture and stacking procedure), which if interpreted as Lyα would indicate $z = 10.0$! The report of these findings was published in Pelló et al. (2004a).

What is the status of this fairly unique candidate? Weatherley et al. (2004) have questioned the reality of the emission line. However, their negative result could be due to the combination of two factors: an error in our absolute wavelength calibration discovered later, and their spectroscopic data reduction technique, where the information is only preserved at the original (wrong) wavelength position and smeared elsewhere (see Pelló et al. 2004b). On the imaging side, deep *V*-band observations with FORS2 (Lehnert et al. 2005) have confirmed its optical non-detection. Our ISAAC *H*-band images have been reanalysed by several groups using different methods (Bremer et al. 2005, Smith et al. 2006) yielding measurements compatible with ours typically within 1 σ. Surprisingly however, this object remained undetected in a deeper NIRI/GEMINI *H*-band image taken approximately 15 months after our ISAAC image (Bremer et al. 2005). In spring 2004 we obtained two *SZ* (~ 1.06 μm) images with ISAAC, where this object is again detected (see Pelló et al. 2005). Taken together these spectroscopic and photometric detections, albeit individually of relatively low significance, indicate that this source is most likely not a spu-

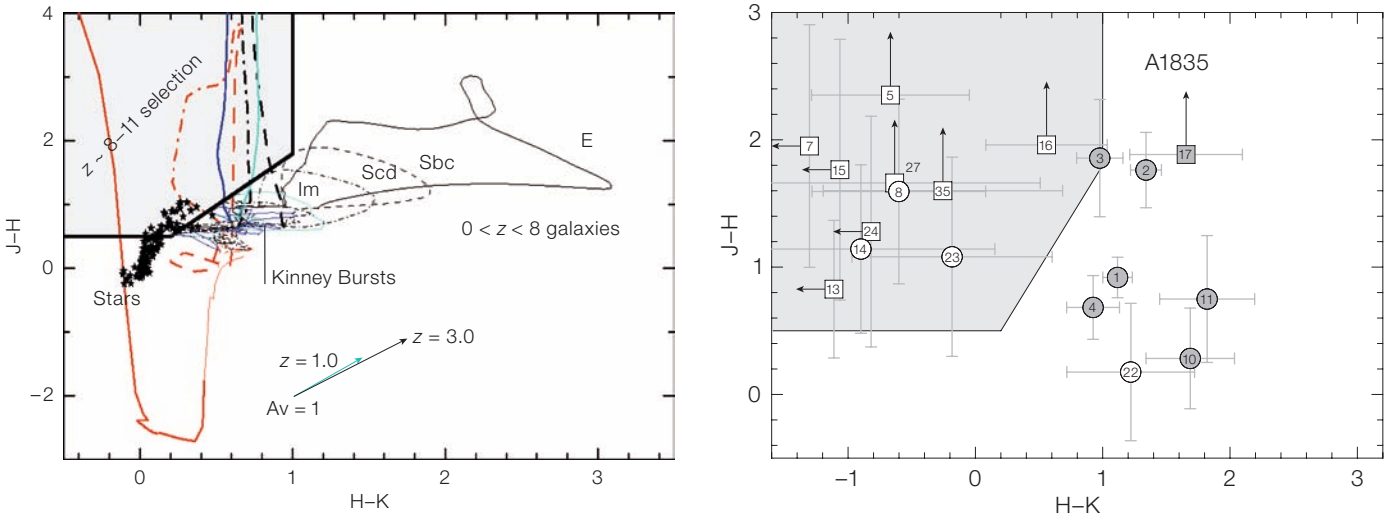

rious, but an intrinsically variable object, as discussed in Richard et al. (2006). Therefore, its nature and precise redshift remain puzzling, and we exclude this object from our list of high-*z* candidates, which we will discuss now.

Applying the above selection criteria to the observations of the two lensing clusters has yielded 13 candidates whose spectral energy distributions (SEDs) are compatible with those of star-forming galaxies at $z \gtrsim 6$ (see Richard et al. 2006). Images and the SEDs of some of them are shown in Figure 2 for illustration. The typical lensing magnification reaches from 1.5 to 10, with an average of ~ 6, i.e. nearly two magnitudes. Their star formation rate, as estimated from the UV restframe luminosity, is typically between 4 and 20 $M_{\odot}$ yr^{-1} after correcting for lensing.

We have used these data to attempt to constrain for the first time the density of star-forming galaxies present at $6 \lesssim z \lesssim 10$ using lensing clusters. After taking into account the detailed lensing geometry, sample incompleteness, and correcting for false-positive detections we have constructed a luminosity function (LF) of these candidates assuming a fixed slope taken from observations at $z \sim 3$. Within the errors the resulting LF is compatible with that of $z \sim 3$ Lyman break galaxies. At low luminosities it is also compatible with the LF derived by Bouwens and collaborators for their sample of $z \sim 6$ candidates in the Hubble Ultra Deep Field (UDF) and related fields. However, the turnover observed by these authors towards the bright end relative to the $z \sim 3$ LF is not observed in our sample. Finally, from the LF we determine the UV star formation rate (SFR) density at $z \sim 6$–10, shown in Figure 3. Our values indicate a similar SFR density as between $z \sim 3$ to 6, in contrast to the drop found from the deep NICMOS fields. Further observations are required to fully understand these differences. Taken at face value, this relatively high SFR density is in good agreement e.g. with the recent hydrodynamical mod-

Figure 1 (Above): Colour-colour diagrams (in the Vega system) showing **(Left:)** the location for different objects over the interval $z \sim 0$ to 11 and our selection region for galaxies in the $z \sim 8$–11 domain and **(Right:)** the location of the individual optical dropouts detected in Abell 1835. Circles and squares correspond to high-*z* candidates detected in three and two filters respectively. Optical dropouts fulfilling the ERO definition are shown in grey.

Figure 2 (Below): Close-up of four high-z candidates in Abell 1835, showing the objects and their surrounding 10 × 10 arcsec fields in optical (*z*) and near-IR bands (*SZ*, *J*, *H*, and *Ks*) as well as their SED. For comparison the image and SED of an intermediate redshift ERO is also shown at the bottom.

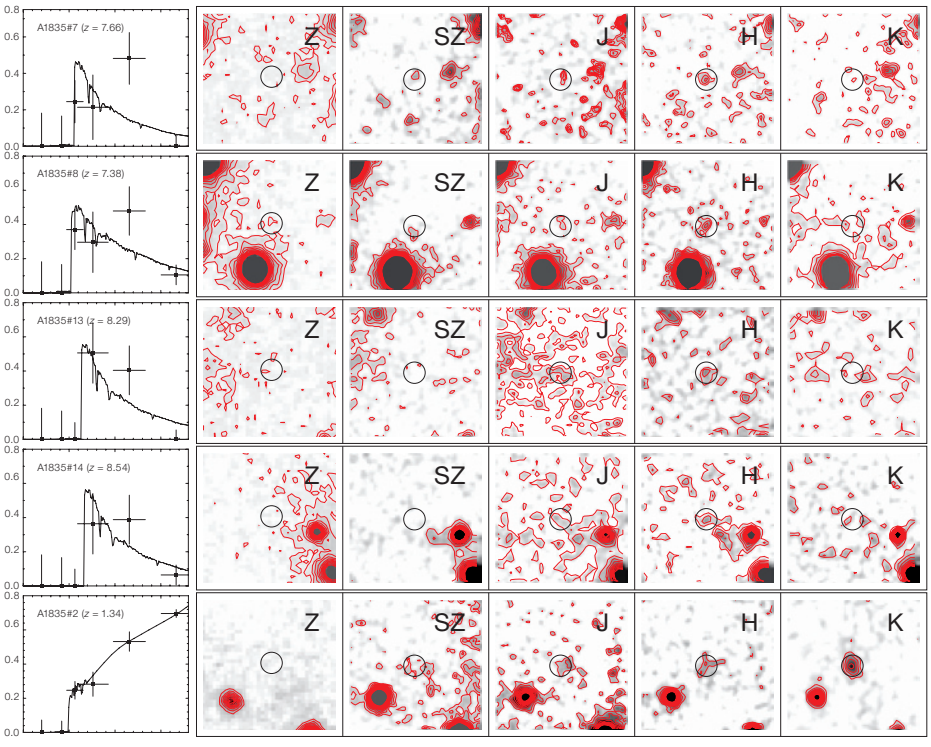

els of Nagamine et al. (2005), with the reionisation models of Choudhury and Ferrara (2005), and also with the SFR density inferred from the past star formation history of observed $z \sim 6$ galaxies (e.g. Eyles et al. 2006).

Follow-up observations

Compared to the data set just described several additional observations were secured on these clusters in the meantime. For example, deep z-band images of both clusters were obtained with the ACS camera onboard HST. These observations confirm that the vast majority (all except one of the above 13) of our high-z candidates are optical dropouts as expected, remaining undetected down to a 1σ limiting magnitude of 28–28.3 mag_{AB} (Hempel et al. 2006). In collaboration with Eiichi Egami we have also access to IRAC/Spitzer GTO images at 3.6, 4.5, 5.8 and 8.0 μm of large sample of lensing clusters including Abell 1835 and AC114. Again, none of our high-redshift galaxy candidates are detected. This is easily understood, since extrapolation of their intrinsically blue SED to IRAC wavelengths shows that their expected fluxes fall below the Spitzer sensitivity. It implies that these objects do not host 'old' stellar populations with strong Balmer breaks, and that they are not affected by significant extinction. A more detailed account of these observations will be presented elsewhere. For comparison a brighter lensed galaxy at $z \sim 7$ has been detected earlier by Spitzer (Egami et al. 2005).

In parallel several attempts were made to detect emission lines from selected candidates using near-IR long-slit spectroscopy with ISAAC on the VLT. See Pelló et al. (2005) for a preliminary report. Presently such observations are tedious, fairly time-consuming, and require excellent seeing conditions. Indeed, given the faintness of the expected lines, the strong IR background, and the need for the highest spectral resolution possible to minimise the impact of the numerous sky lines, a 'scan' of the entire J-band at R ~ 3000 for example requires five settings and a total of ~ 10 ksec to detect an unresolved line of (6–8) × 10^{-18} erg s^{-1} cm^{-2} flux at 5σ with ISAAC.

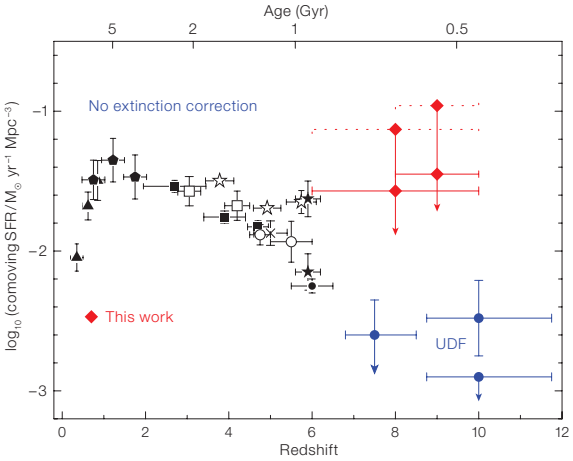

Figure 3: Evolution of the comoving Star-Formation Rate (SFR) density as a function of redshift including a compilation of results at $z \lesssim 6$, our estimates obtained from both clusters for the redshift ranges [6–10] and [8–10] and the values derived by Bouwens and collaborators from the Hubble Ultra-Deep Field (labelled 'UDF'; Bouwens et al. 2004, ApJ 616, L79 and 2005, ApJ 624, L5). Red solid lines: SFR density obtained from integrating the LF of our first category candidates down to $L_{1500} = 0.3\ L^*_{z=3}$; red dotted lines: same as red solid lines but including also second-category candidates with a detection threshold of $< 2.5\sigma$ in H.

One or more emission lines could be detected in few objects, as shown in Figure 4. For example, one of our secondary targets turned out to be a very faint $z = 1.68$ emission line galaxy. Other lines are clearly identified as the [OII] λ3727,3729 doublet from an intermediate redshift galaxy. Finally several objects show a single emission line, which – if identified as Lyα – yields a redshift compatible with the (high) estimated photometric redshift. However, in none of these cases a clear asymmetry of the line, as typical for Lyα from lower-z starbursts, was found. Searches for additional lines in these objects (e.g. CIV λ1550 or HeII λ1640 if at high z, or for [OIII] λ5007 or Hα if at low z) have so far been negative. Therefore the redshifts of these objects are currently difficult to establish, but high-z cannot be excluded on the present grounds. Forthcoming, more efficient near-IR spectrographs should allow a significant breakthrough in this field.

Spin-off projects on EROs and dusty intermediate-z galaxies

Our search for optical dropout galaxies behind lensing clusters yields also other interesting objects, such as extremely red objects (EROs; see Richard et al. 2006). In contrast to the high-z candidates most of them are detected by IRAC/Spitzer. These objects, most likely all at intermediate redshift ($z \sim 1$–3), turn out to have similar properties as e.g. faint IRAC selected EROs in the Hubble UDF, other related objects such as the putative post-starburst $z \sim 16.5$ galaxy of Mobasher et al. 2005, and some sub-mm galaxies (see Hempel et al. 2006). Spectroscopic observations with FORS2 and X-ray Chandra observations are also being secured to clarify the redshift and nature of these interesting optical dropout objects.

Future

With our pilot programme it has been possible to find several very high redshift candidate galaxies by combining the power of strong gravitational lensing with the large collecting area of the VLT. However, differences with other studies based on deep blank fields are found, and already differences between our two clusters indicate that these could at least partly be due to field-to-field variance. Given the relatively low S/N ratio of the high-z candidates and the large correction factors applied to this sample, it is of great interest to increase the number of lensing clusters observed with this technique.

Furthermore, rapidly upcoming new spectrographs such as the second-generation near-IR VLT instruments XShooter and KMOS, the EMIR spectrograph on the Spanish GRANTECAN telescope and others will provide a huge effciency gain for spectroscopic follow-up of faint candidate sources, thanks to their increased spectral coverage and multi-object capabilities. Observations at longer wavelengths, e.g. with HERSCHEL, APEX and later ALMA, are also planned to search for possible dust emission in such high-z galaxies and to characterise more completely other populations of faint optical dropout galaxies. Finally the JWST and

ELTs will obviously be powerful machines to study the first galaxies. Large territories remain unexplored in the early Universe!

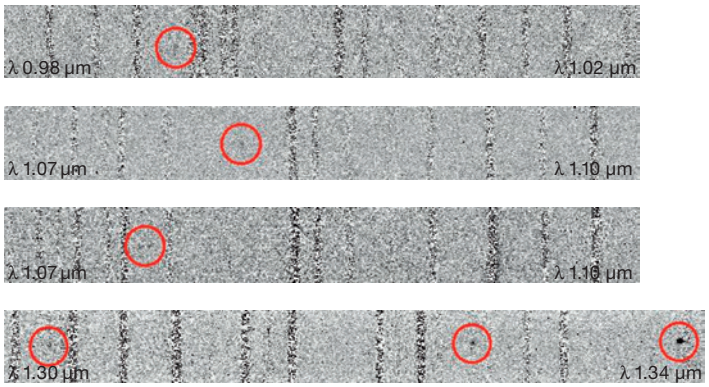

Figure 4: Sky-subtracted 2D ISAAC spectra showing examples of objects with emission line detections marked by red circles in the J band. From top to bottom: A $z = 7.17$ candidate in AC114, a $z = 7.89$ candidate in Abell 1835, an intermediate-z galaxy identified by its [OII] λ3727,3729 doublet, and the $z = 1.68$ emission line galaxy discovered by Richard et al. (2003, A&A 412, L57). The black vertical lines correspond to sky lines.

References

Bremer M. et al. 2004, ApJ 615, L1
Choudhury T. R. and Ferrara A. 2005, MNRAS 361, 577
Egami E. et al. 2005, ApJ 618, L5
Eyles L. et al. 2006, MNRAS, submitted, astro-ph/0607306
Hempel A. et al. 2006, A&A, submitted
Hu E. et al. 2002, ApJ 568, L75
Lehnert M. et al. 2005, ApJ 624, 80
Mobasher B. et al. 2005, ApJ 635, 832
Nagamine K. et al. 2005, New Astronomy Reviews 50, 29
Pelló R. et al. 2004a, A&A 416, L35
Pelló R. et al. 2004b, astro-ph/0407194
Pelló R. et al. 2005, IAU Symp. 225, 373
Richard J. et al. 2006, A&A, in press, astro-ph/0606134
Smith G. P. et al. 2006, ApJ 636, 575
Weatherley S. J. et al. 2004, A&A 428, L29

VLT Images of a Disintegrating Comet

On the night of 23 to 24 April, the VLT observed fragment B of the comet Schwassmann-Wachmann 3 that had split a few days earlier. The ESO astronomers were surprised to discover that the piece just ejected by fragment B was splitting again. Five other mini-comets were also visible. The comet thus seems doomed to disintegrate but the question remains in how long a time.

Comet 73P/Schwassmann-Wachmann 3 (SW 3) revolves around the Sun in about 5.4 years, in a very elongated orbit that brings it from inside of the Earth's orbit to the neighbourhood of Jupiter. In 1995, when it was coming 'close' to the Earth, it underwent a dramatic and completely unexpected thousandfold brightening. Observations in 1996, with ESO's NTT and 3.6-m showed that this was due to the fact that the comet had split into three distinct pieces. Later, in December 1996, two more fragments were discovered. At the last comeback (in 2001), of these five fragments only three were still seen, the fragments C (the largest one), B and E. No new fragmentation happened during this approach, apparently.

Things were different this time, when the comet again moved towards its closest approach to the Sun, and to the Earth. Early in March, seven fragments were observed, the brightest (fragment C) being magnitude 12, while fragment B was 10 times fainter still. In the course of 6 March new fragments were seen.

Early in April, fragment B went into outburst, brightening by a factor 10 and on 7 April, six new fragments were discovered, confirming the high degree of fragmentation of the comet. On 12 April, fragment B was as bright as the main fragment C, with a magnitude around 9. Fragment B seemed to have fragmented again, bringing the total of fragments close to 40, some being most probably very small, boulder-sized objects with irregular and short-lived activity.

The new observations reveal that this new small fragment has split again. The image clearly reveals that below the main B fragment, there is a small fragment that is divided in two and a careful analysis reveals five more tiny fragments almost aligned. Thus, this image alone shows at least seven fragments. The comet has thus produced a whole set of mini-comets. Will this process continue? Will the comet finally totally disintegrate? Further observations are planned.

The observations reported here were made with FORS1 on the VLT. The fragment was observed in four bands (*B*, *V*, *R*, and *I*) for a total of 30 minutes by Emmanuel Jehin, Olivier Hainaut, Michelle Doherty, and Christian Herrera, all from ESO. The astronomers had the telescope track the comet, which explains why the stars appear as trails of coloured dots, each colour corresponding to the order in which the observations were done in the various filters. At the time of the observations, the comet was 26.6 million km away from the Earth, in the constellation Corona Borealis. The final processing of the image was done by Hans Hermann Heyer and Olivia Blanchemain (both ESO).

(From ESO Press Photo 15/06)

Broken fragments of comet SW-3.

Transverse and Longitudinal Correlation Functions in the Intergalactic Medium

Franck Coppolani[1,2]
Patrick Petitjean[2,3]
Félix Stoehr[2]
Emmanuel Rollinde[4,2]
Christophe Pichon[2]
Stéphane Colombi[2]
Martin G. Haehnelt[5]
Bob Carswell[5]
Romain Teyssier[6]

[1] ESO
[2] Institut d'Astrophysique de Paris, France
[3] LERMA, Observatoire de Paris, France
[4] IUCAA, Pune, India
[5] Institute of Astronomy, Cambridge, United Kingdom
[6] DAPNIA, CEA Saclay, Gif-sur-Yvette, France

The Intergalactic Medium can be studied using the imprint left in the spectra of background quasars, the so-called Lyman-α forest. The correlations between absorption features observed along the lines of sight to the quasars have been studied to derive information on the clustering properties of the IGM structures. Very few observations have been performed so far of the correlation of the absorption along two different lines of sight separated by a few arcminutes in the sky. The comparison of the correlation functions along the line of sight (longitudinal direction on a velocity scale) and in the perpendicular direction (on an angular scale) can be used to constrain the geometry of the Universe. We have recently completed a study of the transverse and longitudinal flux correlation functions of the Lyman-α forest in quasar absorption spectra at $z \sim 2.1$ from VLT-FORS and VLT-UVES observations of a total of 32 pairs of quasars with separations in the range $0.6 < \theta < 10$ arcmin and found a correlation signal up to 3–5 arcmin.

The numerous HI absorption lines seen in the spectra of distant quasars, the so-called Lyman-α forest, contains precious information on the spatial distribution of neutral hydrogen in the Universe. Unravelling this information from individual spectra has for a long time proven difficult and ambiguous. Studies of the correlation of the Lyman-α forests observed in the two spectra of QSO pairs have been instrumental in measuring the spatial extent of absorbing structures. Significant correlation between absorption spectra of adjacent lines of sight toward quasars exists for separations of a few to ten arcmin suggesting a size or better a coherence length of the structures larger than 500 h_{70}^{-1} kpc (e.g. Smette et al. 1995; Crotts and Fang 1998; Aracil et al. 2002) and a non-spherical geometry of the absorbing structures (Rauch et al. 2005). On even larger scales, Williger et al. (2000) still find evidence for an excess of clustering on 10 Mpc scales.

The picture of the Lyman-α forest arising from density fluctuations in a warm photoionised Intergalactic Medium distributed as expected in a CDM model explains the statistical properties of individual QSO absorption spectra very well. Most of the baryons are located in filaments and sheets which are only overdense by factors of a few and produce absorption in the column density range $10^{14} < N_{\rm HI} < 10^{15}$ cm^{-2} at $z \sim 2$. On the other hand, most of the volume is occupied by underdense regions that produce absorption with $N_{\rm HI} < 10^{14}$ cm^{-2}. Analytical calculations and numerical simulations of the spatial distribution of neutral hydrogen in ΛCDM models are also able to reproduce the large observed transverse correlation length of the Lyman-α forest in the absorption spectra of QSO pairs (e.g. Rollinde et al. 2003).

As pointed out by several authors a comparison of the transverse correlation to the correlation observed along the line of sight, can be used to carry out a variant of the Alcock and Paczyński (1979) test to put constraints on the geometry of the Universe (e.g. Mc Donald 2003). This provides strong motivation for an accurate measurement of the transverse correlation function.

We have obtained spectra for a very large sample of QSO pairs: 26 pairs with separations in the range 0.6–4 arcmin (corresponding to $\simeq$ 0.2 to 1.4 h^{-1} Mpc proper at $z = 2.1$ for $\Omega_{\rm m} = 0.3$, $\Omega_\Lambda = 0.7$) and six pairs with separations in the range 5–10 arcmin. The results of the survey are published in Coppolani et al. (2006).

Observations

The first release of the 2dF quasar survey has significantly enlarged the number of known quasar pairs with arcmin separation (Outram, Hoyle and Shanks 2001). We have selected pairs with the following criteria: (1) the separation of the two quasars should be in the range 1–4 arcmin where the correlation is expected to be strong; (2) the quasars should be brighter than $m_{\rm V} = 20.30$ to keep observing time in reasonable limits; (3) the emission redshifts of the two quasars should be larger than $z \sim 2.1$ to increase the wavelength range over which high S/N ratio can be obtained (FORS is not sufficiently sensitive below 3 500 Å); (4) the redshift difference should be smaller than $\Delta z \sim 0.5$ (for most of them 0.3) to maximise the wavelength range over which correlations can be studied.

There are 22 quasar pairs in the 2dF survey which meet our criteria of which we observed 20. Twelve previously known pairs have been added to this sample. The spectra of the quasars were obtained with FORS1 and 2 mounted on VLT UT2 and UT3 using grism GR630B and a 0.7 arcsec slit. The final spectral resolution was $R = 1400$ or FWHM = 220 km s^{-1} at 3 800 Å. The exposure times have been adjusted in order to obtain a typical signal-to-noise ratio of ~ 10 at 3 500 Å. At $\lambda \sim 4\,500$ Å the S/N ratio is usually larger than 70. Typical observed spectra of QSO pairs are shown in Figure 1.

To calculate the longitudinal correlation function we also used the data from the Large Programme "The Cosmic Evolution of the IGM" which has produced a sample of absorption spectra of homogeneous quality suitable for studying the Lyman-α forest in the redshift range 1.7–4.5. The spectra of the LP were taken with VLT-UVES and have high resolution (R ~ 45 000) and high signal-to-noise ratio. (30 and 60 per pixel at respectively 3 500 and 6 000 Å.)

Numerical simulations

We used two numerical simulations to estimate the errors and the effect of redshift distortion and of the thermal state of the gas on the correlation functions: a

large-size dark-matter only simulation and a smaller-size full hydrodynamical simulation. For both simulations we assume parameters consistent with the fiducial concordance cosmological model $\Omega_\Lambda = 0.7$, $\Omega_m = 0.3$. The hydrodynamical simulation of 40 Mpc box-size and dark-matter only simulation of 100 h^{-1} Mpc box-size are used to catch both the statistical aspects and the effect of gas physics. The large box-size of the dark-matter only simulation ensures a sufficient statistical sampling on large scales where thermal effects and pressure effects, which are modelled approximately in this simulation, are less important. The hydrodynamical simulation is better suited for investigating the effects of thermal broadening and redshift distortions which are more relevant on small scales. The 40 Mpc box-size of the hydrodynamical simulation offers the best compromise between box-size and resolution.

The observed correlation functions

We define the flux correlation function, $\xi_f(\theta,\Delta v)$, as in Rollinde et al. (2003). In the following we will use $H_0 = 70$ km/s/Mpc, $\Omega_m = 0.3$, $\Omega_\Lambda = 0.7$ to relate scales in redshift space with angular scales. With these parameters $\Delta v = 100$ km s^{-1} corresponds to ~ 1 arcmin at $z = 2$. The observed correlation functions depend strongly on the spectral resolution of the absorption spectra unless the width of all spectral features is fully resolved.

In Figure 2 we show the observed transverse correlation function derived using the 32 pairs of our sample. Each point on this figure corresponds to one pair. The measurement for each quasar pair, $\xi(\theta_i) \equiv \xi_f(\theta_i; \Delta v = 0)$, is shown as a small solid triangle at the angular separation of the pair, θ_i. The transverse correlation is clearly detected on scales < 4 arcmin. If we merge the two bins between 3 and 4 arcmin, the correlation is detected at about the 3σ level.

We have calculated the longitudinal correlation function (the correlation measured along the line of sight to the quasar) from the 58 FORS spectra in the sample at a mean redshift z ~ 2.1. We also have estimated the longitudinal correlation function measured from the high-resolution spectra obtained in the course of the UVES-VLT Large Programme. The two correlation functions agree very well after the high-resolution VLT-UVES spectra is convolved with a Gaussian filter of FWHM = 220 km s^{-1} to take into account the difference in resolution between the UVES and FORS spectra.

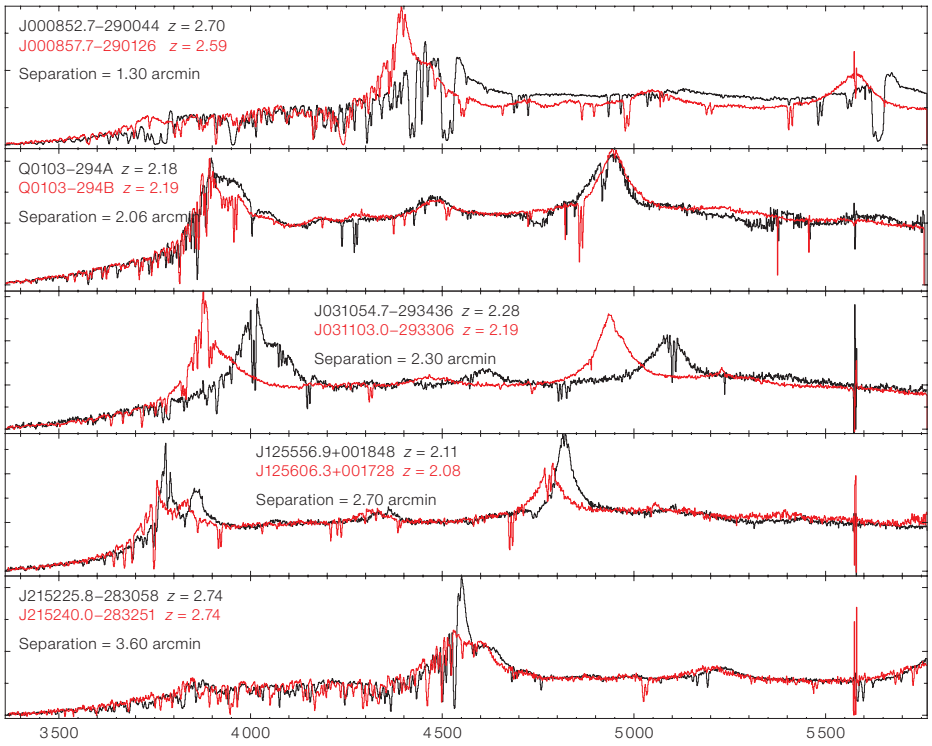

Figure 1 (Above): Typical observed spectra of QSO pairs in order of increasing right ascension. QSO names, emission redshifts and angular separations are given in the top-left corner of each sub-panel.

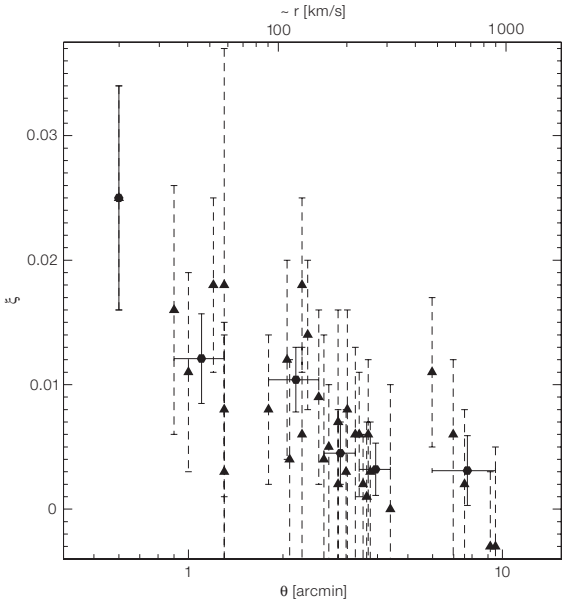

Figure 2 (Left): The observed transverse correlation coefficient for individual pairs (black triangles, dashed error bars) and a binned estimate of the transverse correlation function (solid error bars). Note that the first bin at the smallest separation contains only one measurement.

Comparison of observed and simulated correlation functions

The ability of ΛCDM models to reproduce the longitudinal correlation function of the Lyman-α forest has been demonstrated by many authors (e.g. Rollinde et al. 2003) and the same is true for our simulations. The curves from the hydro-

dynamical simulation in Figure 3 for $z = 2$ and $z = 3$ nicely bracket the observed correlation function obtained from the high-resolution data with a median redshift of $z = 2.39$.

The transverse correlation contains precious direct information on the physical size/coherence-length of the absorbing structures as it is less affected by redshift space distortions than the longitudinal correlation function. Furthermore, a comparison of the longitudinal and transverse correlation functions can – at least in principle – strongly constrain cosmological parameters in particular Ω_Λ.

The thick solid curve in Figure 4 shows our estimate of the transverse correlation function from the full hydrodynamical simulation at $z = 2$. It agrees well with our measurement of the observed transverse correlation function (mean redshift ~ 2.1).

Despite the larger sample (about three times more pairs at $\theta < 3$ arcmin than in Rollinde et al. 2003) and the correspondingly smaller errors, we cannot yet distinguish between different values of Ω_m. However, the result shown here is very encouraging as it shows that clustering signal is present up to about 4 arcmin, consistent with the predictions of ΛCDM models.

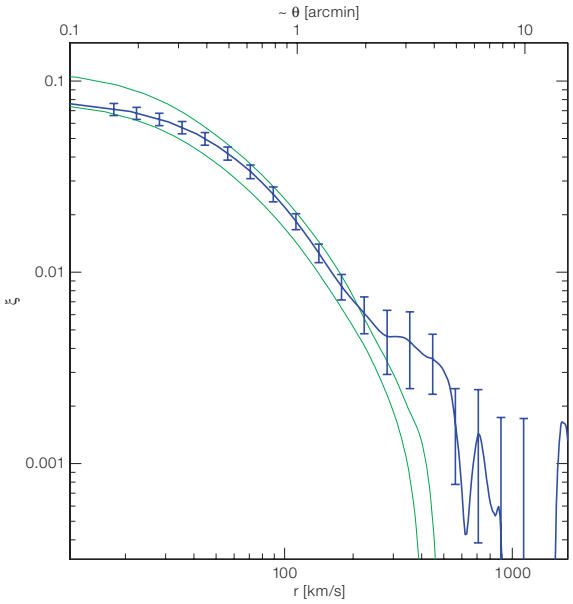

Figure 3: The observed longitudinal correlation function from the high-resolution UVES spectra (thick solid curve) compared to the longitudinal correlation function as measured in the full hydrodynamical simulation at $z = 2$ (lower thin curve) and $z = 3$ (upper thin curve), respectively.

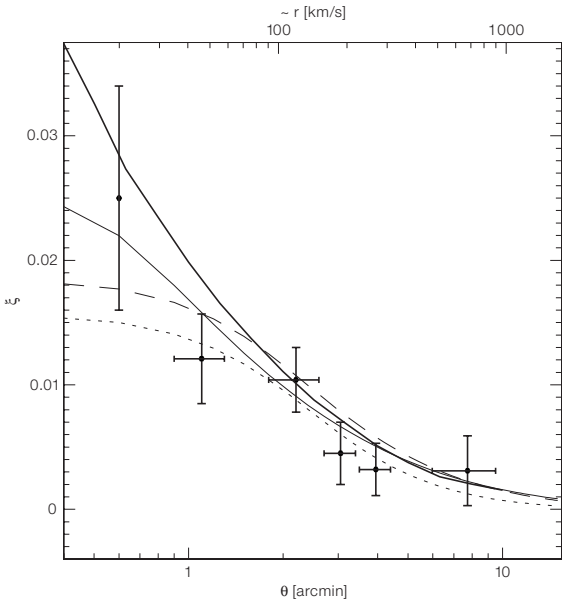

Figure 4: The binned estimate of the observed transverse correlation function (solid error bars) is shown together with the estimate of the transverse correlation function from the full hydro-simulation (thick solid curve) and linear predictions for $\Omega_m = 0.1$, 0.3 and 1 (thin solid, dashed and dotted lines respectively, assuming a flat Universe: $\Omega_\Lambda + \Omega_m = 1$). The linear theory predictions are normalised to reproduce the longitudinal correlation function at large scales.

Metal absorption systems

Our sample of quasar pairs is also well suited to study the spatial distribution of the gas responsible for the associated metal absorption in QSO spectra. We have selected after identification a sample of 139 C IV systems distributed over a redshift path $\delta z = 38$, corresponding to a density of 3.7 systems per unit redshift. We apply the Nearest-Neighbour method, as described in Aracil et al. (2002) to the corresponding list of C IV systems.

We do not find any statistically significant signal of correlation in the transverse direction. This is consistent with the models by Scannapieco et al. (2006) who have shown that, at $z \sim 3$, the longitudinal C IV correlation function is consistent with a model where C IV is confined within bubbles of typical radius ~ 2 Mpc comoving surrounding halos of mass ~ 10^{12} $M_\odot$. At this redshift, this corresponds to a separation of about 2 arcmin, smaller than the median separation in our sample.

However, there is a possible small excess of clustering of C IV systems on scales smaller than 5 000 km s^{-1}. This scale is larger than the typical correlation length, of about 1000 km s^{-1}, seen in the longitudinal correlation function of C IV systems (e.g. Scannapieco et al. 2006). This is due to an excess of associations in the velocity bin $\Delta v \sim 4\,000$ km s^{-1}. However, the corresponding C IV associations are located in the peculiar field containing the quartet Q 0103-294A&B, Q 0102-2931 and Q 0102-293 (all four quasars are separated by less than 10 arcmin). Along these lines of sight the density of C IV systems is 6.4 per unit redshift and the number of coincidences within 4 000 km s^{-1} is about twice larger than the mean density of coincidences in the overall sample. In addition, there is no C IV system between $z = 1.955$ and 2.051, a redshift range over which the H I absorption in front of the quartet is much reduced (Rollinde et al. 2003). Note also that the correlation between the Lyman-α forests of Q 0102-2931 and Q 0103-294B,

two quasars of the group with ~ 6 arcmin separation, is measured to be quite high (ξ = 0.011).

A similar overdensity of C IV systems has been observed in the field of Tol 1037–2704 (e.g. Jakobsen et al. 1986) and has been interpreted as being due to the presence of a supercluster. The dimensions of this supercluster would be at least 80 and 30 h^{-1} Mpc along and perpendicular to the line of sight, respectively. To our knowledge no deep imaging of these fields exist and it would be very interesting to search for possible concentrations of galaxies.

Future prospects

We have detected the transverse correlation of the intergalactic medium at the 3σ level up to separations of about 3–5 arcmin. The shape and correlation length of the transverse correlation function of the absorbing gas is in good agreement with expectations for absorption by density fluctuations in the warm photoionised Intergalactic Medium as described in CDM-like structure formation models. Our measurement is thus an important further independent confirmation that the Lyman-α forest is indeed caused by the filamentary and sheet-like structures of the cosmic web predicted by these models. In agreement with predictions of previous theoretical studies we find that our sample is still too small to obtain significant constraints on cosmological parameters. The improved errors of our larger sample compared to the sub-sample of Rollinde et al. (2003) suggest however that meaningful constraints on Ω_Λ can be obtained. For this, a larger sample and a careful analysis of the systematic uncertainties with a large suite of full hydrodynamical simulations are necessary. Mc Donald (2003) estimated that this requires a sample of 13$(\theta/1')^2$ pairs on scales up to 10 arcmin.

In addition, our results open the prospect to reconstruct the 3D density field directly (see Pichon et al. 2001). For this a network of lines of sight in the same field should be observed. Intermediate and/or low spectral resolution is sufficient but the distance between lines of sight is crucial and should be smaller than about 5 arcminutes.

Acknowledgements

Franck Coppolani thanks IUCAA-Pune (India) for hospitality during the time part of this work has been completed, ESO-Vitacura for a Ph.D. studentship and Cédric Ledoux for his supervision during the time spent in Chile.

References

Alcock C. and Paczyński B. 1979, Nature 281, 358
Aracil B. et al. 2002, A&A 391, 1
Coppolani F. et al. 2006, MNRAS 370, 1804
Crotts A. P. J. and Fang Y. 1998, ApJ 502, 16
Mc Donald P. 2003, ApJ 585, 34
Outram P. J., Hoyle F. and Shanks T. 2001, MNRAS 321, 497
Petitjean P., Mücket J. P. and Kates R. E. 1995, A&A 295, L9
Pichon C. et al. 2001, MNRAS 326, 597
Rauch M. et al. 2005, ApJ 632, 58
Rollinde E. et al. 2003, MNRAS 341, 1299
Scannapieco E. et al. 2006, MNRAS 365, 615S
Smette A. et al. 1995, A&AS 113, 199
Williger G. M. et al. 2000, ApJ 532, 77

Extrasolar Planets and Brown Dwarfs: A Flurry of Results

Three ESO press releases on extrasolar planets and brown dwarfs in the last few months testify to the pace of activity in this field at the moment. They are summarised briefly here, and are available in complete form on the ESO website (PR 19/06, 28/06, 29/06).

Planetary-Mass objects surrounded by discs

Two new studies show that objects only a few times more massive than Jupiter are born with discs of dust and gas, the raw material for planet making. This suggests that miniature versions of the solar system may circle objects that are some hundred times less massive than our Sun.

For a few years it has been known that many young brown dwarfs, 'failed stars' that weigh less than eight per cent the mass of the Sun, are surrounded by a disc of material. This may indicate that these objects form the same way as did our Sun. The new findings confirm that the same appears to be true for their even smaller cousins, sometimes called planetary-mass objects or 'planemos'. These objects have masses similar to those of extrasolar planets, but they are not in orbit around stars – instead, they float freely through space.

"Now that we know of these planetary-mass objects with their own little infant planetary systems, the definition of the word 'planet' has blurred even more", adds Ray Jayawardhana (University of Toronto, Canada), lead author of the study. "In a way, the new discoveries are not too surprising – after all, Jupiter must have been born with its own disc, out of which its bigger moons formed."

Unlike Jupiter, however, these planetary-mass objects are not circling stars.
In their study, Jayawardhana and Ivanov (ESO) used the VLT and NTT to obtain optical spectra of six candidates identified recently by researchers at the University of Texas at Austin. Four of the six turned out to have masses between five to 15 times that of Jupiter. All four of these objects are 'newborns', just a few million years old, and are located in star-forming regions about 450 light years from Earth. They show infrared emission from dusty discs that may evolve into miniature planetary systems over time.

In another study, Subhanjoy Mohanty (Harvard-Smithsonian Center for Astrophysics, CfA), Ray Jayawardhana (University of Toronto), Nuria Huelamo (ESO) and Eric Mamajek (also at CfA) used the VLT and NACO to obtain images and spectra of a planetary-mass companion

discovered at ESO two years ago around a young brown dwarf that is itself about 25 times the mass of Jupiter. This planetary-mass companion is the first-ever exoplanet to have been imaged. The brown dwarf, dubbed 2M1207 for short and located 170 light years from Earth, was known to be surrounded by a disc. Now, this team has found evidence for a disc around the eight-Jupiter-mass companion as well.

A brown dwarf – white dwarf pair

A rather unusual system has been found, in which two planet-size stars, of different colours, orbit each other. One is a rather hot white dwarf, weighing a little bit less than half as much as the Sun. The other is a much cooler, 55 Jupiter-mass brown dwarf.

"Such a system must have had a very troubled history", said Pierre Maxted, lead author of the paper that reports the study in the 3 August issue of Nature. "Its existence proves that the brown dwarf came out almost unaltered from an episode in which it was swallowed by a red giant." The two objects, separated by less than 2/3 of the radius of the Sun or only a few thousandths of the distance between the Earth and the Sun, rotate around each other in about 2 hours.

The two stars were not so close in their past. Only when the solar-like star that has now become a white dwarf was a red giant, did the separation between the two objects diminish drastically. During this fleeting moment, the giant engulfed its companion. The latter spiralled in towards the core of the giant. The envelope of the giant was finally ejected, leaving a binary system in which the companion is in a close orbit around a white dwarf. The separation between the two stars will slowly decrease.

The low-mass companion to the white dwarf (named WD0137-349) was found using spectra taken with EMMI on the NTT. The astronomers then used the UVES spectrograph on the VLT to take 20 spectra and so measure the period and the mass ratio.

The team members are Pierre Maxted (Keele University, UK), Ralf Napiwotzki (University of Hertfordshire, UK), Paul Dobbie and Matt Burleigh (University of Leicester, UK).

A pair of planetary-mass objects

The cast of exoplanets has an extraordinary new member. Astronomers have discovered an approximately seven-Jupiter-mass companion to an object that is itself only twice as massive. Both objects have masses similar to those of extrasolar giant planets, but they are not in orbit around a star – instead they appear to circle each other. The existence of such a double system puts strong constraints on formation theories of free-floating planetary-mass objects.

Ray Jayawardhana (University of Toronto, Canada) and Valentin D. Ivanov (ESO) reported the discovery in the 3 August issue of Science Express. "This is a truly remarkable pair of twins – each having only about one per cent the mass of our Sun", said Jayawardhana. "Its mere existence is a surprise, and its origin and fate a bit of a mystery."

Roughly half of all Sun-like stars come in pairs. So do about a sixth of brown dwarfs, 'failed stars' that have less than 75 Jupiter masses and are unable to sustain nuclear fusion in their cores. During the past five years, astronomers have identified a few dozen even smaller free-floating planetary-mass objects in nearby star-forming regions. Oph 162225-240515, or Oph1622 for short, is the first one found to be a double.

The researchers discovered the companion candidate in an optical image taken with the NTT. They took optical spectra and infrared images of the pair with the VLT to make sure that it is a true companion, instead of a foreground or background star that happens to be in the same line of sight. These follow-up observations indeed confirmed that both objects are young, at the same distance, and much too cool to be stars. This suggests the two are physically associated.

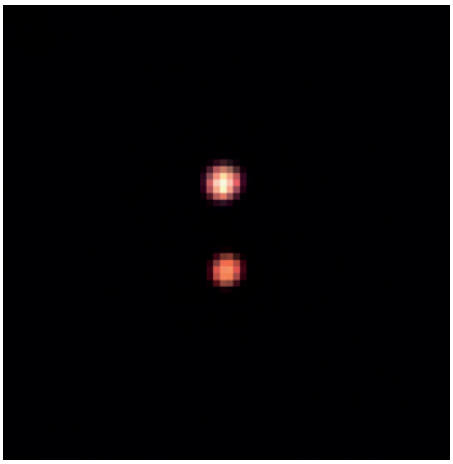

The System Oph1622 (ISAAC/VLT).

The companion is estimated to be about seven times the mass of Jupiter, while the more massive object is about 14 Jupiter masses. The newborn pair, barely a million years old, is separated by about six times the distance between the Sun and Pluto, and is located in the Ophiuchus star-forming region approximately 400 light years away.

Planets are thought to form out of discs of gas and dust that surround stars, brown dwarfs, and even some free-floating planetary-mass objects. But, "it is likely that these twins formed together out of a contracting gas cloud that fragmented, like a miniature stellar binary", said Jayawardhana. "We are resisting the temptation to call it a 'double planet' because this pair probably didn't form the way that planets in our Solar System did", added Ivanov.

Oph1622B is only the second or third directly imaged planetary-mass companion to be confirmed spectroscopically, and the first one around a primary that is itself a planetary-mass object. Its existence poses a challenge to a popular theoretical scenario, which suggests that brown dwarfs and free-floating planetary-mass objects are embryos ejected from multiple protostar systems. Since the two objects in Oph1622 are so far apart, and only weakly bound to each other by gravity, they would not have survived such a chaotic birth.

SPHERE: a 'Planet Finder' Instrument for the VLT

Jean-Luc Beuzit[1]
Markus Feldt[2]
Kjetil Dohlen[3]
David Mouillet[1]
Pascal Puget[1]
Jacopo Antici[5]
Andrea Baruffolo[5]
Pierre Baudoz[4]
Alessandro Berton[2]
Anthony Boccaletti[4]
Marcel Carbillet[6]
Julien Charton[1]
Riccardo Claudi[5]
Mark Downing[7]
Philippe Feautrier[1]
Enrico Fedrigo[7]
Thierry Fusco[8]
Raffaele Gratton[5]
Norbert Hubin[7]
Markus Kasper[7]
Maud Langlois[3]
Claire Moutou[3]
Laurent Mugnier[8]
Johan Pragt[9]
Patrick Rabou[1]
Michel Saisse[3]
Hans Martin Schmid[10]
Eric Stadler[1]
Massimo Turrato[5]
Stéphane Udry[11]
Rens Waters[12]
François Wildi[11]

[1] Laboratoire d'Astrophysique de Grenoble, France
[2] Max-Planck-Institut für Astronomie, Heidelberg, Germany
[3] Laboratoire d'Astrophysique de Marseille, France
[4] Laboratoire d'Etudes Spatiales et d'Instrumentation en Astrophysique, Paris, France
[5] INAF – Osservatorio Astronomico di Padova, Italy
[6] Laboratoire Universitaire d'Astrophysique de Nice, France
[7] ESO
[8] Office National d'Etudes et de Recherches Aérospatiales, Chatillon, France
[9] Stichting ASTRonomisch Onderzoek in Nederland, the Netherlands
[10] Eidgenössische Technische Hochschule Zürich, Switzerland
[11] Observatoire de Genève, Switzerland
[12] Universiteit van Amsterdam, the Netherlands

Direct detection and spectral characterisation of extrasolar planets is one of the most exciting but also one of the most challenging areas in modern astronomy. For its second-generation instrumentation on the VLT, ESO has supported two phase A studies for a so-called 'Planet Finder' dedicated instrument. Based on the results of these two studies, a unique instrument, SPHERE, is now considered for first light in 2010, including a powerful extreme adaptive optics system (SAXO), various coronagraphs, an infrared differential imaging camera (IRDIS), an infrared integral field spectrograph (IFS) and a visible differential polarimeter (ZIMPOL).

The prime objective of the Spectro-Polarimetric High-contrast Exoplanet REsearch (SPHERE) instrument for the VLT is the discovery and study of new extrasolar giant planets orbiting nearby stars by direct imaging of their circumstellar environment. The challenge consists in the very large contrast between the host star and the planet, larger than 12.5 magnitudes (or 10^5 in flux ratio), at very small angular separations, typically inside the seeing halo. The whole design of such an instrument is therefore optimised towards reaching the highest contrast in a limited field of view and at short distances from the central star (Mouillet et al., 2001). Both evolved and young planetary systems will be detected, respectively through their reflected light (mostly by visible differential polarimetry) and through the intrinsic planet emission (using IR differential imaging and integral field spectroscopy). Both components of the near-infrared arm of SPHERE will provide complementary detection capabilities and characterisation potential, in terms of field of view, contrast, and spectral domain.

SPHERE will greatly contribute to the field of extrasolar planet studies, already very active, particularly by offering direct detections of planets more massive than Jupiter at various stages of their evolution, in the key separation regime 1 to 100 AU. Migration mechanisms will then be better understood. The complementarities of direct imaging with other detection methods such as radial velocities and photometric transits, in terms of targets, detection biases and measured planetary parameters, and more specifically the combination with results from other projects like HARPS, COROT, VLTI/PRIMA, JWST and Kepler, will offer promising avenues. The present indications that massive distant planets could be numerous will be firmly confirmed or denied by SPHERE, if the number of observed targets with relevant detection limits is statistically acceptable, i.e. of the order of 300 to 400.

This would in particular fully justify a large effort in an extended observational survey of several hundred nights concentrating on the following classes of targets:
– *Nearby young associations* will offer the best chance of detecting low-mass planets, since they will have brighter substellar companions, and therefore the greatest number of planets per star observed.
– *Stars with known planets*, especially any that exhibit long-term residuals in their radial-velocity curves, indicating the possible presence of a more distant planet.
– *Nearest stars:* measuring these targets will probe the smallest orbits and will thus provide the only opportunities for detecting planets by directly reflected light.
– *Stars aged from 100 Myr to 1 Gyr:* The planets will still be over-luminous as compared to Solar System planets, so the mass limit will be lower than for old systems.

With such a prime objective, it is obvious that many other research fields will benefit from the large contrast performance of SPHERE: protoplanetary discs, brown dwarfs, evolved massive stars and marginally, Solar System and extragalactic science. These domains will nicely enrich the scientific impact of the instrument. Their instrumental needs should however not be in conflict with the high-contrast requirements.

Science requirements and observing modes

The key scientific requirements deriving from the science analysis and driving

the design of the instrument are summarised below:

– High contrast to reach giant planets 14 to 16 magnitudes fainter than their host star.
– Access to very small angular separations, 0.1″ to 3″ from the host star.
– Sensitivity and optimal performance for targets up to visible magnitude ~ 10, for building a potential target list in which the sample volume is consistent with the objectives (more than 400 targets in total, with 100 high-priority targets).
– Sensitivity to faint companions down to magnitude H ~ 24.
– Access to an extended spectral domain at low resolution, for the characterisation of the detected objects, at a resolving power ~ 30.
– Sensitivity to extended sources down to ~ 17 magnitudes per square arcseconds at less than 0.2″ from the host star.

Three main observing modes have been defined in order to draw the maximum benefit of the unique instrumental capabilities of SPHERE.

The *NIR survey mode* is the main observing mode which will be used for ~ 80 % of the observing time. It combines IRDIS dual imaging in *H* band with imaging spectroscopy using the IFS in the *Y*+*J*-bands by the aid of dichroic beam separation after the coronagraph. This configuration permits to benefit simultaneously from the optimal capabilities of both dual imaging over a large field (out to ~ 5″ radius) and spectral imaging in the inner region (out to at least 0.7″). In particular, it allows to reduce the number of false alarms and to confirm potential detections obtained in one channel by data from the other channel. This will be a definitive advantage in case of detections very close to the limits of the system.

The *NIR characterisation mode*, in which IRDIS is used alone in its various modes, will allow obtaining observations with a wider FOV in all bands from Y to short-K, either in dual imaging or in broad and narrow-band filters. This will be especially interesting in order to obtain complementary information on already detected and relatively bright targets (follow-up and/or characterisation). Spectroscopic characterisation at low or medium resolution will be possible in long-slit mode.

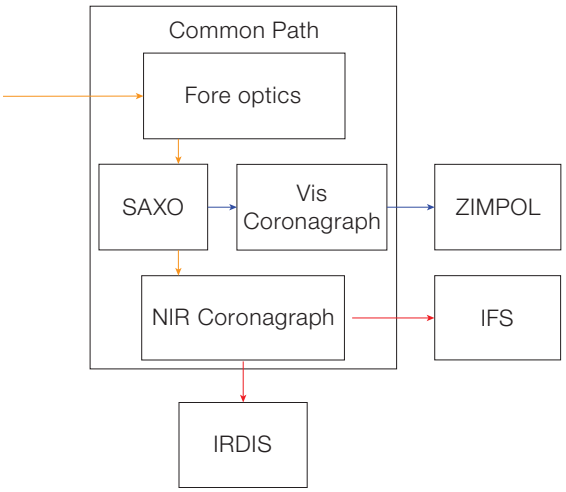

Figure 1: Global concept of the SPHERE instrument, indicating its four sub-systems: Common Path Optics, IRDIS, IFS, and ZIMPOL. It also includes the main functionalities within the Common Path sub-system. Optical beams are indicated in red for NIR, blue for visible and orange for Common Path.

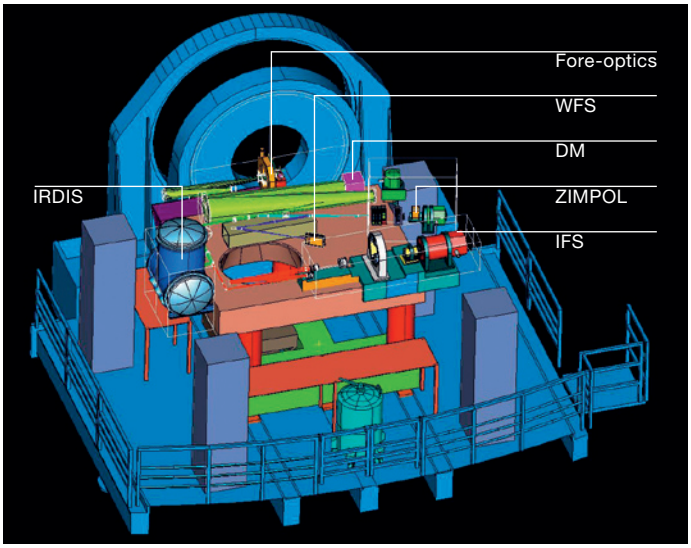

Figure 2: Implementation of SPHERE on the Nasmyth platform.

Additional science cases will also benefit from these observing modes (discs, brown dwarfs, etc.). This will be a very useful capability for the ESO community at a time when NACO will most likely no longer be offered.

The *visible search and characterisation mode*, will benefit from ZIMPOL polarimetric capacities to provide unique performance in reflected light very close to the star, down to the level required for the first direct detection in the visible of old close-in planets, even if on a relatively small number of targets. ZIMPOL also provides classical imaging in the visible, offering unique high-Strehl performance in an era when the Hubble Space Telescope (HST) will probably have been decommissioned.

Instrument concept

To fulfil these requirements, the proposed SPHERE instrument is divided into four sub-systems as illustrated by Figure 1.

Common Path Optics

The Common Path Optics, transmitting the telescope beam via the various correcting elements of the adaptive optics system (pupil tip-tilt and pupil de-rotator, deformable mirror, image tip-tilt mirror, atmospheric dispersion compensator ...) and via the coronagraphic unit (apodizer, coronagraphic mask, Lyot stop) to the adaptive optics wavefront sensor and to the science channels. The proposed implementation of SPHERE on the VLT Nasmyth platform is presented in Figure 2.

Extreme adaptive optics

The design of the SPHERE Adaptive optics for eXoplanet Observation (SAXO), resulting from a global trade-off combining optical design, technological aspects, cost and risk issues, leads to the use of a 41 × 41 actuator DM of 180 mm diameter with inter-actuator stroke > ±1 μm and maximum stroke > ± 3.5 μm, and a two-axis tip-tilt mirror (TTM) with ± 0.5 mas resolution (Fusco et al. 2006). The wavefront sensor is a 40 × 40 lenslet Shack-Hartmann sensor, with a spectral range between 0.45 and 0.95 μm equipped with a focal plane filtering device of variable size (from λ/d to $3\lambda/d$ at 0.7 μm, where d is the projected microlens diameter) for aliasing control. A temporal sampling frequency of 1.2 kHz is achieved using a 240 × 240 pixel electron multiplying CCD detector (CCD220 from EEV) with a read-out noise < 1 electron and a 1.4 excess photon noise factor. The global AO loop delay is maintained below 1 ms.

Image and pupil stability are essential in high-contrast instruments. Differential image movements due to thermo-mechanical effects and ADC mechanism precision are therefore measured in real time using an auxiliary NIR tip-tilt sensor located close to the coronagraphic focus and corrected via a differential tip-tilt mirror in the WFS arm. Likewise, pupil runout is measured by analysis of the WFS sub-pupil intensity along the pupil edge and corrected by a pupil tip-tilt mirror close to the telescope focal plane at the entrance of the instrument. Non-common path aberrations are measured offline using a phase diversity algorithm and compensated on-line by reference slope adjustments.

Coronagraphs

Efficient coronagraphy is important for reaching the science goals of SPHERE. Its action is twofold: reduce the intensity of the stellar peak by a factor of at least 100 and eliminate the diffraction features due to the pupil edges. Stellar coronagraphy is a quickly evolving research field and it is important to leave the instrument open for future evolution by allowing exchangeable masks both in the coronagraphic focus and in its entrance and exit pupil planes.

The baseline coronagraph suite will include an achromatic four-quadrant phase mask coronagraph (A4Q) based on precision mounting of four half-wave plates (HWP), and both a classical Lyot coronagraph (CLC) and an apodised Lyot coronagraph (ALC). The A4Q has recently been demonstrated in the visible, where the main difficulties of precision edge-polishing and mounting of the HWPs have been addressed and excellent performance has been demonstrated (Mawet et al., 2006). Extension of these techniques to the NIR is ongoing. While the CLC option, with mask diameter of about 10 λ/D, is within the realm of classical manufacturing, the ALC option requires an apodiser in the coronagraph entrance pupil. Prototyping is ongoing, and a promising technology using graded metal deposition has been identified. An alternative technology based on ion implantation is also considered, but this technology gives discrete steps in the apodization profile. The effects of this are being quantified by simulations.

Infra-Red Dual-beam Imaging and Spectroscopy

The Infra-Red Dual-beam Imaging and Spectroscopy (IRDIS) sub-system constitutes the main science module of SPHERE. The main specifications for IRDIS include a spectral range from 950 to 2320 nm and an image scale of 12.25 mas per pixel consistent with Nyquist sampling at 950 nm. A FOV greater than 11″ square is required for both direct and dual imaging, leaving a slight margin for system optimisation when using two 'quadrants' of a 2k × 2k detector. The main mode of IRDIS is the dual imaging, providing images in two neighbouring spectral channels with minimised (< 10 nm rms) differential aberrations. Ten different filter couples are defined corresponding to different spectral features in modelled exoplanet spectra. In the direct imaging mode, 12 broad, medium and narrow-band filters are defined. In addition to direct and dual imaging, long-slit spectroscopy at resolving powers of 50 and 500 is provided, as well as a dual polarimetric imaging mode. A pupil-imaging mode for system diagnosis is also implemented.

Dual imaging separation is done using a beam-splitter combined with a mirror, producing two beams in parallel. Each beam has its own camera doublet and band-limiting filter. The main challenge is to achieve the required 10 nm differential aberrations requirement, but an error budget based on high-quality classical polishing technology is found to satisfy the requirement. This option has been favoured over the alternative Wollaston-based option used for example in the NACO SDI camera (Lenzen et al., 2004) because it eliminates spectral blurring problems, which would limit the useful FOV, and allows the use of high-quality materials with high homogeneity.

The proposed opto-mechanical design of IRDIS is shown in Figure 3.

Integral Field Spectroscopy

While an integral field spectrograph (IFS) for planet imaging is conceptually challenging, it is widely recognised as a potentially extremely useful science module for a planet-searching instrument. The reasons for this are twofold: Firstly the IFS can be built with virtually zero differential aberrations, and secondly the multiple spectral channels allow for better correction of speckle chromaticity and even data-analysis strategies that do not rely on the presence of *a priori* assumed features in the planet's spectrum.

For SPHERE we are pursuing a microlens-based IFS concept related to the classical TIGER concept, modified for the case of high-contrast diffraction-limited observations. The required 5σ detectivity at 0.5″ is 10^{-7} with a goal of 10^{-8} with respect to the un-occulted PSF peak, and the spectral range of the IFS is limited to the *Y-J* bands (0.95–1.35 μm), allowing the use of a single detection channel and parallel operation of IRDIS and IFS. A resolving power per pixel of 30 is maintained, with a minimum FOV of 1.35″ square and a strong goal of 3″ square. Nyquist-limited spatial sampling at 0.95 μm is imposed as for IRDIS. Optimised commonality between IFS and IRDIS in terms of detector and associat-

ed equipment is seen as an important system goal. The same 2k × 2k detector format is therefore adopted, and it is highly likely that the long-wavelength cut-off defined for IRDIS will also be acceptable for IFS. The opto-mechanical concept including micro-lens array, collimation optics, an Amici Prism providing zero beam deviation and constant resolution within the entire wavelength range, camera optics, and the detector cryostat is illustrated in Figure 4.

Imaging Polarimeter

The Zurich Imaging Polarimeter (ZIMPOL) sub-system is a high-precision imaging polarimeter working in the visual range, covering at least 600 to 900 nm. The instrument principle (Gisler et al., 2004) is based on fast modulation, using a ferro-electric retarder, and demodulation of the polarisation signal, using a modified CCD array, as illustrated in Figure 5. Key advantages of this technique are the simultaneous detection of two perpendicular polarisations (the modulation is faster than seeing variations), and the recording of both images on the same pixel. Thanks to this approach, a polarimetric precision of 10^{-5} or even better should be achieved. The CCD will cover a Nyquist sampled field of 3″ × 3″ square and it is foreseen that the FOV can be moved around the bright star so that a field with a radius of 4″ can be covered. In addition to polarimetric imaging, ZIMPOL provides the possibility for high-resolution imaging in the visual range using a set of broad and narrow-band filters. This capability will be unique in the post-HST era.

Expected performances

Various numerical simulation approaches have been developed by different groups during the Phase A studies of the SPHERE instrument. All these efforts are being gathered into a single instrument simulator developed on the CAOS platform in order to provide the technical and scientific community with a tool to predict the instrument performance. We present here the basic approach and key results of the AO/IRDIS simulator developed in Phase A, invoking a double subtraction, dual imaging approach.

Figure 3: IRDIS opto-mechanical implementation.

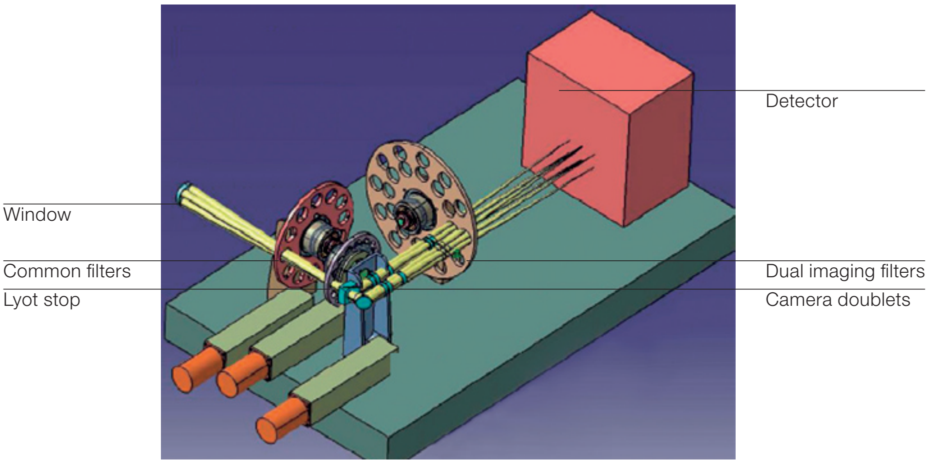

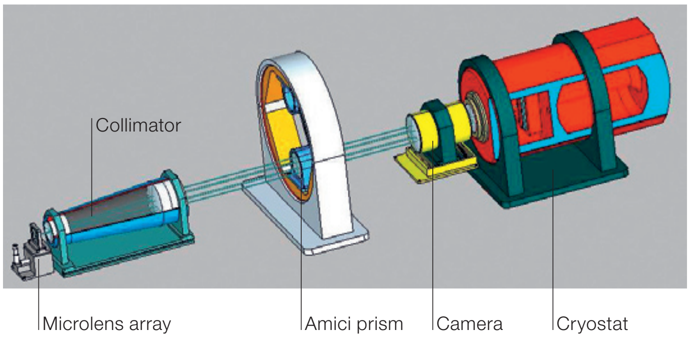

Figure 4: Opto-mechanical design of the IFS.

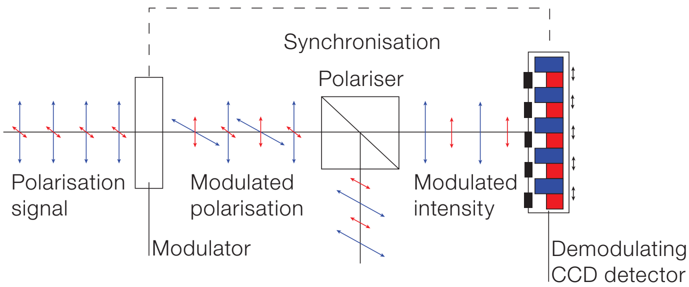

Figure 5: Basic polarimetric principle.

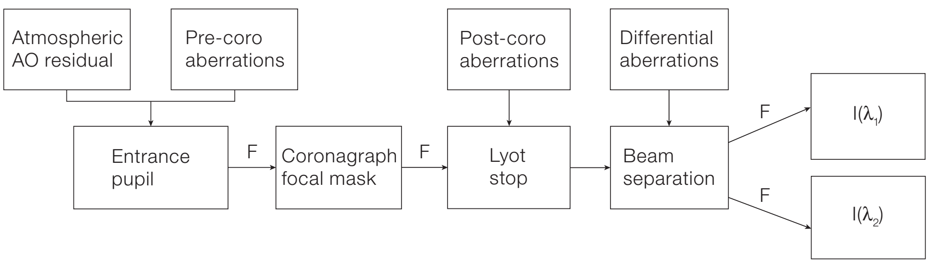

Figure 6: Basic structure of the dual-imaging performance model.

Figure 6 shows the structure of the dual imaging performance simulator. Through a series of three Fourier transforms (denoted F in the figure), the coronagraphic action on a perturbed wavefront and the influence of post-coronagraphic aberrations are simulated. The coronagraphic entrance wavefront is affected by time-variable residuals of the AO correction of atmospheric turbulence, as well as quasi-static instrumental aberrations. Instrumental aberrations include actual phase maps representing the VLT mirrors, and estimated phase maps of instrument optics generated using a power spectral density (PSD) with an inverse square-law radial profile, assumed to represent typical high-quality optical surfaces. All the optics upstream of the dichroic beam-splitter is high-pass filtered with a cut-off at the AO cut-off spatial frequency (20c, denoting cycles per pupil diameter). All optics downstream of the dichroic is high-pass filtered with a cut-off at 4c, representing the expected limit of instrumental calibration based on phase-diversity techniques. Post coronagraphic aberrations represent aberrations within the IRDIS science module. While common aberrations, as predicted by theoretical studies, are of little influence on the speckle reduction process, differential aberrations are extremely important. This leads to the strict differential aberrations budget imposed upon the IRDIS design. Other factors included in the simulations include image decentring on the focal plane mask, both dynamic (jitter), chromatic (ADC residual) and fixed offset, coronagraph defaults (e.g. deviation from π phase shifts in the 4QPM mask), etc.

In the complete double difference simulation, this simulation is performed twice, once for the object star and once for a reference star, using uncorrelated atmospheric screens and introducing small differences, in particular in terms of fixed offset of the star on the coronagraph and transverse and rotational alignment error between telescope phase screens and instrument phase screens. A sensitivity analysis has confirmed the great importance of controlling these parameters to great precision (image centring < 0.5 mas, pupil shift < 0.2 %, pupil rotation < 0.1°), imposing the pupil and image stabilisation optics and control loops described above.

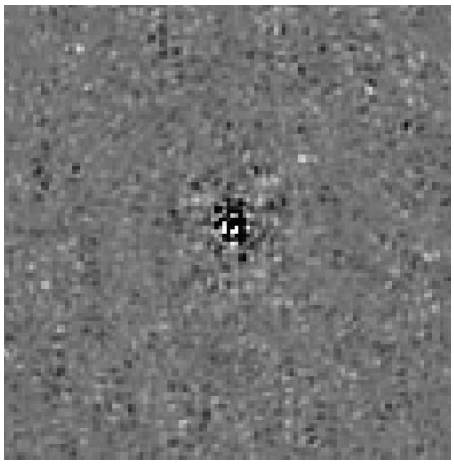

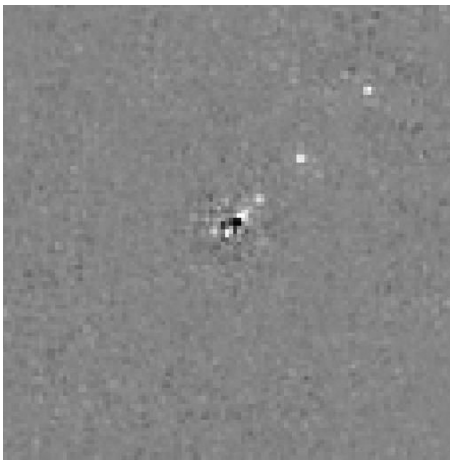

Figure 7: Residuals after simple dual-band subtraction (left) and double subtraction (right). Gray scale is linear between +/– 5 10^{-6} of the non-coronagraphic PSF maximum. Residual noise is subtracted down to a level much lower than companion flux.

Figure 7 shows the resulting processed image after dual wavelength subtraction (left) and the complete double difference subtraction involving a reference star. The object here is a young (10 Myr) M0 star at 10 pc, with 1 MJ companions located at 0.1 to 0.4 arcsec from the star. These companions have a difference in magnitude of 12 with respect to their host star, representing a contrast of 1.3 10^{-5}. Through an extensive simulation of test cases involving various stellar ages and distances and a series of different-sized companions at different orbital separations, we find in particular that 1 MJ planets are detectable down to angular separations of 0.2″ for a young (10 Myr) M0 star at 40 pc, and that 10 MJ planets are detectable down to angular separations of 0.1″ for an older (1 Gyr) M0 star at 10 pc.

Project organisation

Following two concurrent phase A studies, the ESO Scientific and Technical Committee recommended in April 2005 to investigate the feasibility and interest of benefitting from both studies by proposing an optimised instrument including the XAO system, coronagraphic devices and differential imaging camera proposed by one consortium as well as the Integral Field Spectrograph and ZIMPOL visible dual imaging polarimeter proposed by the other consortium. A post-phase A study has validated the interest of such an approach in terms of scientific return and its feasibility in terms of system analysis and project management.

The new consortium includes several European institutes, namely: Laboratoire d'Astrophysique de Grenoble (P.I. institute), Max-Planck-Institut für Astronomie in Heidelberg (co-P.I. institute), Laboratoire d'Astrophysique de Marseille, Laboratoire d'Etudes Spatiales et d'Instrumentation en Astrophysique de l'Observatoire de Paris, Laboratoire Universitaire d'Astrophysique de Nice, ONERA, Observatoire de Genève, Osservatorio Astronomico di Padova, Institute of Astronomy of the Zurich College of Technology, Astronomical Institute of the University of Amsterdam, ASTRON and ESO.

The kick-off meeting took place in March 2006 and the current development plan, foresees first light for SPHERE in late 2010.

Conclusion

The SPHERE instrument, optimised for very high-contrast imaging around an extensive sample of stars, and its operation model including in particular a large survey strongly supported by the build-

ing consortium, will allow the direct detection of a sample of giant planets in a variety of conditions. Such a return in the proposed schedule (first light in 2010) will provide a timely and critical contribution to the highly competitive research field of extrasolar planets: formation, evolution and characterisation. This observational approach will provide specific information, complementary to other observational techniques (radial velocities, photometric transits, thermal IR imaging, etc.) and absolutely necessary to prepare for the foreseen next-generation challenges, from the ground with Extremely Large Telescopes or from space with coronagraphic imaging telescopes (TPF-C) and interferometric instruments (DARWIN, TPF-I).

The science return of SPHERE will be optimised through the observation of a large enough number of targets in survey(s). Large homogeneous data sets allow for the derivation of statistically significant data on the incidence and properties of planets, from both detection and non-detection, and for a better discussion of the false alarms. The SPHERE consortium proposes to dedicate most of its GTO allocation to such a moderately large survey, covering a few of the identified science goals on a sub-set of the possible SPHERE targets, and endorses the proposal to have a broader community involved in a much wider and more complete survey. ESO and the consortium are currently exploring the possibility to promote such a SPHERE large survey.

References

Claudi R. et al. 2006, Proc. SPIE 6269, in press
Fusco T. et al. 2006, Proc. SPIE 6272, in press
Gisler D. et al. 2004, Proc. SPIE 5492, 463
Lenzen R. et al. 2004, Proc. SPIE 5492, 970
Mawet D. et al. 2006, A&A 448, 801
Mouillet D. et al. 2001, Proc. "Scientific Drivers for ESO Future VLT/VLTI Instrumentation" conference, 258

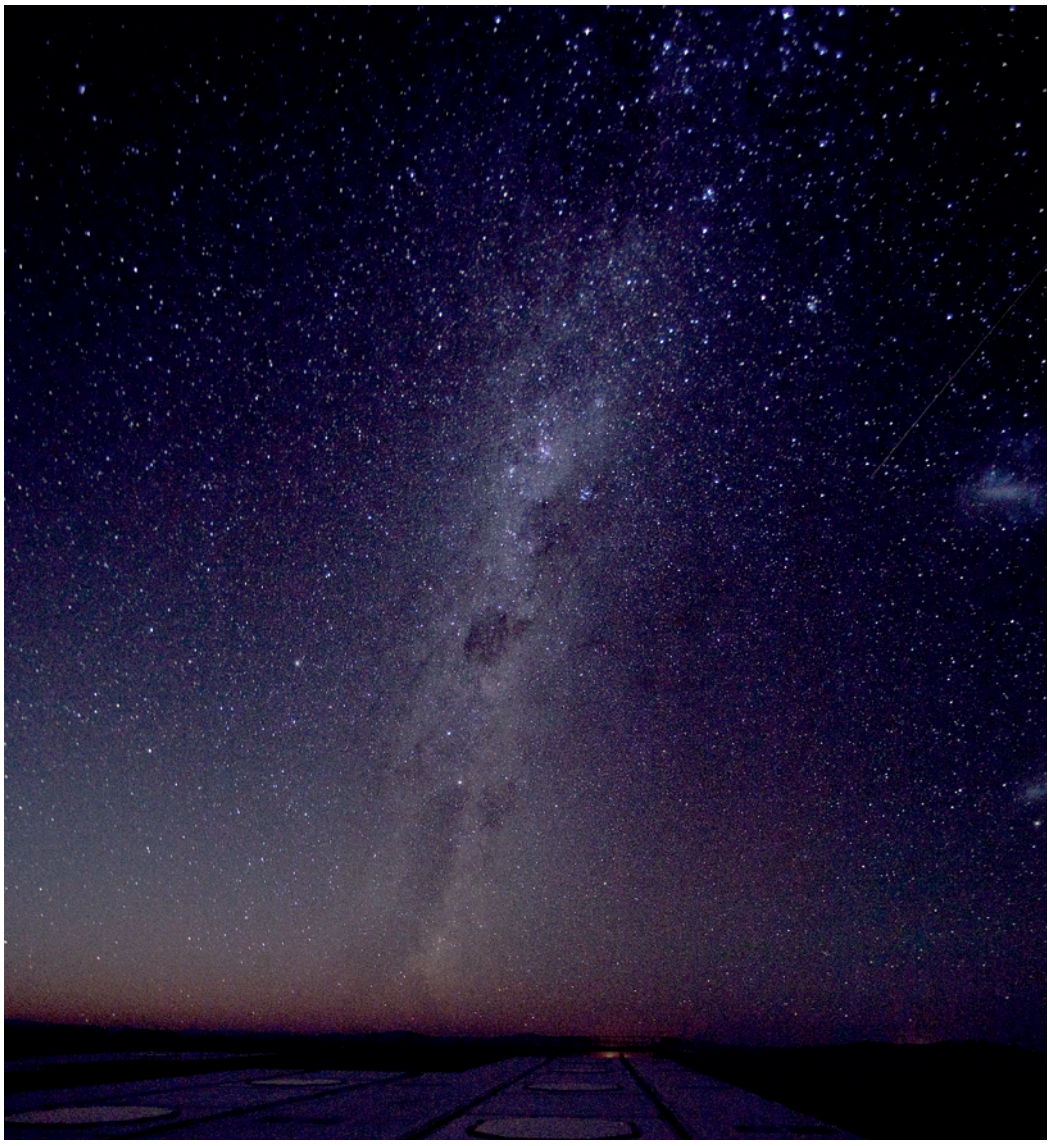

The sky above Paranal. The Milky Way is clearly visible in all its majesty, as well as the Magellanic Clouds on the right. This image was obtained on 11 December 2005 by Hans Hermann Heyer (ESO) with a Canon EOS 5D.

Second-generation VLTI Instruments: a First Step is Made

Andrea Richichi, Alan Moorwood (ESO)

As the VLTI continues its successful science operations with the first scientific instruments, MIDI and AMBER, plans are already under way for the horizon beyond 2010. To maintain the VLTI at the top of the international competition, a next generation of instruments is being evaluated: more versatile, more complete, but also more complex and technically challenging. Phase A studies for three candidates have just started, and we provide here a brief summary of their characteristics.

It took the work of dozens of engineers and astronomers, a decade of planning, design and testing, hundreds of thousands of lines of code, the (occasionally unorthodox) use of telescopes from 40 cm to 8.2 m in diameter, and a lot of sweat in the dry Paranal air. But the goals set back in the nineties, to make interferometry a standard technique at ESO and make the VLTI the most powerful facility of its kind in the world, have been achieved. To be sure, some problems remain, mainly in the form of unwanted vibrations: a lot of work has been devoted to this, particularly by the so-called Interferometric Task Force, and several solutions are being considered. But it is undeniable that the VLTI constitutes today the term of reference for interferometry, in terms of sensitivity, angular resolution and accuracy. The 8.2-m Unit Telescopes and the movable 1.8-m Auxiliary Telescopes represent a unique combination of large collecting areas and long, flexible baselines which remains unmatched not just in performance but also in ease of operation. The two facility instruments, MIDI and AMBER, are offered to the community and carry out routine observations both in visitor and in service mode. Altogether, about 80 interferometric proposals are received at ESO in each semester, totalling approximately 10 % of the Paranal scientific requests. MIDI is a unique mid-infrared beam combiner, and it can be fairly said that each observation with this instrument is the first of its kind for any given astronomical target. AMBER is unique in its ability to combine beams from three 8-m telescopes at a time, providing so-called closure phases which are a key to measure not just the size of a target but also its asymmetries and rough geometrical appearance. Both instruments are equipped with the possibility of generous spectroscopic dispersion. Counting in also the very prolific production from the previous VINCI test instrument, the VLTI has generated already in its commissioning period and early scientific operation many dozens of refereed papers, dominating the relatively restricted field of interferometric results world-wide.

One might think that all this is reason enough to lay back for a moment and enjoy the fruits of a long effort: nothing could be further from the truth. In its resolution on scientific strategy of December 2004, with the first scientific results from the VLTI in hand, the ESO Council sanctioned that it was a priority to exploit the unique capabilities of this facility. Faithful to this directive, a Workshop was organised in Garching in April 2005, among other things to identify the ideas and visions in the community about the development of interferometry at Paranal. At this venue, nine technical and instrumental concepts were presented. These were evaluated by the ESO STC, which recommended to study a subset of them. Four instruments were subsequently investigated, and at their meeting of October 2005 the ESO STC praised their scientific potential but recommended further optimisation of synergies as well as a formal call for proposals. This was done, and finally in April 2006 three second-generation instrumental concepts for the VLTI were formally introduced: MATISSE, VSI and GRAVITY. ESO STC recommended to go ahead with Phase A studies, and these started in June 2006 with an expected duration of about 15 months.

MATISSE is the natural successor to MIDI. It will cover the 10 micron spectral window as does the latter, but additionally extend coverage to the *L*-, *M*-bands (3 to 5 microns) and possibly the *Q*-band at 20 microns. Especially the shorter wavelengths are an interesting addition, since they are not covered by the first-generation instruments and in fact by almost any other interferometer. MATISSE will combine four beams, which represents an enormous jump from MIDI with two baselines only: this will yield six baselines simultaneously (MIDI only one) and provide three closure phases, providing the first-ever possibility of interferometric imaging in the mid-infrared. Of course, caution has to be taken, as with all optical interferometers, that here imaging means the simple combination of a limited number of visibilities and phases in Fourier space, and would not be at the level of quality we are used to from radio interferometers. Nevertheless, this represents a quantum step in optical interferometry observations. Scientific objectives are a natural continuation of those of MIDI, with a focus on cool dusty environments in many classes of stars and including the challenging goals of AGNs and exoplanets. With MATISSE, it would be possible to add substantially more information on the geometry and spatial distribution of the dust.

VSI is the natural successor to AMBER, from which it adopts many design aspects including the use of monomode fibres as spatial filters to clean the wavefronts from high-order perturbations before achieving interference. VSI represents an evolution of AMBER in the number of beams, which would be boosted from the current three to four or even six (this being the maximum number allowed by the VLTI delay lines). Remembering that the number of baselines and closure phases increases approximately with the square of the number of beams, the advantage is obvious especially concerning the imaging possibilities of this instrument. With six beams, VSI would provide simultaneously 15 baselines and 10 closure phases, compared with 3 and 1 respectively for AMBER. Another innovative aspect, currently under evaluation, could be the use of integrated optics for beam combination, i.e. replacing large bulk optics with a single stamp-sized optical chip. This has an obvious advantage for the alignment and the stability of the instrument, as well as opening up the possibility of adding beams in a quasi-modular fashion. As in the previous parallel between MATISSE and MIDI, the science goals of VSI would also follow closely in the footsteps of AMBER, with the additional important goal of increasing dramatically the amount of information on the geometry and the spatial distribution of the sources.

GRAVITY is, in a sense, the new kid on the block. It is born out of the need to address a brand new observational mode, i.e. the ability to perform extremely accurate astrometric measurements on very faint sources. Interferometers can perform narrow-angle astrometry, by using a nearby reference source and measuring "the number of fringes" between the reference and the target. This concept is used for example in PRIMA, another VLTI development which is well underway and which will permit us to use a nearby bright star to either make observations of faint scientific targets, and/or to perform astrometry with a goal of 50–100 microarcseconds. However, the ultimate accuracy of the astrometric measurements depends, among other things, on the angular distance between target and reference. PRIMA is designed to cover distances up to one arcminute, and the beams pointing to the target and the reference are separated upstream in the optical train, close to the telescopes. GRAVITY proposes to separate them downstream instead, close to or inside the instrument. This will limit the possible angular distance to less than 2 arcseconds, but will in turn permit much higher astrometric accuracy, up to 10 micro-arcseconds. The main goal, though not the only one, is to investigate the motion of stars very close to the Sgr A* source in the Galactic Centre (see Figures 1 and 2), which is normally accepted to be a massive black hole based on evidence obtained at various wavelengths but without very high angular resolution. GRAVITY would go far beyond, by observing the relativistic effects in the orbits of the stars around the black hole and permitting the direct estimation of the BH mass as well as other parameters.

All these three instruments have exciting scientific goals, and represent significant improvements over the first-generation AMBER and MIDI. However, they also imply a number of technological challenges. Just to name one as an example, GRAVITY will need IR wavefront sensors in the lab (as opposed to the current MACAO visual adaptive optics systems at the UT telescopes) and a high-performace fringe-tracker for four beams, as well as internal metrology of accuracy comparable to that of PRIMA.

Figure 1: Simulated GRAVITY observations (axes in μas) of a hot spot orbiting the Galactic Centre black hole at a few Schwarzschild radii (RS ~ 9 μas). **Left:** Already a single observation of a flare will allow us to trace the overall motion at high significance. **Right:** Combining the data from several flares will reveal general relativistic effects (e.g., multiple images from lensing), probing the space-time around the supermassive black hole (Eisenhauer et al. 2005, Paumard et al. 2005).

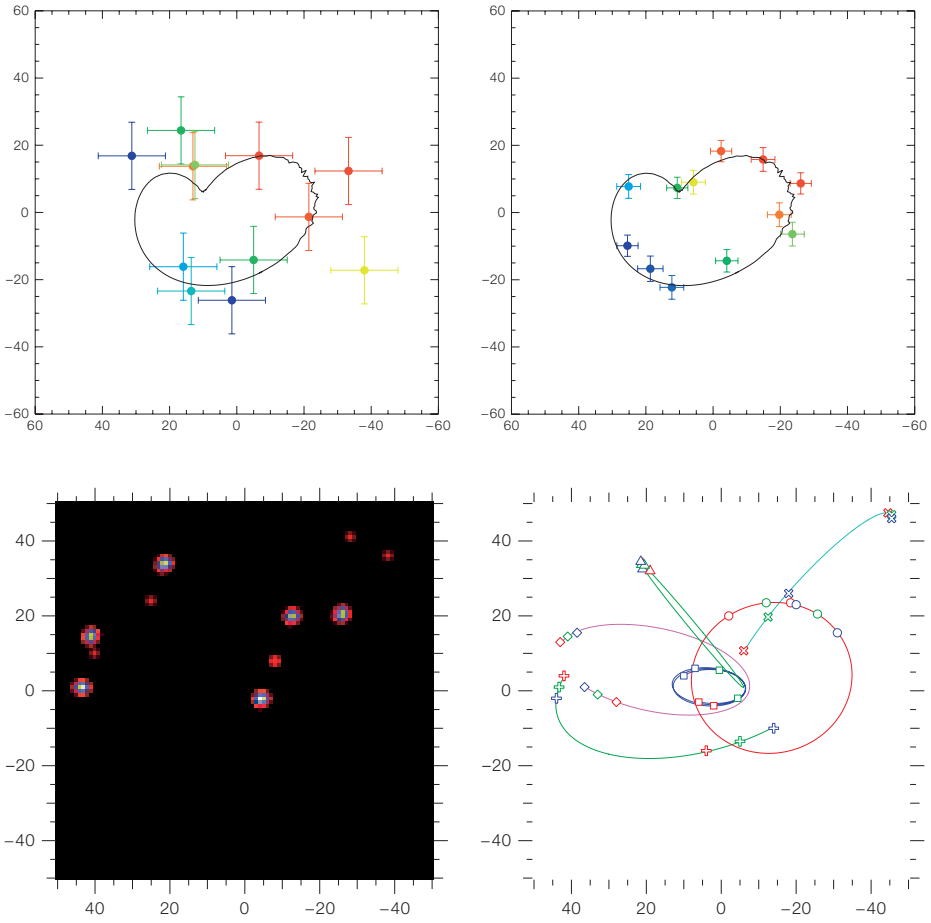

Figure 2: Simulated GRAVITY observations (axes in mas) of the stars in the central cusp of the Galactic Centre. **Left:** Image of the innermost 100 mas of the Galaxy as seen with GRAVITY in a nine-hour observation with the 4 UTs. Noise has been added to the visibilities and phases, and the image has been synthesised and deconvolved using the standard CLEAN algorithm. **Right:** 15 months of astrometry using the image synthesis technique allow tracing the orbits of the stars. Several stars have completed at least one orbit, exhibiting periastron shifts from relativistic effects and from the extended mass distribution in the Galactic Centre (Eisenhauer et al. 2005, Paumard et al. 2005).

The three Phase A studies which have just started will have the task to investigate in detail these scientific challenges, identify potential showstoppers, prove feasibility and provide insight on actual costs and schedule of each instrument. ESO will not be just a spectator in this game. In addition to the usual role of supervision and involvment in the studies, a number of strategic choices need to be addressed internally. Will PRIMA need to be extended as well to meet the needs of the second generation? Will it be necessary to have a dedicated fringe tracker for each new instrument, or will a common one suffice? How many telescopes can be effectively combined for routine operations? Last but not least, what is the VLTI ultimate performance after the technical interventions currently in progress?

We hope to know the answers in a few Messengers from now.

References

Paumard T. et al. 2005, Proc. of the ESO Workshop on "The Power of Optical/IR Interferometry: Recent Scientific Results and Second-generation VLTI Instrumentation"

Eisenhauer F. et al. 2005, Proc. of the ESO Workshop on "The Power of Optical/IR Interferometry: Recent Scientific Results and Second-generation VLTI Instrumentation"

The ALMA Back-End

Alain Baudry[1]
Fabio Biancat Marchet[2]
Hervé Kurlandcyk[2]
Silvio Rossi[2]

[1] Observatoire Aquitain des Sciences de l'Univers de Bordeaux, Floirac, France
[2] ESO

The Atacama Large Millimeter Array is designed to produce excellent images in spectral lines and continuum, to detect distant galaxies like our Milky Way and to image proto-stellar discs in the nearest molecular clouds. To accomplish these goals, signals from the ALMA antennas must be processed and transmitted to the technical building in a format ready to be accepted by the correlator. The ALMA Back-End provides this in a loss-free, reliable and flexible way. In the following an overview is given of the ALMA Back-End subsystems developed in various European Institutes under ESO coordination.

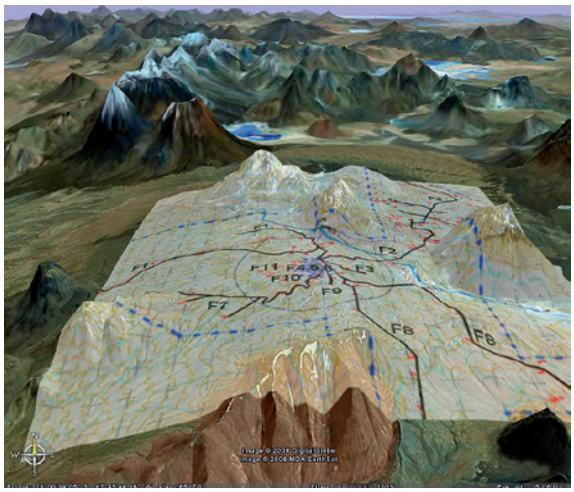

Figure 1: The fibre network on the Chajnantor site. The fibre network is an essential part of the Back-End allowing the data transfer from each antenna to the technical building. The distance of the farthest stations to the technical building is approximately 15 km. The network will encompass more than 100 km of multi-fibre cables for a total of installed fiber length exceeding 10 000 km. In order to attain the thermal insulation required by the photonic local oscillator the cables will be directly buried at a depth of 0.6–1 m.

The signal of frequency up to 950 GHz captured by each antenna of the array is converted to a pair of Intermediate Frequency (IF) signals, one for each polarisation, in the range of 4–12 GHz by the Front-End cryogenic receivers, digitized and transferred to the technical building as a 120 Gbit/second raw data stream through one single optical fibre. A sketch of the fibre network at Chajnantor is shown in Figure 1.

In the technical building (right side of Figure 2) a custom processor, the correlator, cross-correlates the signals from all antennas and pre-processes the data flow before passing it to the computing system for further processing. The IF signal processing and digitization in the antenna as well as the data transmission system that transfers the signal to the correlator are part of the ALMA Back-End subsystem (left side of Figure 2).

The severe environment deserves special attention: at 5000 m altitude the heat dissipation capability is greatly reduced, in addition the remote location and the lack of oxygen heavily impact the possibility of performing maintenance on site. This calls for low power dissipation, high reliability and easy maintenance equipment.

Although the most advanced information and communication applications are fast approaching the ALMA needs, meeting the ALMA requirements was only possible by pushing the technology beyond the state of the art and Application Specific Integrated Circuits (ASICs) were developed where commercial solutions are not yet available.

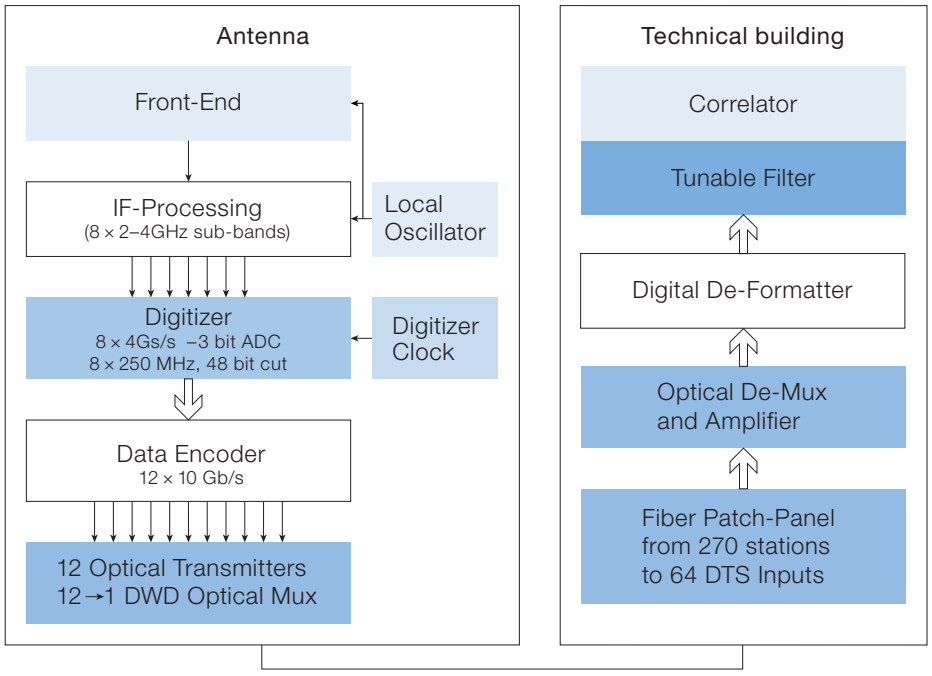

Figure 2: A schematic view of the ALMA system, showing the location of the Back-End subsystems between the Front-End receivers and the correlator. The Data Transmission System within the Back-End in the antenna processes, digitizes at 4 Gsamples/s and converts the 'low' frequency (4–12 GHz) signals output by the Front-End receivers in a multi-colour light beam that through one single fibre is transferred at the rate of 120 Gbit/s to the technical building where it is converted back to an electrical signal and fed into the correlator. The Back-End also includes the photonics Local Oscillator that provides an extremely phase accurate signal to all antennas.

Data Transmission System

The Data Transmission System (DTS) in the antenna performs two main tasks: it digitizes the processed IF frequency signals and converts them to a format suitable for digital transmission along one single optical fibre. In the DTS the scientific signal is converted into 12 10 Gbit/s digital serial streams each one driving a laser emitter with slightly different colour. The 12 light beams are optically mixed together and injected into one single optical fibre (Dense Wavelength Division Modulation).

In the technical building the incoming light beam is optically de-multiplexed to separate the 12 original beams. These are converted to electrical signals and fed into the correlator. In order to reliably operate at the required light frequency and with the proper power and sensitivity throughout their whole lifetime both the laser emitters and receivers need a sophisticated control system for current and temperature.

The Digitizer Assembly

The ALMA Digitizer Assembly is part of the Data Transmission System. It digitizes the two incoming signals, one for each polarisation, at a rate of 4 Gsamples/s and parallelises them into six 16-bit words at a rate of 250 MHz. These words are sent to the Data Encoder that formats them for the optical transmission.

The heart of the Digitizer Assembly is the digitizer chip, VEGA (see Figures 3 and 4), a band-pass 2–4 GHz 3-bit flash analog to digital converter operating at the sampling rate of 4 Gsamples/s. Although at present the market offers components that nominally meet some of the requirements, the suitable combination of sampling rate, resolution, maximum input frequency (4 GHz) and power consumption is not available. Therefore, an Application Specific custom device (ASIC) needed to be developed. The power dissipation represents an additional constraint as the low air density at the operating altitude makes the ventilation rather inefficient, especially considering that the Digitizer Assembly needs to be enclosed in a sealed case to reduce radio frequency interference.

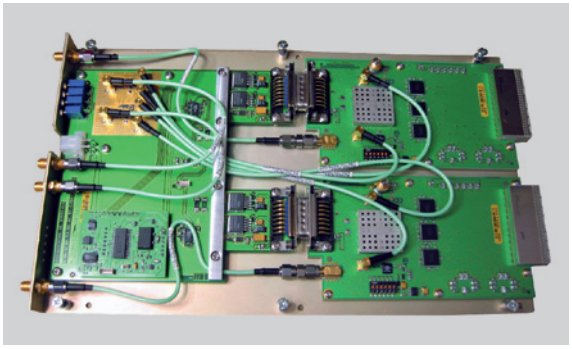

Figure 3: The Digitizer Assembly contains two VEGA digitizer chips (enclosed in the small metal boxes) and six PHOBOS de-multiplexer chips (the square black devices on the right side). The Digitizer Assembly converts two 2–4 GHz pass-band signals sampled at 4 Gsample/s into six 16-bit parallel streams at 250 MHz. The left side of the assembly contains the power supplies, the clocks distribution circuits and the low frequency circuits for communication and remote control.

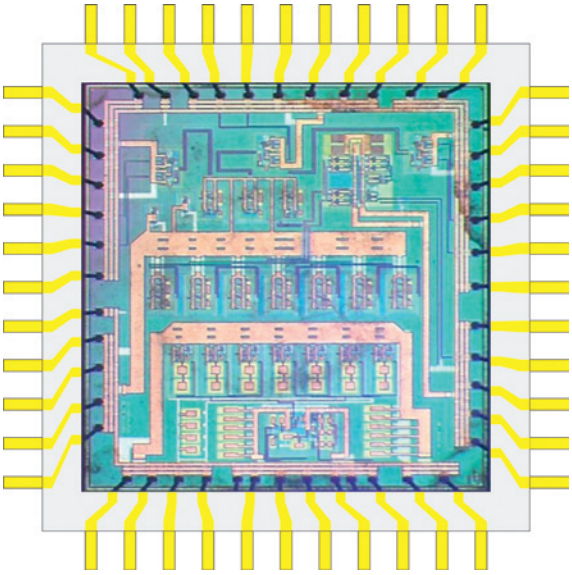

Figure 4: This microphotography shows the internal layout of the VEGA digitizer chip a 4 Gsample/s 3-bit analog to digital converter. A second chip, PHOBOS, de-multiplexes (i.e. parallelises) the VEGA serial stream output. Both devices are custom developments and are operated at clock frequencies as high as 4 GHz. They are implemented in the Silicon-Germanium BiCMOS technology that allows to design transistors with transition frequency as high as 75 GHz, but with power dissipation significantly lower than other high frequency technologies (InP, GaAs). The power consumption for the two devices is in the range of 1 W, which allows enclosing the whole Digitizer Assembly into a RF tight box without any special heat sink.

In order to meet the high speed and low power requirements, the digitizer uses the Silicon-Germanium technology and BiCMOS 0.25 µm process. This technology allows the fabrication of high speed and low dissipation hybrid analog/digital devices. The nominal voltage supply is 2.5 V and the average power consumption is 1.5 W. The device has a high temporal stability, a key requirement for radio astronomy. A self-diagnostic block is included in the chip in order to verify after the production or during maintenance that the device exhibits toggling outputs.

A companion demultiplexing chip, PHOBOS, was also developed. It parallelises an incoming 4 Gbit/s serial stream in 16-bit words at a rate of 250 MHz. Three of these devices are connected to each one of the three VEGA output lines. Despite the higher pin-out and complexity and even lower power dissipation constraints (less than 1 W per chip), the development of PHOBOS was less critical being a fully digital device with no analogue parts.

VEGA and PHOBOS are the result of a combined effort between the Observatoire de Bordeaux, the IXL Laboratory of the Université de Bordeaux and a commercial partner. All design, simulations and qualification tests have been performed by the two institutes while the commercial partner provided the software tools and the production facilities.

Local Oscillator

To operate the array in the interferometric mode the ALMA Front-End receivers require a phase-stabilised Local Oscillator (LO) coherent among all antennas to convert the incoming astronomical signal to lower frequencies. Receiving frequencies as high as 950 GHz and baselines up to 15 km set an extremely tight phase stability requirement for the LO.

To generate and effectively distribute such a stable reference all over the array, a photonic approach has been adopted. Two laser beams whose frequency difference equals the LO frequency (before multiplication in the Front-End) are injected in one single fibre that brings the signal from the technical building to the antenna. At the antenna the two beams are combined in a photomixer and the resulting electrical signal, whose frequency is the difference of the incoming beams frequency, is fed into the Front-End receiver.

The laser synthesizer is based on an extremely stable master laser to which a second laser, the slave, is phase locked with a frequency difference (the actual LO frequency) that is set by a tuneable microwave generator.

The tight requirements in terms of operating frequency and sensitivity of the photomixer are met by a custom device designed and produced at Rutherford Appleton Laboratory (UK), where a modified commercial photodiode has been integrated in a special package (Figure 5) providing fibre optic connection, bias connection, filtering and output waveguide.

Since the propagation time along the fibre affects the phase of the LO signal, to reduce the phase variations, the changes in length of the fibre must be kept as small as possible. In the LO system the fibre length variations are limited by both passive means and active control. The active control is based on an interferometric subsystem which measures the round trip length and acts on fibre stretching actuators to compensate for the length variations. The length of the link combined with the light speed in the fibre sets the bandwidth of the line length corrector which is constrained to about 1 kHz. Therefore, only disturbances (including acoustic ones) well below this frequency and of limited amplitude can effectively be compensated, the others must be kept low by passive means. Passive means include thermal-stable installation of the fibre, thermal insulation, and mechanical insulation. In order to keep the cost of the system affordable utilisation of special fibres (like low temperature coefficient) was not considered.

The complete LO system has been tested in the lab (with the proper length of fibre) and is currently undergoing field tests at the Alma Test Facility (at the VLA Observatory, in New Mexico).

The fibre system

As mentioned above, the antennas will be connected to the technical building through a network of optical fibre cables. Each antenna will be reached by eight single-mode optical fibres, allocated as follows:

– one fibre for the Data Transmission System (the data resulting from observation)
– one fibre for the Photonics Local Oscillator reference signal
– two fibres for the monitoring and control signals (Ethernet network)
– four spare fibres

There will be approximately 200 possible locations (antenna pads) among which the antennas will be relocated. The fibres from each one of the antenna pads are connected at the technical building to a central patch panel (with up to 270 antenna connections, see Figure 2). Here, the through connections from the optical equipment at the antennas to the optical equipment in the technical building will be made. The maximum and minimum distances between antenna pads and technical building will be 15 km and 500 m respectively. The relatively long maximum distance calls for low attenuation and reduced amount of splices along the links and the topology of the network must be optimised in these respects. In addition, the design shall take into account the extreme sensitivity of the Local Oscillator to both temperature variations and vibrations. This sets tight requirements on the layout of the system where good thermal and mechanical insulation must be achieved. For this purpose the cable will be directly buried underground, including the fibre splices. This solution provides high thermal and mechanical insulation. In order to fully exploit the insulation characteristics of the soil, no ducts or other protections that could allow air flow around the cable are foreseen (with some possible exceptions at road crossings). Therefore, the cable needs to be suitable for direct burial. Similarly, the cable joints will be directly buried and the fibre splices as well as the terminations at the station vault will be properly protected against the environment by suitable enclosures.

Unlike the Local Oscillator and the Data Transmission System, the links carrying the monitor and control signals from all pads will be permanently connected to the equipment and the switching to the active pads will be performed automatically, not requiring a manual patching. Although currently under investigation, a similar automatic connection does not seem feasible for the LO and DTS links because of the tighter requirements and higher costs.

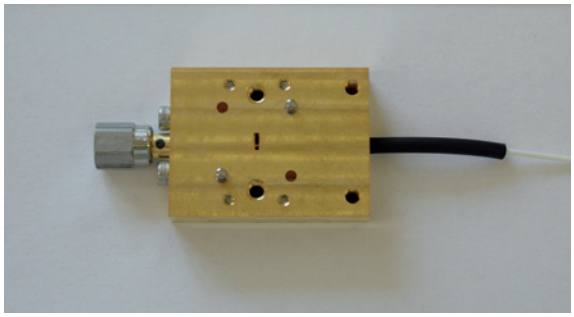

Figure 5: The photomixer is a tiny but fundamental component of the ALMA photonics LO. It converts the two icoming (through the fibre on the left side of the picture) light beams into an electrical signal whose frequency is the difference of the frequencies of the light beams. Pushing the performance close to the theoretical limit, Rutherford Appleton Laboratory managed to enclose a photodiode into a 'photomixer block' capable of delivering up to 1 mW at frequencies as high as 140 GHz.

Fibre splicing at 5 000 m

Experience from the APEX project, which also operates at Llano de Chajnantor, suggests that the harsh operating environment (dust, strong wind, extreme temperatures and low air density) might prevent any contractor from reliably meeting the 0.15 dB splice loss (at the sea level) assumed as a standard in the industry and as a baseline for the optical budgets used in ALMA. As a matter of fact, no splicing equipment existed that was rated for that altitude.

For the LO link specifically, the quality of the splice is important because the Photonic LO signal is limited in terms of launch power by Brillouin backscattering (because of the extremely narrow line width) and in terms of received power because of the low saturation power of the photomixers. Poor splices may also result in other polarisation effects which may affect the LO signal phase.

In order to provide the technical teams involved in the project with a realistic expectation of the yield and quality of splices attainable at the Chajnantor site and to identify the most suitable splicing equipment, a splicing trial activity has been carried out at the site. The outcome of the splice trial showed that it is possible to make excellent splices at 5000 m and that the two industrial splicing machines tested on site are suitable for the fibre optic installation work once they are properly adjusted. It is confirmed that, provided that cleanliness precautions are taken during installation, the 'sea-level' splice loss can be adopted also for the ALMA site.

Acknowledgements

The development of the Back-End subsystems described above is the result of a combined effort of various European Institutes. Many thanks to the people that made it possible: Jean-Baptiste Begueret from IXL Bordeaux and Laurent Dugoujon from STmicroelectronics for the development of the digitizer ASICS. Peter Huggard from Rutherford Appleton Lab, Nathan Gomes, Pengbo Shen from University of Kent for the Photonics LO development. Roshene McCool, Ralph Spencer, Bryan Anderson, Dave Brown from Jodrell Bank Observatory for the development of the optical Data Transmission System. Guy Montignac, Stephane Gauffre, Cyril Recoquillon from Université de Bordeaux for the development of the Digitizer. Special thanks to Rolando Medina from ESO Paranal and Christophe Jacques from NRAO who actively participated in the splice trial on site and to the ALMA safety team that made it possible in an effective and safe way.

The Irregular Galaxy NGC 1427A. Based on *U*, *V* and *H*-alpha observations with FORS1 obtained in service mode for Andreas Reisenegger and his colleagues in November 2002 and January 2003. North is on the left and West is up. Henri Boffin (ESO) did the final processing of the image. See ESO Press Photo 27c/06 for more details.

The 2006 ESO Science Archive Survey

Nausicaa Delmotte[1]
Markus Dolensky[1]
Alberto Micol[2]
Paolo Padovani[1]
Bruno Rino[1]
Piero Rosati[1]
Andreas Wicenec[1]
Jörg Retzlaff[1]
Charles Rité[1]
Remco Slijkhuis[1]
Benoît Vandame[1]
My Ha Vuong[1]

[1] ESO
[2] ST-ECF

We present the results of the 2006 ESO science archive survey aimed at improving services to the astronomical community. Future archive development plans will be based on user feedback.

The ESO Science Archive Facility

The ESO Science Archive Facility (SAF) has been operational at ESO Headquarters in Munich since 1991. It contains data from ESO telescopes located at the La Silla, Paranal and Chajnantor observatory sites. Since June 2005 it also contains data from the UKIRT Infrared Deep Sky Survey taken with the Wide Field Infrared Camera. The SAF is operated by ESO in collaboration with the Space Telescope European Coordinating Facility and also provides access to Hubble Space Telescope data for the HST user community. Except for a few special cases, all ESO science observations have a proprietary period of one year. After this period the archival data sets and abstracts of the successful ESO proposals are available worldwide to the general astronomical community. All calibration data are public immediately after the observations. The ESO archive also contains high-level science data products packaged and delivered to the community via special releases: e.g. VLT Commissioning and Science Verification data, ESO Imaging Survey, Advanced Data Products.

The 2006 ESO Science Archive Survey

The survey was an initiative of the Virtual Observatory (VO, Padovani and Quinn 2005) Systems department at ESO. It focused on the ESO part of the ESO/ST-ECF SAF only. It was designed to determine which services and interfaces are best suited to the user needs and which features they would like to see added. This short on-line survey was issued on 1 March 2006 and ran for one month. The announcement for the survey was sent by e-mail to all registered archive users. A further announcement was posted on the main archive web page. The participation rate of the community was very good. 558 participants returned the questionnaire out of 1600 active users. The survey contained questions addressing four main areas: user profile, current ESO archive services, publications based on ESO data and future of the ESO SAF. All the survey responses for each question, including various graphics, can be accessed on-line at *http://archive.eso.org/archive/stats/survey/survey_results.html.*

Composition of the user community

The scope of the first questions was to characterise the ESO archive user community. Basically, 84 % of the survey respondents are not affiliated to ESO, 60 % are Principal or Co-Investigators of some ESO observing programme(s), 61 % are professional or post-doc astronomers and one fourth are students. Amateur astronomers account for a non-negligible part of the user community (7 %) whereas teachers, educators and journalists account for only 1 %. A majority of respondents (58 %) use the ESO archive a few times a year and 29 % of the respondents use it several times a month.

ESO archive services

The ESO SAF offers a number of on-line information services (Rossat et al. 2005) relevant to ESO users and to the community at large, among which are: several archive browsers (for observations, observing programmes and scheduling, user publications), access to the ambient conditions database, and to the Digitized Sky Survey and catalogue servers (GSC, USNO-A2.0, astrometric catalogues). The main ESO archive query form is widely used (91 %). It was re-designed last year for the worldwide opening of the ESO archive on 4 April 2005 (Delmotte et al. 2005). It is intended to aid first-time users of the ESO archive and astronomers with no previous experience with ESO instruments. See Figure 1 for a more detailed usage of the various ESO archive services. The primary reasons for using the ESO archive services are scientific research (86 %) and planning of future observations (51 %). Satisfaction levels for interface, documentation and operation related matters are already quite good, if not excellent (Figure 2).

Publications based on ESO data

63 % of the survey respondents have published papers based on ESO data and 72 % of those respondents actually published papers based on genuine archival data, that is, not belonging to their own observing programmes. This is a noteworthy trend for a ground-based observatory. As already noticed by other astronomical data centres (Walsh and Hook 2006), archive-based research is indeed becoming prominent. However, the size and variety of data are rising fast, meaning more complexity for the end users of the ESO archive. Thus, to improve the scientific return of the archive, the ESO VO Systems department is actively involved in producing and publishing Advanced Data Products (ADPs), i.e. highly processed ESO data products, ready for immediate scientific use, e.g. the GOODS/ISAAC data release (Retzlaff et al. 2005). The largest fraction of ADPs will be provided by the astronomical community, e.g. the Garching-Bonn Deep Survey/WFI data release. Public Survey data products from VISTA and from OmegaCAM at the VLT Survey Telescope will also populate the SAF. In addition, as of Period 75, Principal Investigators of ESO Large Programmes are required to return their data products to the ESO archive at the time of publication of their scientific results (Pirenne and Quinn 2004). The survey analysis revealed that already one third of archival papers are based on high-level data products (ADPs, EIS, Science Verification, Commissioning data),

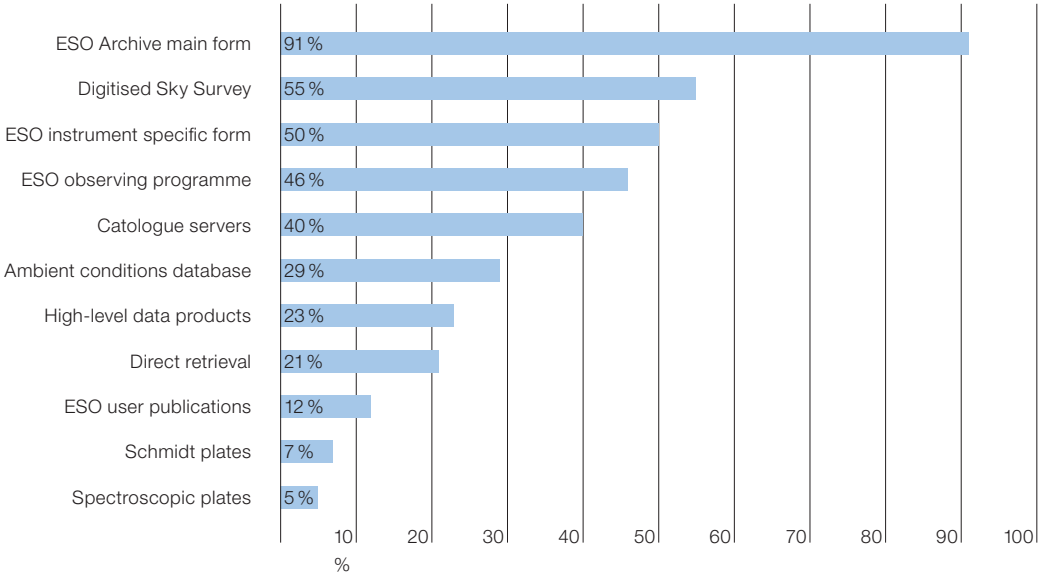

Figure 1: Percentage of usage of ESO SAF services by the survey repondents.

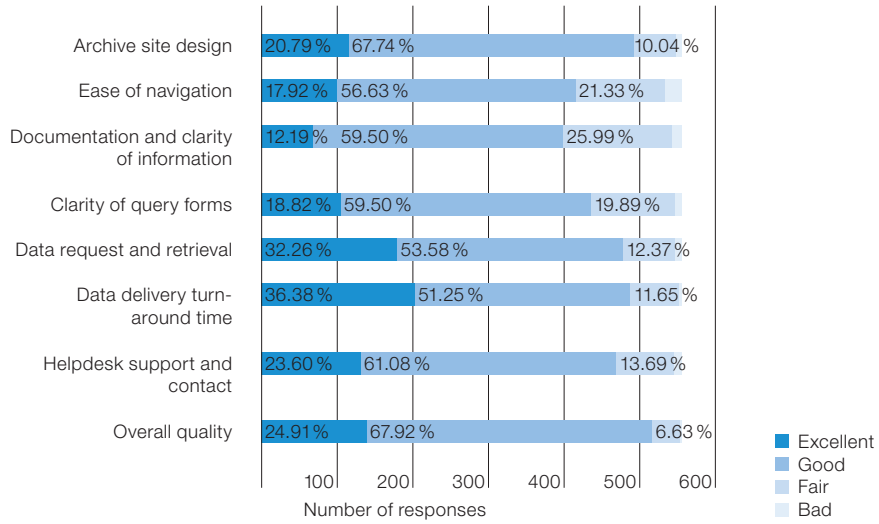

Figure 2: Measures of satisfaction of the survey respondents with the ESO archive.

as opposed to raw data. Given that the ESO archive contains more than 3 000 raw data sets and around 100 high-level data sets, the survey responses in Figure 3 (top) were weighted to better reflect the science productivity based on either raw data or high-level data products. Thus a high-level data set is approximately 15 times more likely to lead to a scientific publication than a raw data set (Figure 3, bottom). Similar trends are apparent from other archive facilities, such as HST. This is one more indication that ADPs are valuable components of the ESO SAF and are likely to foster its scientific exploitation.

ESO SAF development plan

Answers and satisfaction levels gathered from the present survey helped identifying areas needing improvement and this will drive the actual archive development. The analysis of responses, including free input text comments and suggestions, revealed that most users already consider the SAF services satisfactory but indicate areas of improvements. The main user requests are: more complex/powerful query capabilities but still with easy/light interface, more ADPs and data reduction support, easy and direct access to calibrations, and better characterisation of data. In particular, the possibility to search the ESO archive by input list of coordinates, to quickly access data previews, and the ability to search by object class being the most frequently requested new features (see Figure 4), these will be taken into high consideration. Finally, 41 % of the survey participants consider they are not sufficiently kept informed about what is new in the ESO archive. As a solution, regular archive headlines will be published in the ESO Messenger in addition to the news and announcements that are currently advertised on the main archive web page.

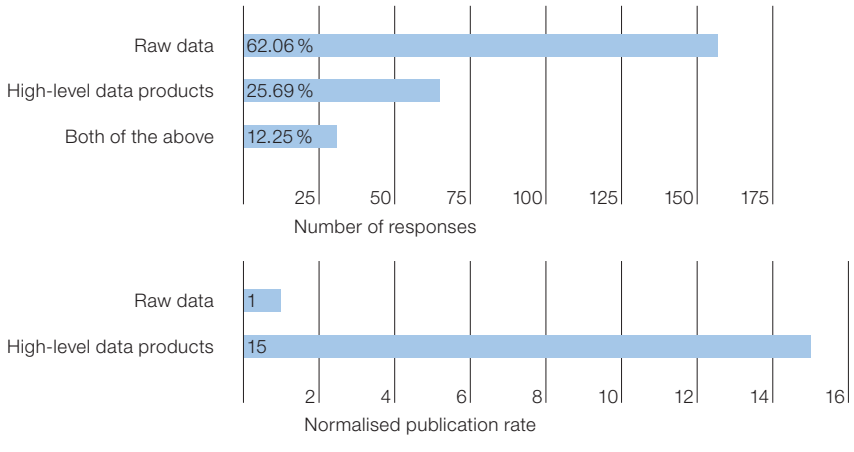

Figure 3: Top: Nature of the data used in ESO archival papers. **Bottom:** Scientific productivity of raw versus high-level data sets, given a quantity ratio of raw to high-level of 3 000 : 100.

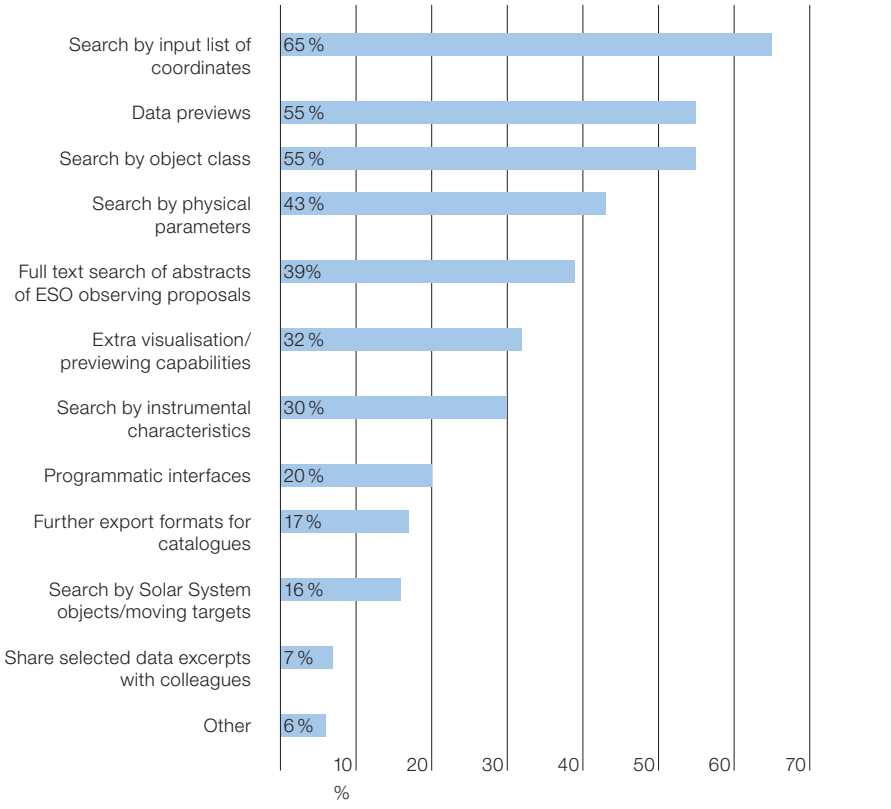

Figure 4: List of features the survey respondents would like to see in the ESO science archive interface.

Latest News

After the completion of the survey, a number of improvements have already occurred at the ESO SAF. The possibility to upload a list of both coordinates and object names has been added to the main ESO archive query form. The first APEX-2A Science Verification data were released and the APEX instrument specific query form is now available. Finally, the VO Systems department has already started to implement services compliant with the VO access methods and formats. As a way to receive more feedback and to ensure that the ESO SAF continues to address its user needs, more surveys will be issued in the future. New survey results will help focus efforts to develop and enhance the ESO SAF services to the astronomical community.

Acknowledgements

We would like to thank all the ESO archive users and respondents of the present survey for their time and valuable comments.

References

Science Archive Facility: *http://archive.eso.org/*

Delmotte N. et al. 2005, to appear in ADASS XV ASP Conf. Proc.

Retzlaff J. et al. 2005, to appear in ADASS XV ASP Conf. Proc.

Rossat N. et al. 2005, ADASS XIV ASP Conf. Series 347, 674

Padovani P. and Quinn P. 2005, The Messenger 122, 22

Pirenne B. and Quinn P. 2004, The Messenger 116, 48

Walsh J. and Hook R. 2006, ST-ECF Newsletter 40, 6

FriOWL: A Site Selection Tool for the European Extremely Large Telescope (E-ELT) Project

Marc Sarazin[1]
Eddie Graham[2]
Hervé Kurlandczyk[1]

[1] ESO
[2] University of Fribourg/University of Berne, Switzerland

A systematic approach to site characterisation has been undertaken by ESO with the development of a geographical information tool dedicated to astroclimatology at the Department of Geography, University of Fribourg (Switzerland).

FriOWL for Global Analysis

FriOWL is a tool dedicated to tracking climatic trends and has been developed for ESO by the Department of Geography of the University of Fribourg, Switzerland (Graham et al. 2005). This tool has the primary function of helping to locate the most promising areas worldwide on the basis of the long-term average of various climate parameters. It also allows the estimation of the seasonal variability of these climate parameters at a given location, as well as their sensitivity to long-term climate change. FriOWL also allows the calculation of the anomaly coefficient of each climatic parameter with respect to the long-term average.

FriOWL (*http://archive.eso.org/friowl*) is a geographical information system with a spatial resolution of 2.5 degrees (ca. 300 km), It is composed of many different climatic layers containing a minimum of 15 years of data stored as monthly averages (the final goal is to have 45 years of data of all variables). The study of the temporal variability of the different layers gives new information on the seasonal and long-term climatology of the areas with selected sites. The nature of each of the layers has been chosen according to the expected sensitivity of ELT science to the different atmospheric parameters.

FriOWL Version 2.1 deals mainly with global climatological data, known as *reanalyses*. Reanalyses are the best available consensus of the global atmospheric system at any one time. They consist of reconstructions of the daily weather patterns from the 1950s to the present, using the latest numerical weather prediction and assimilation models. Reanalyses data come from two main centres, namely the joint National Centers for Environmental Prediction/National Center for Atmospheric Research in the USA (henceforth known as NCEP/NCAR) and the European Reanalysis products from the European Centre for Medium Range Weather Forecasting (henceforth known as ERA). Additional data, such as Outgoing Longwave Radiation (OLR) from NOAA, and the Aerosol Index from the Total Ozone Mapping Spectrometer (TOMS) satellite, are also included in the FriOWL database.

The FriOWL (latest version 2.1) database uses a temporal resolution of monthly means, with the total database ranging in length from 15 to 55 years, depending on the variable in question. Later, it will be possible to include higher temporal resolutions (e.g. daily, or possibly up to six-hourly). Most of the NCEP/NCAR parameters start in 1948, running through to the present, giving over 50 years of good quality data. The ERA dataset used in FriOWL Version 2.1 consists of data mostly from the ERA-15 project, a reanalysis covering the fifteen years between 1979 and 1993. A new, much longer 44-year reanalysis product, known as ERA-40, has been recently released and spans the period from September 1957 to August 2002. We hope to include ERA-40 in a later version of FriOWL.

Climatological analysis: the VLT site survey revisited

Identifying potential candidates for major ground-based astronomical projects is hardly a simple process and many factors other than science performance may sometimes blur the picture. But how can we be sure that no areas with strong potential have been ignored? Also the time schedules for project completion are often shortened because of the competition for funding and science delivery. Thus the site characterisation period which precedes the site selection process is often reduced to a minimum, typically 12 to 24 months. Therefore, how can we know whether the relatively short testing period is representative of the long-term history of the areas studied?

Within the next three years, more than 10 sites will be fully characterised by the various ELT groups in the world. And because much care was taken to use instruments which, if not always identical, are very similar and in any case repeatedly cross-calibrated, the data accumulated can easily be merged and the sites cross-compared for the benefit of all institutions. FriOWL will allow the assessment of the sensitivity of the candidate sites to climate change.

It is tempting of course to use FriOWL to verify that the previous astronomical projects have been well sited. In Figure 1, the cloud cover during the VLT site survey period (1984–1990) has been re-situated within the twice longer time span available in FriOWL (1979–1993) as an illustration of the power of FriOWL to detect climatological anomalies. In this figure, the pixels surrounding Paranal show a very low anomaly while the Amazon basin was 10 % clearer than usual and the north-west of the continent was up to 10 % cloudier. Note that the current spatial resolution of FriOWL is sufficient for the analysis of climatological fluctuations which are linked to large-scale synoptic patterns (i.e. the 'highs' and 'lows' on a weather chart). On the other hand, the longer time coverage provided by ERA-40 is required for a better variability assessment.

Site short-listing

Most existing observatories housing international facilities have high standards and are natural candidates for future projects, unless they suffer from a lack of space or environmental restriction, such as Mauna Kea (Hawaii), providing only second-choice areas compared to the summit ridge (e.g. TMT). Several ELT sites surveys are currently conducted on well-known places such as La Campanas in Chile (GMT), San Pedro Martir in Mexico (TMT) and Roque de los Muchachos in Canary Islands (E-ELT). With the perspective of a lower weather downtime than in the Canary Islands during winter, the anti-Atlas mountain ridge is also considered for the siting of the Euro-

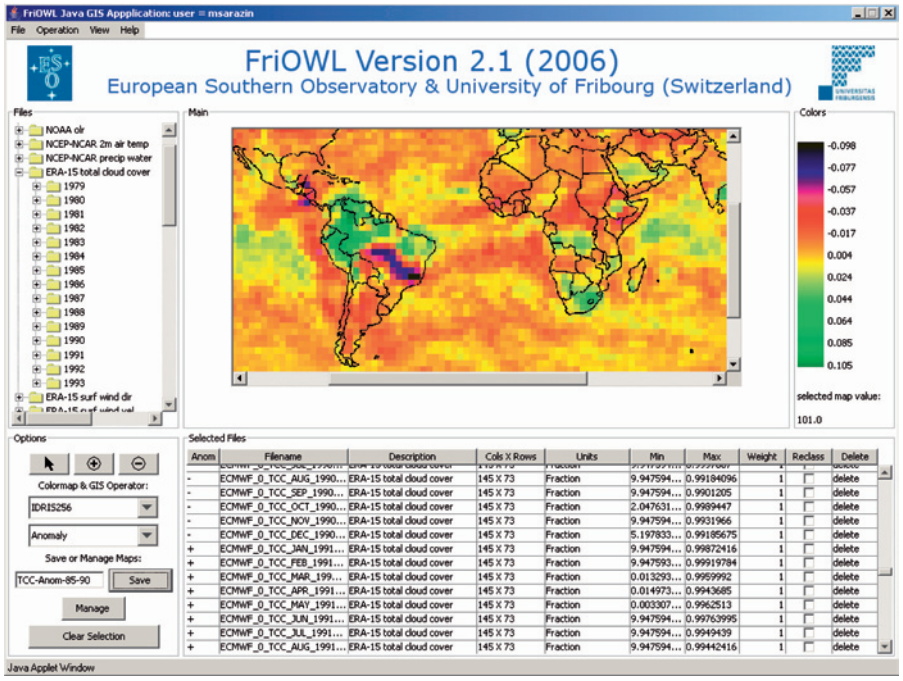

Figure 1: Total cloud cover anomaly of the VLT site testing period (1984–1990) with respect to the longer term average (1979–1993). The Paranal pixel shows a very low anomaly while the Amazon basin was 10 % clearer than usual and the north-west of the continent was up to 10 % cloudier.

pean ELT. In the 'photon valley' where the VLT Observatory of Paranal (Chile) resides, ESO plans to characterise a summit ~ 20 km to the north (La Chira) for the E-ELT, while TMT is studying an earlier candidate of the VLT site survey (Armazones) ~ 20 km further to the east.

For middle and far infrared observations, a lower external temperature reduces the thermal background. High elevation mountains also provide low precipitable water vapour (PWV) content. This is the case of the 4 600-m site in the Macon ridge in NW Argentina studied by ESO and Cordoba Observatory which, in addition to low PWV, presents only half the seismic risk of Paranal. This is also the case of the new Franco-Italian Antarctic scientific station of Concordia at Dome C, whose proponents claim that it offers such favorable observing conditions that even a significantly smaller ELT would be highly competitive in some scientific areas.

In addition to topography, FriOWL is currently composed of 11 layers, among which are total cloud cover and precipitable water vapour (PWV). It is possible to combine the FriOWL layers with different weights so as to compose dedicated maps of suitability. An example is given in Figure 2 where topography, PWV and cloudiness have been used as reference parameters for infrared astronomy. It is easy to see that only a few regions on earth are suitable, but these still cover enough area to provide many possible candidate sites.

The wider the observation spectrum of the astronomical facility, the more layers must be added and the narrower the choice becomes. For instance, in UV and V photometry, despite their high number of clear nights, the central Saharan regions where the desert sand is blown upwards before travelling to Europe, Brazil or to the Middle East depending on the seasons, have to be discarded for they contain high aerosol contamination. Note that the aerosol index available in FriOWL (Figure 3) is believed to be related to atmospheric extinction, but this is still debated (Siher, 2004; Varela et al., 2004).

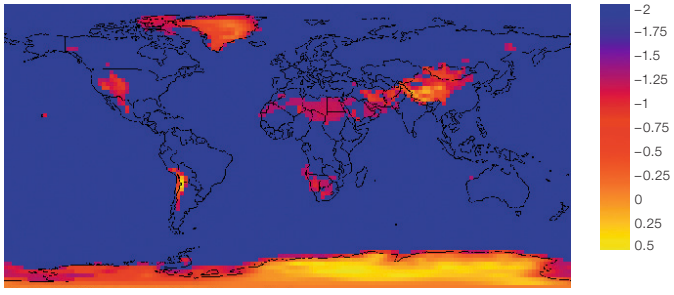

Figure 2: Overlay distinguishing areas providing high summits and low cloudiness as well as low PWV (arbitrary scale) 2.5 degree square pixels.

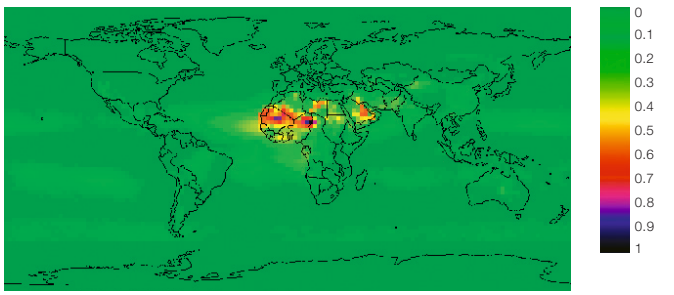

Figure 3: Mean aerosol index (arbitrary scale) as measured by TOMS UV satellite for the period 1980–2002, 2.5 degree square pixels.

Another layer specific to high-resolution observation with adaptive optics is the high-altitude wind speed. Based on radiosoundings performed at the VLT and Gemini sites in Chile by the LUAN (Nice), Sarazin and Tokovinin (2002) have shown that the wind speed at the jet stream level (12 km altitude asl, or 200 hPa pressure level) could be related to the temporal coherence of the wave front to be corrected by adaptive optics. Note that the numerical relation derived for Chilean sites was further confirmed at San Pedro Martir, but not on an island like La Palma (Varela et al., 2004). The experience accumulated at the VLT-NAOS facility shows that the performance of the wavefront correction decreases considerably when the coherence time is shorter than about 3 ms. At Paranal, the coherence time is longer than 3 ms about 80 % of the time in summer, but only 40 % of the time during the rest of the year (Figure 4). The large differences in the 200 hPa FriOWL wind layer for the first (Figure 5a) and the third (Figure 5b) trimester of the year imply that, rather than relying on yearly averages, estimating the efficiency of AO observing on a candidate site should take seasonal variations into consideration.

In order to identify the best candidates within a FriOWL pixel area, the low spatial resolution information can be complemented by the direct use of geostationary satellite imagery. With a resolution better than the size of the observable sky of a ground-based facility, the technique developed by Erasmus (2006) for cloudiness and PWV assessment has proven its usefulness.

European astronomy managed to converge towards a single funding request to the European Commission FP6 framework programme. This gave birth to the 2005–2008 ELT Design Study, a technology development programme coordinated by ESO and conducted by research institutes and industrial companies in Europe. The study covers the development of enabling technologies and concepts required for the eventual design and construction of a European extremely large optical and infrared telescope, with a diameter in the 30- to 60-m range. Site characterisation, exploratory instrument designs, and an assessment of the performance of a segmented aperture

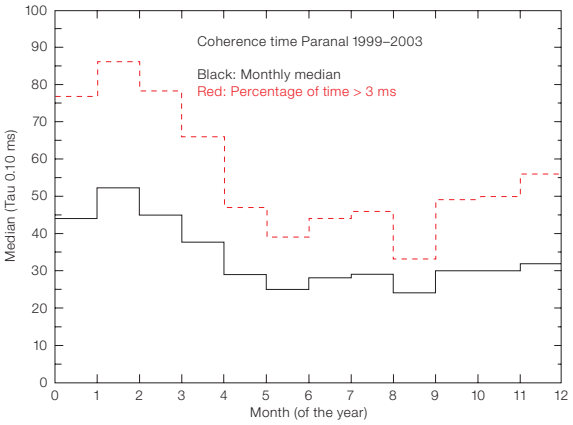

Figure 4: Statistics of the atmospheric coherence time at Paranal showing a strong seasonal trend.

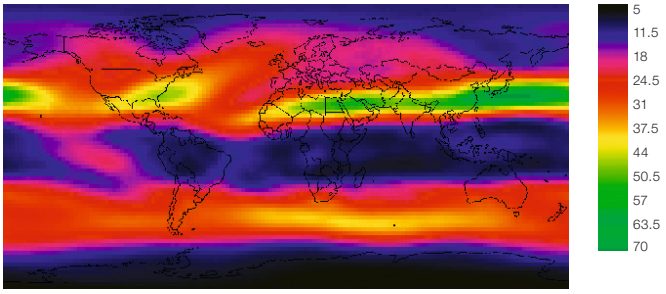

Figure 5a: Mean wind speed at 200 hPA (ca. 12 km above sea level) in m/s for the months of January, February and March during the period 1979–1993, 2.5 degree square pixels.

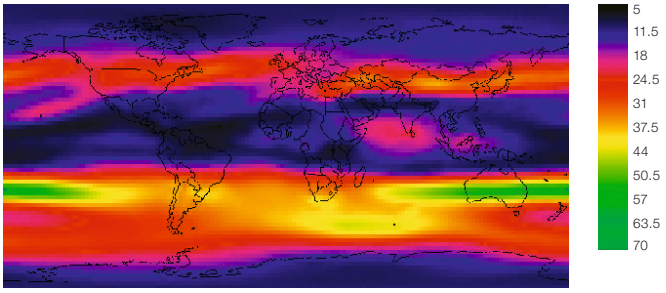

Figure 5b: Same as Figure 5a, but for the months of July, August and September.

exposed to wind on a representative site are also included. Considering the available funds, the site characterisation work package under the responsibility of Nice University (IAC and ESO as deputies) has been limited to four sites (Chile, Canary Islands, Argentina, Morocco) and will be compared to Dome C in Antarctica. It also includes actions for a better understanding of the physics of the turbulence at large scales proposed by Arcetri Observatory, LUAN and ONERA. At the end of the site characterisation period, the E-ELT site selection process will start with the participation of the ESO community at large through the ELT Standing Review Committee (ESRC) in which site activities are covered by Roland Gredel.

Verification of the ALMA site

For the site selection of the ALMA telescope some specific climatic and meteorological requirements were necessary. In particular in order to achieve good observational conditions, Outgoing Longwave Radiation (OLR) and Precipitable Water Vapour (PWV) were identified as key parameters among others to determine suitable sites for millimetre and submillimetre wavelength radio astronomy.

OLR is inversely related to cloud cover and directly related to surface temperature (in the absence of clouds). Increased cloud cover will reduce OLR reaching the top of the atmosphere from the earth's

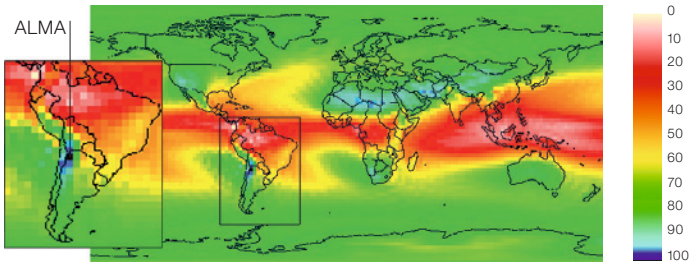

Figure 6: Sum overlay of Outgoing Longwave Radiation (OLR) measured from 1974–2001 and the Precipitable Water Vapour (PWV) measured from 1948–2001. The darkest pixel corresponds to the most appropriate place on the non-icy earth that combines both parameters. The ALMA site (Chajnantor) is included in that dark pixel.

surface and vice versa (Erasmus 2006). Typically the highest values of OLR indicate the high temperature of the earth – because hot regions radiate the greatest amounts of longwave radiation to space. However, thin cirrus clouds trap a significant amount of OLR – thus, lower values of OLR indicate higher than normal presence of cirrus clouds but may also indicate lower than normal surface temperatures (in the absence of clouds). Therefore the icy region such as the poles will not be considered here. The model used in this example has a 2.5° horizontal resolution for the period from June 1974 to December 2001. The units are watts per square metre (W/m^2).

Precipitable water vapour (PWV) is provided as a monthly mean of integrated total column precipitable water vapour in kg/m^2 (which is equivalent to millimetres). It is the mean total amount of water that could be precipitated from the atmosphere. Values typically range from a few mm in cold regions to over 50 mm in the tropics. In the Chajnantor pixel of FriOWL, the PWV is around 2,5 mm which is particularly low. Note that the real Chajnantor PWV value is lower (0.68 mm), because the climate model height at this pixel (approx. 4 000 m) is lower than the real height of Chajnantor (over 5 000 m).

As an example a qualitative composite map was made, by combining the mean Outgoing Longwave Radiation and Precipitable Water Vapour maps of FriOWL. Firstly, in order to have comparable values, the scales of the different units were adjusted and then the PWV values were inverted since we wanted to avoid high values of PWV. Finally, both maps were overlaid upon one another. The result (Figure 6) confirms the Chajnantor pixel as the best possible combination of both parameters on the whole non-icy earth.

References

Erasmus A. D. 2006, Proc. of the IAUS 232, 510
García-Lorenzo B. M. et al. 2004, SPIE Proc. 5489, 130
Graham E. et al. 2005, Meteorological Applications, Vol. 12, Issue 1, 77
Sarazin M. and Tokovinin A. 2002, Proc. to ESO Conference and Workshops 58, 321
Siher E. A. et al. 2004, SPIE Proc. 5489, 138
Varela A. M. et al. 2004, SPIE Proc. 5571, 105

Image of the Robert's Quartet group of galaxies, from *B*, *V*, *R* and *I* observations made with FORS2 on the VLT. Image processing by Henri Boffin, Kristina Boneva and Hans Hermann Heyer (all ESO). See ESO Press Photo 34a/05 for more details.

The ESO-ESA Working Group on Fundamental Cosmology

John Peacock[1]
Peter Schneider[2]

[1] Royal Observatory Edinburgh, United Kingdom
[2] University of Bonn, Germany

In September 2003, the executives of ESO and ESA agreed to establish a number of working groups to explore possible synergies between these two major European astronomical institutions on key scientific issues. The first two working group reports (on Extrasolar Planets and the Herschel-ALMA Synergies) were released in 2005 (Perryman and Hainaut) and 2006 (Wilson and Elbaz), and the report on Fundamental Cosmology has recently been completed (Peacock and Schneider 2006). In this article, we present the major findings and recommendations of this working group (hereafter WG) whose members are John Peacock (Chair, ROE Edinburgh), Peter Schneider (Co-Chair, AIfA Bonn), George Efstathiou (IoA Cambridge), Jonathan R. Ellis (CERN), Bruno Leibundgut (ESO), Simon Lilly (ETH Zürich) and Yannick Mellier (IAP Paris). A number of colleagues made further essential contributions to the report. Support for several face-to-face meetings in Garching was provided by the ST-ECF, particularly Bob Fosbury and Wolfram Freudling.

The WG's mandate was to concentrate on fundamental issues in cosmology. We have thus excluded direct consideration of the exciting recent progress in astrophysical cosmology, such as the formation and evolution of galaxies, the processes of reionisation and the first stars, etc. However, many of our recommended actions will produce vast datasets of general applicability; these will also have a tremendous impact on these broader areas of astronomy.

This is an appropriate time to take stock of the field. The past 10–15 years have seen huge advances in our cosmological understanding, to the point where there is a well-defined standard model that accounts in detail for (nearly) all cosmologically relevant observations. Very substantial observational resources have already been invested, so the next generation of experiments is likely to be expensive. Indeed, the scale of future cosmological projects will approach that of particle physics, both in financial and in human terms. We therefore need to identify the problems that are both the most fundamental, and which offer the best prospects for solution. In doing this, it is hard to look too far ahead, as our views on priorities will doubtless evolve; but planning and executing large new experiments will take time. We intend our report to cover the period up to about 2020, so that ESA's Cosmic Vision 2015–2025 document has been an essential part of our discussion.

Considerations

The recommendations of the WG are based on a number of considerations, given here in approximately decreasing order of relative weight:

What are the essential questions in fundamental cosmology?

The standard model consists of a Universe described by Einstein's theory of general relativity, with a critical energy density dominated by a component that is neither matter nor radiation, but a new entity termed 'dark energy', which corresponds to endowing the vacuum with energy. The remaining energy consists of collisionless 'cold dark matter' (about 22 %) and ordinary 'baryonic' material (about 4 %), plus trace amounts of radiation and light neutrinos. The Universe is accurately homogeneous on the largest scales, but displays a spectrum of inhomogeneities whose gravitationally-driven growth is presumed to account for the formation of galaxies and large-scale structure. The simplest consistent theory for the origin of these features is that the Universe underwent an early phase of 'inflation', at which time the density in dark energy was very much higher than at present. Given this background, there follows a natural set of key questions: (1) What generated the baryon asymmetry? Why is there negligible antimatter, and what set the ratio of baryons to photons? (2) What is the dark matter? Is it a relic massive supersymmetric particle, or something (even) more exotic? (3) What is the dark energy? Is it Einstein's cosmological constant, or is it a dynamical phenomenon with an observable degree of evolution? (4) Did inflation happen? Can we find observational relics of an early vacuum-dominated phase? (5) Is standard cosmology based on the correct physics? Are features such as dark energy artefacts of a different law of gravity, perhaps associated with extra dimensions? Could fundamental constants actually vary?

Which of these questions can be tackled, perhaps exclusively, with astronomical techniques?

It seems unlikely that astronomical observations can currently contribute any insight into baryogenesis. Furthermore, the nature of dark matter may well be best clarified by experiments at particle accelerators, in particular the Large Hadron Collider, or by direct dark matter searches in deep underground laboratories. This particle astrophysics approach may also tell us much about other fundamental issues, such as the law of gravity, extra dimensions, etc.

However, astronomical tools will also make essential contributions to these problems. They can constrain the dark matter constituents via their spatial clustering properties and/or their possible annihilation signals. Astronomy is also probably the best way to measure any time variability of the fundamental 'constants'. Finally, the nature of dark energy and the physics of inflation can be empirically probed, according to our current knowledge, only in the largest laboratory available – the Universe itself.

What are the appropriate methods with which these key questions can be answered?

Studies of the dark energy equation of state can profit from four different methods: the large-scale structure of the three-dimensional galaxy distribution, the abundance of galaxy clusters, weak gravitational lensing, and the distance-redshift relation as measured from distant supernovae. An attempt was made to judge the relative strengths of these meth-

ods, where we took into account the detailed quantitative investigation of the USA's Dark Energy Task Force (*http://www-astro-theory.fnal.gov/events/detf.pdf*). All methods will require a substantial improvement of measurement accuracies, so that that unanticipated systematic limits may become a problem. Given the central importance of this key question, pursuing only a single method therefore bears an unacceptable risk.

The physics of inflation can be studied by three main methods: the direct detection of gravitational waves from the inflationary epoch; the B-mode polarisation signal of the cosmic microwave background (CMB) generated by gravity waves; and a precise measurement of the slope and curvature of the density fluctuation power spectrum. These are bounded by CMB measurements at the largest scales, and weak lensing and Lyα forest studies at the smallest scales.

Which of these methods appear promising for realisation within Europe, or with strong European participation, over the next ~ 15 years?

This issue is subject to considerable uncertainty, as it depends on the funding situation as much as on international developments, in particular when it comes to cooperation with partners outside Europe. Nevertheless, much work has been invested in planning for potential future projects, so in many cases there is a strong basis on which to pick the best future prospects. Certainly, there is no shortage of input, and it is a sign of the scientific vitality of European cosmology that there are unfortunately more attractive ideas than can feasibly be funded. Given the interagency nature of this WG, we have naturally chosen to emphasise particularly timely opportunities for collaboration between these two major players in European astronomy.

Which of these methods has a broad range of applications and a high degree of versatility even outside the field of fundamental cosmology?

Given that the next major steps towards answering the key cosmological questions will in any case require substantial resources, it is desirable that the projects to be pursued should lead to datasets of general applicability. Whereas the cosmological issues are the prime science drivers of these projects, and determine their specifications, a broad range of applications will increase the scientific value of the investments, and boost their level of support in the community.

Recommendations

Based on these considerations, our recommendation are as follows:

1. ESA and ESO have the opportunity to collaborate in executing an imaging survey across a major fraction of the sky by constructing a space-borne high-resolution wide-field optical and near-IR imager and providing the essential optical multi-colour photometry from the ground. The ESO Public Surveys VST/KIDS and VISTA/VIKING will be essential pathfinders for this sort of data, but substantial increases in grasp and improvements in image quality will be needed in order to match or exceed global efforts in this area. Near-IR photometry is essential for obtaining reliable photometric redshifts, in particular for galaxies beyond redshift unity, but also to minimise the fraction of outliers at lower redshifts. VISTA will be able to perform this role to some extent with regard to KIDS. However, imaging in space offers huge advantages in the near-IR via the low background, and this is the only feasible route to quasi all-sky surveys in this band that match the depth of optical surveys. Therefore,
   - ESA should give the highest immediate priority in its astronomy programme to a satellite that combines this near-IR photometry with high-resolution optical imaging, and in parallel,
   - ESO should give high priority to expanding its wide-field optical imaging capabilities to provide the required multi-band photometric data.
   - Furthermore, since the calibration of photo-*z*'s is key to the success of this plan, ESO should aim to conduct large spectroscopic surveys spread sparsely over ~ 10 000 deg^2, involving > 100 000 redshifts. This will require the initiation of a large key programme with the VLT, integrated with the imaging survey.

   This project will be an invaluable asset for several of the methods mentioned before. It will provide the necessary data for weak lensing and large-scale structure studies of the dark energy component in the Universe. Furthermore, it will provide an indispensable dataset for statistical studies of dark energy using galaxy clusters, yielding the means to determine redshifts and optical luminosity of X-ray and SZ-selected clusters, as provided by, e.g., eROSITA and Planck. In addition, such a project (essentially 2MASS with a 7 magnitude increase in depth plus an SDSS imaging survey 4 magnitudes deeper and with ~ 3 times larger area), together with highly accurate photometric redshifts for galaxies and quasars, would be a profound resource for astronomy in general, a legacy comparable in value to the Palomar surveys some 50 years ago. Among the numerous applications of such a dataset, we mention the selection of targets for deep spectroscopic studies, either for the VLT, the JWST and finally an ELT.

2. The existence of major future imaging surveys presents a challenge for spectroscopic follow-up. For some applications, such as weak gravitational lensing, photometric redshifts with few per cent precision are sufficient. But some science questions need true spectroscopy, and this presents a problem of grasp. A capability for massive multiplexed deep spectroscopy (at the level of several thousand simultaneous spectra over a field of order one degree) is required for this. Such a facility would permit surveys of > 10^6 redshifts needed to probe dark energy using the galaxy power spectrum as a standard ruler, and there are a number of international plans for instruments of this sort. ESO should secure access to such an instrument, either through the development of such a facility for the VLT, or as a collaborative arrangement with an external project,

perhaps in conjunction with sharing some of Europe's proposed imaging data.

3. A powerful multi-colour imaging capability can also carry out a supernova survey extending existing samples of $z = 0.5$–1 SNe by an order of magnitude, although this requires the imager to be of 4-m class. In order to exploit the supernova technique fully, an improved local sample is also required. The VST could provide this, provided that time is not required for other cosmological surveys, in particular lensing.

4. Whereas the WG sees the main science drivers for a European Extremely Large Telescope (E-ELT) as lying in other fields of astronomy, we recommend that the following applications in fundamental cosmology should be regarded as forming an essential part of the E-ELT capability:
– Supernova surveys need to be backed up with spectroscopy to assure the classification for at least a significant subsample and to check for evolutionary effects. The spectroscopy requires access to the largest possible telescopes, and an E-ELT will be essential for the study of distant supernovae with redshifts $z > 1$.
– A European ELT will also be important in fundamental cosmology via the study of the intergalactic medium. Detailed quasar spectroscopy can limit the nature of dark matter by searching for a small-scale coherence length in the mass distribution. These studies can also measure directly the acceleration of the Universe, by looking at the time dependence of the cosmological redshift. Furthermore, by providing information of the density fluctuation power spectrum at the smallest scales, the Lyman-α forest provides the biggest lever arm on the shape of the power spectrum, and thus on its tilt and its potentially running spectral index.
– E-ELT quasar spectroscopy also offers the possibility of better constraints on any time variation of dimensionless atomic parameters such as the fine-structure constant α and the proton-to-electron mass ratio. There presently exist controversial claims of evidence for variations in α, which potentially relate to the dynamics of dark energy. It is essential to validate these claims with a wider range of targets and atomic tracers.

5. In the domain of CMB research, Europe is well positioned with the imminent arrival of Planck. The next steps are (1) to deal with the effects of foreground gravitational lensing of the CMB and (2) to measure the 'B-mode' polarisation signal, which is the prime indicator of primordial gravitational waves from inflation. The former effect is aided by the optical/near-IR imaging experiments discussed earlier. The latter effect is potentially detectable by Planck, since simple inflation models combined with data from the WMAP CMB satellite predict a tensor-to-scalar ratio of $r \simeq 0.15$. A next-generation polarisation experiment would offer the chance to probe this signature in detail, providing a direct test of the physics of inflation and thus of the fundamental physical laws at energies $\sim 10^{12}$ times higher than achievable in Earth-bound accelerators. For reasons of stability, such studies are best done from space; we thus recommend such a CMB satellite as a strong future priority for ESA and the support of corresponding technological developments.

6. An alternative means of probing the earliest phases of cosmology is to look for primordial gravity waves at much shorter wavelengths. LISA has the potential to detect this signature by direct observation of a background in some models, and even upper limits would be of extreme importance, given the vast lever arm in scales between direct studies and the information from the CMB. We thus endorse space-borne gravity-wave studies as an essential current and future priority for ESA.

7. A future Square Kilometre Array would provide colossal advances in the field of radio astronomy and, depending on its design, also in fundamental cosmology. It might be able to provide a spectroscopic (21 cm) redshift survey of $\sim 10^8$ galaxies and to study the large-scale structure and its baryonic oscillations with unprecedented accuracy out to redshifts $z \sim 11.5$. This project will operate on a longer timescale, and is a natural successor to the studies described above. A strong European participation in the SKA is therefore essential.

References

Peacock J. A. and Schneider P. 2006, Fundamental Cosmology, ESA-ESO Working Groups Report (see *http://www.stecf.org/coordination/esa_eso/wg.php?working_group=cosmology*)

Perryman M. and Hainaut O. 2005, Extra-solar planets, ESA-ESO Working Groups report (see *http://www.stecf.org/coordination/esa_eso/extrasolar/report.pdf*)

Wilson T. L. and Elbaz D. 2006, The Herschel-ALMA Synergies, ESA-ESO Working Groups report

Image of the Sombrero Galaxy, from the VLT Photo Gallery.

Report on

The XXVIth IAU General Assembly

held in Prague, Czech Republic, 14–25 August 2006

Peter Shaver (ESO)

Photos: H. H. Heyer, ESO (2)

The IAU President of the past three years, Dr. Ron Ekers, addressing the Opening General Assembly.

The recent XXVIth General Assembly of the International Astronomical Union, held on 14–25 August in Prague, was a great success. These triennial events always provide a unique opportunity to experience first-hand the progress across the entire range of astronomy, as well as to meet friends and colleagues from one's own and other sub-fields, and this General Assembly certainly lived up to expectation. Some 2 800 participants from around the world attended this event.

There were six full symposia during these ten days, seventeen joint discussions (many of which were also more than a day in length), nine special sessions including two on recent 'Hot Topics', as well as meetings of the twelve divisions and forty-one commissions, and the opening and closing general assemblies themselves. Still other scientific meetings took place, including the annual meeting of the European Astronomical Society and meetings on Gaia and ALMA. Thus, the highly-publicised discussion on the definition of Solar-System planets was just one amongst an enormous range of topics, from the history of astronomy to discussions of possibilities for astronomy on the Moon, from business meetings to future large-scale facilities, from NEOs to black holes to the frontiers of cosmology. The scale of an IAU General Assembly is truly vast.

The setting of this year's General Assembly was magnificent Prague, which also hosted the 1967 General Assembly, and the evenings and weekends provided ample opportunities for participants and guests to experience this city and its great astronomical history. Social events included a traditional ensemble performance, a concert by the Prague Philharmonia, the official dinner with the theme "Back to the Thirties", and a comprehensive suite of tours of Prague and elsewhere in the Czech Republic. Our Czech colleagues were wonderful hosts, and the overall organisation of the myriad aspects of this huge assembly was absolutely professional and flawless.

Highlights of the General Assemblies include plenary invited discourses, and this year they were given by Jill Tarter ("The Evolution of Life in the Universe"), Alan Title ("The Magnetic Field and its Effects on the Solar Atmosphere as Observed at High Resolution"), Shuang Nan Zhang ("Similar Phenomena at Different Scales: Black Holes, Sun, Supernovae, Galaxies and Galaxies Clusters"), and Reinhard Genzel ("The Power of New Experimental Techniques in Astronomy: Zooming in on the Black Hole in the Centre of the Milky Way"). A cosmology prize from the Peter Gruber Foundation and co-sponsored by the IAU was awarded to John Mather for his work on the cosmic microwave background.

A meeting such as this is far too vast to summarise, especially as events took place in parallel. But for any one participant there was a wonderful range of topics to choose from – a unique opportunity to broaden one's horizons and learn about many different fields as well as one's own. There will of course be publications covering all the symposia, and many of the other events will be recorded in various ways, including web sites and publications.

Here we can at least list the range of topics covered by the symposia and joint discussions, and mention a few of the special meetings held in addition. The six symposia covered galaxy evolution, near-earth objects, triggered star formation in a turbulent interstellar medium, black holes across the range of masses, convection in astrophysics, and binary stars in contemporary astrophysics. The joint discussions covered cosmic particle acceleration, pulsar emission, solar active regions and magnetic structure, the ultraviolet Universe, the top of the stellar M-L relation, neutron stars and black holes in star clusters, the Universe at $z > 6$, solar and stellar activity cycles, supernovae one millennium after SN 1006, planetary exploration missions, pre-solar grains as astrophysics tools, long wavelength astrophysics, large surveys for galactic astronomy, dense stellar systems, new cosmology results from the Spitzer

The large and prominent ESO stand presented ESO's activities to the participants of the General Assembly.

Space Telescope, nomenclature/precession/new models in fundamental astronomy, and seismology of the Sun and sun-like stars.

The special sessions included astronomical facilities of the next decade, teaching and learning astronomy methods, the Virtual Observatory, 'Hot Topics', astronomy for the developing world, astronomical data management, and astronomy in Antarctica. Amongst the future astronomical facilities discussed were JWST, ALMA, LOFAR, the SKA, the TMT, the GMT, the European ELT, high-energy facilities, gravity-wave facilities, neutrino facilities, and the Virtual Observatory. A following session covered future plans from NASA, ESA, Japan, China, the NSF, European strategic planning, and the OECD. Working groups and other activities included astronomical libraries, women in astronomy, young astronomers, 'Universe Awareness' geared to small children primarily in developing countries, and plans for the Year of Astronomy in 2009. In the back-ground to all of this, of course, were the many business meetings of the IAU executive and the divisions and commissions, essential for the world's organisation on astronomy. Resolutions and definitions important to astronomy are decided upon at the general assemblies, and a well-known outcome of this General Assembly was the definition of a planet in the Solar System; the final version resulted in eight Solar-System planets (Mercury, Venus, Earth, Mars, Jupiter, Saturn, Uranus and Neptune), with Pluto having the distinction of being the prototype of a new category of trans-neptunian objects. The final version of the two relevant resolutions can be found at *http://www.iau.org/fileadmin/content/pdfs/resolution_ga26-5-6.pdf.*

Photo: L. H. Nielsen, IAU

Dr. Catherine Cesarsky (right), fully engaged in discussions at the Women in Astronomy luncheon.

Photo: H. H. Heyer, ESO

Two former Directors General of ESO, who were both also Presidents of the IAU, attended the General Assembly: Prof. Adriaan Blaauw (IAU President 1976–1979; shown in this photo), and Prof. Lodewijk Woltjer (IAU President 1994–1997).

The IAU General Assembly is where the new officers of the IAU executive, divisions and commissions are elected every three years. The new officers of the executive include Prof. Karel A. van der Hucht of SRON, Netherlands, new IAU General Secretary, Dr. Robert Williams of the Space Telescope Science Institute, new President-Elect, Dr. Catherine Cesarsky, ESO Director General and new President, and Dr. Ian Corbett (ESO), new Assistant General Secretary. Dr. Cesarsky is the first woman to have the high distinction of being the President of the IAU. The full lists of new IAU officers can be found on the IAU website *http://www.iau.org/.*

Further details about the recent IAU General Assembly in Prague can be found at *http://www.astronomy2006.com/* including PDF copies of the daily newspaper "*Dissertatio cum Nuncio Sidereo III*" at *http://astro.cas.cz/nuncius/.*

The IAU General Assemblies provide by far the best opportunity for all astronomers from around the world, and particularly young astronomers, to learn about the frontiers of all areas of astronomy, and to meet the leaders in all fields. Narrow topical specialist meetings obviously play a very important role in astronomy today, but they cannot possibly provide the breadth, perspective and learning opportunities of an IAU General Assembly. Also, when one has worked in a variety of fields, this is the only way to meet one's colleagues from all of those fields. An IAU General Assembly is a truly global experience, in the widest sense.

Photo: E. Janssen, ESO

New IAU Officers: from left to right, Prof. Karel A. van der Hucht of SRON, Netherlands, new IAU General Secretary, Dr. Robert Williams of the Space Telescope Science Institute, new President-Elect, Dr. Catherine Cesarsky, ESO Director General and new President, and Dr. Ian Corbett (ESO), new Assistant General Secretary.

The new IAU President, Dr. Catherine Cesarsky, addressing the Closing General Assembly.

Photo: E. Janssen, ESO

The next IAU General Assembly will take place in Rio de Janeiro, in 2009. The year 2009 will be a very special one for astronomy, as it is the 400th anniversary of Galileo's first observations with a telescope. The IAU has proposed that 2009 should be designated the International Year of Astronomy; UNESCO has endorsed this resolution, and it is hoped that the UN will soon follow. This will provide an exceptional opportunity to highlight astronomy's role in world culture and science, and many related initiatives will be undertaken in countries and internationally around the world. 2009 is also the 90th anniversary of the IAU, and on 22 July of that year the longest duration total solar eclipse of the 21st century will take place. Thus, the 2009 General Assembly will be a very special one – the centrepiece of the International Year of Astronomy activities.

Report on the Conference on

Library and Information Services in Astronomy: LISA V

held in Cambridge, Massachusetts, USA, 18–21 June 2006

Uta Grothkopf (ESO)

LISA V, the latest in the series of conferences on Library and Information Services in Astronomy, was held in Cambridge, Massachusetts, in June 2006. More than 100 astronomy librarians, data archive specialists, publishers, and astronomers from 24 countries discussed tools and trends in information retrieval and management. As with previous conferences, ESO played a major role in the organisation and support of LISA V.

Information retrieval, access and storage are changing at a fast pace. Traditionally, astronomy has often been a leader in pursuing and implementing evolving technologies earlier than other subject areas. The reasons are the comparatively small number of core journals and databases in astronomy that are excellent testbeds for new tools and techniques, as well as generous funding from space agencies and non-profit organisations. Hence, astronomy librarians are often already applying technologies in their day-to-day work with which colleagues in other disciplines are just becoming acquainted. LISA (Library and Information Services in Astronomy) conferences provide an excellent forum to keep astronomy librarians informed about news in the fields of networked databases, digital data creation and preservation as well as experimental navigation and knowledge discovery tools.

So far, five LISA conferences have been held: the first international meeting ever held specifically for astronomy librarians took place in Washington, DC in 1988; LISA II was hosted by ESO in Garching, Germany in 1995; LISA III and IV were held in Puerto de la Cruz, Tenerife, Spain in 1998 and Prague, Czech Republic in 2002, respectively.

In June 2006, the fifth LISA conference took place in Cambridge, MA, USA, co-hosted by the Libraries of the Harvard-Smithsonian Center for Astrophysics and Massachusetts Institute of Technology. The conference was attended by 105 participants from 24 countries. Among them were once again almost 20 colleagues who attended thanks to financial aids provided through the Friends of LISA (FOL) committee; FOL traditionally raises funds from vendors, professional societies, institutions, and individuals in order to help astronomy librarians in resource-poor countries to attend LISA conferences. ESO traditionally has made generous donations to FOL. In addition, the local organisers managed to col-

lect funds from an impressive number of commercial and institutional sponsors.

The conference motto, "Common Challenges, Uncommon Solutions", reflected on the fact that LISA conferences provide an opportunity for astronomy librarians from all over the world to exchange ideas with their colleagues about professional problems they have encountered in their own libraries, as well as the solutions they have found. LISA is unique in this sense as no other meeting showcases so many individual projects from our subject area.

The meeting organisers (with Uta Grothkopf, ESO, and Christina Birdie, IIA, co-chairing the SOC and Donna Coletti from Harvard CfA chairing the LOC) were able to attract the highest number of invited speakers ever. This was possible thanks to the excellent conference location with invited speakers from Harvard University and MIT, among them keynote speaker John Huchra, Professor at Harvard University, and Owen Gingerich, Professor Emeritus at the Harvard-Smithsonian Center for Astrophysics.

The programme consisted of 37 talks, organised in eight sessions, as well as 35 posters, a poster review and a panel discussion. Some of the highlights of the conference included talks on libraries in the VO era, citation analysis for observatories, the history of astronomy and astronomical archives as well as the future of scientific publishing.

Figure 1 illustrates a few subjects covered by LISA conferences and how their fraction of the programme has changed over time. *Collection Development*, including topics like literature acquisition from foreign countries and handling of non-print material, outnumbered all other topics at LISA I, but played a far smaller role during subsequent meetings. *Electronic Journals* started to become available around LISA II (with the electronic *ApJ Letters* first being published in 1995) and had developed into a well-established topic by the time LISA III was held in 1998. E-journals introduced new business models in libraries where traditional purchasing of material is supplemented or even substituted by licensing (leasing) contracts; this, in turn, led to the *Open Access* movement that aims at open availability of scientific literature without subscription fees.

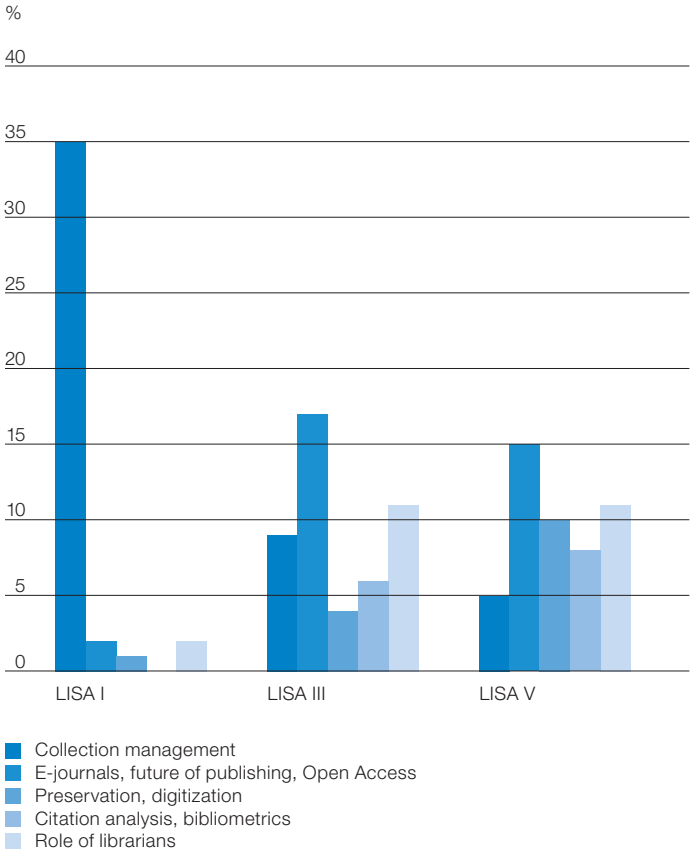

Figure 1: Selected subject areas covered by LISA I, III and V and their fraction of the programme. For explanation, see the text.

In order to guarantee future access to print as well as electronic documents, a long-term archiving strategy must be in place. *Preservation* and *Digitization* were strongly represented topics at LISA conferences in particular during recent meetings. *Citation Analysis and Bibliometrics* are comparatively 'young' subject areas that are receiving more and more interest by managements and funding authorities; in most observatories, librarians are engaged in compiling telescope bibliographies and deriving statistics. Our final example of topics, the *Role of Librarians*, has been a constant matter of attention at LISA conferences as the work area of astronomy librarians evolves and opens new professional opportunities.

The conference proceedings will be published in print and electronic format in the ASP conference series and will be edited by Sandra Ricketts (AAO), Eva Isaksson (University Helsinki Observatory) and Christina Birdie (Indian Institute of Astrophysics). Given the fast pace with which technologies and work procedures in libraries are changing, many participants felt that the current four-yearly cycle of LISA conferences should be shortened. So, after the proceedings have been published, it may be time to start planning LISA VI ...

Related websites

LISA V information: *http://cfa-www.harvard.edu/library/lisa/*
Author instructions and news regarding the proceedings: *http://www.astro.helsinki.fi/library/lisa5/authors/*
General website for information on past and future LISA conferences: *http://www.eso.org/libraries/lisa.html*

Further reading

Corbin B. G. and Grothkopf U., LISA – The Library and Information Services in Astronomy conferences. In: Organisations and strategies in astronomy (OSA), Vol. 7, Heck A. (ed.), Springer, Dordrecht, ISBN 1-4020-5300-2, in press (*http://www.eso.org/libraries/lisaconferences.pdf*)

New ALMA Site Museum Preserves Valuable Local Culture

Gonzalo Argandoña, Felix Mirabel (ESO)

The construction of ALMA close to the village of San Pedro de Atacama is making contributions to other sciences besides astronomy.

More than 10 000 years ago, human beings arrived at the Atacama Desert for the very first time. For generations, they managed to survive in this harsh environment, giving birth to a myriad of unique cultures and traditions, whose origins and evolution are still subject to intense research by anthropologists, historians, archaeologists, geneticists and linguists.

Thanks to the environmental studies that have been an essential part of ALMA construction since the beginning of the works, including archaeological surveys of the area, scientists now have fresh knowledge of the old history of Chajnantor and nearby areas. Part of this significant comprehension is expressed in the new ALMA site museum, which was inaugurated in July 2006 at 3 200 m altitude, close to the Operations Support Facility (OSF). The museum is a realistic reconstruction of one of the twenty old *estancias* that have been discovered in the area, between 2 800 and 4 000 metres altitude, by the Chilean archaeologist and ALMA consultant, Ana María Barón.

The corrals and dormitories made of stone may seem basic at first glance, but they are the material expression of an old, vanishing way of life, in which Andean shepherds used to stay in an *estancia* as long as they had enough water and vegetation for their cattle. When the moment came, complete families moved to a different *estancia*, with more water and food for their animals.

In recent decades, those families have tended to move closer to the lower and more benign lands of the *Salar de Atacama*, leaving behind the ancient high *estancias* due to the growing scarcity of rain. In fact, the *Estancia Barrios* – where the ALMA site museum is now placed – was finally abandoned in the '60s by the family of Pedro Cruz, who spent part of his infancy on the high-land *estancias* that now are silent witnesses of the progress of ALMA construction. Pedro Cruz was one of the main guests at the inauguration event of the site museum, in a very symbolic ceremony that was hosted by Massimo Tarenghi, ALMA director, and ALMA executives in Chile.

Photo: J. Atvujar, El Mercurio

Pedro Cruz (left) explains to Felix Mirabel, ESO Representative in Chile, his early years at *Estancia Barrios*, one of the twenty old *estancias* located at an altitude between 2 800 and 4 000 metres that were abandoned in the last decades. *Barrio* was rebuilt and transformed into a site museum. At the back, Marcela Hernando, Intendenta of Chile's Region II, and Sandra Berna, major of San Pedro de Atacama.

The Intendenta Marcela Hernando, representative of the President of Chile in Region II, celebrated the integration of different cultures in the same land, under one of the clearest skies of the world. The major of San Pedro de Atacama, Sandra Berna, expressed her gratitude to ALMA for its contribution to the understanding and protection of Atacama cultural heritage.

In the future, when ALMA is completed, the site museum will be open to the public, as part of a special visits programme that will also include an ALMA Information Centre at the OSF and a viewpoint at Chajnantor for those who are fit enough for an altitude of 5 000 metres.

Young students from local schools of San Pedro de Atacama and Toconao also attended the event. They symbolically received the first copies of the book "Footprints in the Desert" (*Huellas en el Desierto*), which presents the main findings of the archaeological surveys in the ALMA area. This publication, written by Ana María Barón and edited by ESO, was donated to all schools in Chile's Region II, to expand the new knowledge of the Atacama Desert and its culture to younger generations. It is available electronically at the Spanish website *http://www.eso.cl*, and an English edition is now under production.

Cover of the new book "Footprints in the Desert" (*Huellas en el Desierto*), which presents the latest findings on the old history of the Llano of Chajnantor and nearby areas, which was donated to all schools in Chile's Region II.

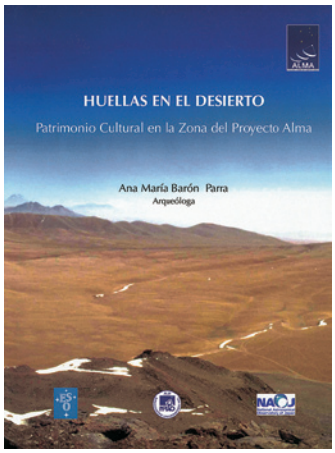

At the end of the ceremony, Pedro Cruz and other members of the local communities spontaneously performed their own rituals for the inauguration of the site museum. They paid their respects to the high mountains and to the *Pachamama* (Mother Earth), in an old tradition that was joined by ALMA executives and Chilean authorities, asking for prosperity and harmony for all the people living now in this arid and ancient ground.

Photo: C. Romero

Massimo Tarenghi, ALMA director, performing the local ritual of 'payment' to *Pachamama* (Mother Earth), at the inauguration ceremony of the new site museum.

ESO-Chile Fund for Astronomy: 10 Years of Productive Scientific Collaboration

Gonzalo Argandoña, Felix Mirabel (ESO)

In a ceremony in Santiago in June 2006, ESO and the Chilean Ministry of Foreign Affairs celebrated the 10th Anniversary of the Supplementary Agreement. This agreement granted to Chilean astronomers up to 10 % of the total observing time on ESO telescopes and established an annual fund for the development of astronomy, managed by the 'ESO-Chile Joint Committee'.

At the ceremony to celebrate the 10th Anniversary of the ESO-Chile Joint Committee: (from left to right) Felix Mirabel (ESO Representative and Head of the Science Office in Chile), Dr. Catherine Cesarsky (ESO Director General), Dr. Leonardo Bronfman (Director of Astronomy Department, Universidad de Chile; representative of the Chilean scientific community within the ESO-Chile Joint Committee), and, speaking, Ambassador Luis Winter (Director of Special Policy, Ministry of Foreign Affairs of Chile).

The celebration event was hosted by ESO Director General, Dr. Catherine Cesarsky, and the Director of Special Policy for the Chilean Ministry of Foreign Affairs, Ambassador Luis Winter. "ESO's commitment is, and always will be, to promote astronomy and scientific knowledge in the country hosting our observatories", said Dr. Cesarsky. "We hope Chile and Europe will continue with great achievements in this fascinating joint adventure, the exploration of the Universe."

On behalf of the government of Chile, Ambassador Luis Winter outlined the historical importance of the Supplementary Agreement, ratified by the Chilean Congress in 1996. "Such is the magnitude of the ESO-Chile Joint Committee that, only in 2005, this annual fund represented eight per cent of all financing sources for Chilean astronomy, including those from government and from universities", Ambassador Winter said. The appointed Chilean astronomer for the ESO-Chile Joint Committee, Dr. Leonardo Bronfman, also took part in the ceremony, along with ambassadors in Chile of ESO mem-

The ESO-Chile Fund has supported the improvement of astronomy teaching at schools for children and young people. In the picture, CADIAS, the Astronomy Teaching Support Centre, funded by the annual fund.

Photo: CADIAS

The book "10 Years Exploring the Universe" presents a global view of recent developments of astronomy in Chile thanks to the ESO-Chile Annual Fund.

ber states, and representatives of the Chilean government and the scientific community.

History and impact of the ESO-Chile fund

The formal relations between ESO and its host country, the Republic of Chile, were first established through the Convention of 1963, which allowed the successful construction and operation of the La Silla Observatory. Decades later, during the years of VLT construction, an Interpretative and Supplementary Agreement to the Convention was signed and was ratified by the Chilean Congress on September 1996. The new agreement guaranteed to Chilean astronomers privileged access to the state-of-the-art telescopes installed at La Silla, Paranal and Chajnantor for deserving research projects. To make the most of this vast scientific wealth, an annual fund was established for the development of astronomy and related sciences in the country.

A decade after the launch of this initiative, ESO edited a special book, based on the reports of the beneficiaries of the annual fund, to review the impact of the numerous projects financed so far. The book, entitled "10 Years Exploring the Universe", was launched in the same celebration event at ESO Vitacura. The publication presents a global view of recent developments of astronomy in Chile.

Since the beginning, the ESO-Chile fund has granted over 2.5 million euros to finance new positions of post-doc and astronomy professors at major Chilean universities, development of research infrastructures, organisation of scientific congresses, workshops for science teachers and astronomy outreach programmes for the public.

In addition to the 400 000 euros given annually by ESO to the ESO-Chile Joint Committee, around 550 000 euros are granted every year to finance regional collaboration programmes, fellowships for students in Chilean universities, and the development of radio astronomy through the ALMA-Chile Committee. In total, apart from the 10 % of the observing time at all ESO telescopes, ESO contributes 950 000 euros annually for the promotion of astronomy and scientific culture in Chile.

As a consequence of these funds and other positive stimulating factors in Chile in recent years, there has been a rapid development in the size and scientific impact of the national astronomical community. According to a study by the Chilean Academy of Sciences in 2005, the number of astronomers has doubled over the last 20 years and there has been an eightfold increase in the number of scientific publications. The same study stated that astronomy could be the first scientific discipline in Chile with the standards of a developed country, with additional benefits in terms of technological improvement and growth of human resources.

The book "10 Years Exploring the Universe" can be downloaded in PDF format from *http://www.eso.cl* (Spanish version) and *http://www.eso.org/outreach/press-rel/pr-2006/pr-21-06.html* (English version). The report by the Chilean Academy of Sciences, "Analysis and Projections of 2005 Chilean Sciences – Chapter: Astronomy" is available at *http://www.sochias.cl/extras/astro2005_final.pdf.*

Evolution of the number of astronomy positions at the major Chilean universities.

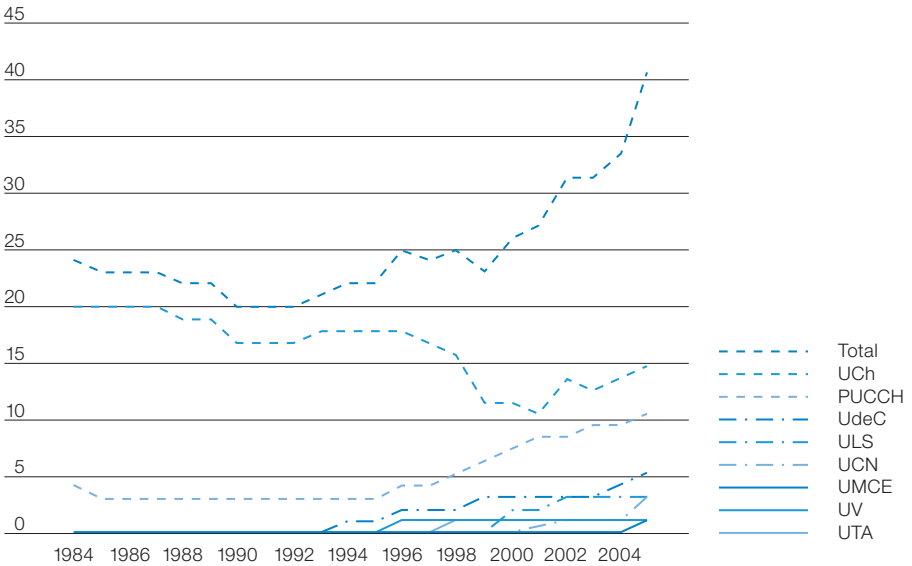

Fellows at ESO

Rubina Kotak

Although I spent the first two years of my life in the south-western corner of Tanzania, I grew up near the equator, in Kenya. Having obtained my Masters degree from Canterbury (Kent), I decided that it was time to venture somewhere a little more exotic. Hence I moved north, to southern Sweden to start a PhD at Lund Observatory.

Here I worked on time-resolved spectroscopy of cool white dwarf pulsators with a view to simultaneously tapping their asteroseismological potential and constraining the properties of the convection zone in a novel way. Having (temporarily) exhausted all the targets that could be observed in this way, using the largest (optical) telescope on the planet, it was time to move on. So I found myself at Imperial College London, working as part of a concerted European effort to decipher the physics of thermonuclear supernovae (SNe). Partly as a result of the numerous side-projects that sprouted out of this, two of my current preoccupations are the characterisation and use of circumstellar matter surrounding SNe to determine the nature of the progenitor star(s), and whether core-collapse SNe are able to produce significant quantities of dust at all redshifts.

I arrived at ESO-Garching less than a year ago and am still negotiating my way around the intriguing maze of corridors, doors, and dead ends, making navigation using images e.g. of the Horsehead Nebula, a necessity! My duties at ESO include working in the PR department which is both fun and stimulating. Being at ESO gives that child-in-a-sweetshop feeling: lots of interesting talks, experts in every field, and a general feeling of being at the hub of events and decisions that will shape the future for decades to come. My time at ESO is sadly coming to an end, but I'm looking forward to taking up a staff positon at Queen's University Belfast. Definitely time to invest in umbrellas!

Photo: G. Dremel, ESO

Rubina Kotak

The Starburst Galaxy NGC 908. Image based on data obtained with FORS2 on the VLT, using B, V, and R filters. North is up and East is to the left. The data were extracted from the ESO Science Archive and further processed by Henri Boffin (ESO). More information can be found in ESO PR Photo 27a/06.

Corrigendum

The caption of the second photo in the report on the Walloon Space Days in the last issue of The Messenger mentioned Mme Simonet, Minister for Science, New Technologies and External Relations of the Walloon Regional Government, while the photo showed Dr. Monnik Desmeth, Belgian delegate and Vice President of the ESO Council. The picture here shows Mme Simonet at the press conference at AMOS.

Photo: S. Tarquinio, AMOS

ESO

European Organisation
for Astronomical
Research in the
Southern Hemisphere

ESO is opening two positions as

Operations Staff Astronomer

The successful candidate will be part of the Science Operations Department of the La Silla Paranal Observatory with duty station on Paranal. She/he will support observations in both visitor and service mode. The tasks to be performed include short-term (flexible) scheduling of queue observations, calibration and monitoring of the instruments, and assessment of the scientific quality of the astronomical data.

Operations Astronomers may be members of the ESO Science Faculty, with an appointment at the level of Assistant or Associate Astronomer. 105 nights per year are spent at the Observatory carrying out functional duties, usually in a shift of 8 days on Paranal, 6 days off. The rest of the time is spent in the Santiago office. They will be expected and encouraged to actively conduct astronomical research during that time. Depending on qualification, expertise, and personal interest, Operations Astronomers may alternatively be offered an appointment with 135 nights per year to be spent on the Observatory with the reminder of the time being available for personal research.

The position requires a Ph.D. in Astronomy, Physics or equivalent.

We are seeking a staff astronomer with substantial observing experience (at least three years). The ideal candidate will be an active researcher and have excellent observation-oriented research records, will be familiar with a broad range of instrumental, data analysis, archiving and observational techniques, and must be conversant with at least one major data reduction package such as MIDAS, IRAF or IDL. Of special value would be a record of instrumental experience, such as the participation in the design, construction or calibration of existing instruments and/or previous experience in the operation of an astronomical facility.

For details and to download an application form, please consult our homepage: *http://www.eso.org*. If you are interested in working in a stimulating international research environment and in areas of frontline science and technology, please send us your application in English to:

ESO Personnel Department
Karl-Schwarzschild-Straße 2
85748 Garching near Munich, Germany
e-mail: vacancy@eso.org

ESO is an equal opportunity employer.
Qualified female candidates are invited to apply.

ESO. Astronomy made in Europe

Personnel Movements

Arrivals (1 July–30 September 2006)

Europe	
Calçada, Luis (P)	Media Laboratory Assistant
Castro, Sandra Maria (BR)	Software Engineer
Dietrich, Jörg (D)	Fellow
Eder, Brigitta (A)	Student
Hilker, Michael (D)	User Support Astronomer
Kempf, Andreas (D)	Electronics Engineer
Mainieri, Vincenzo (I)	Fellow
Moins, Christophe (F)	Software Engineer
Szasz, Gabriel (SK)	Student
van der Plas, Gerrit (N)	Student
Vernet, Joel Daniel Roger (F)	Instrument Scientist
Weigand, Michael (D)	Paid Associate
Weiser, Sabine (D)	Accounting Assistant

Chile	
Conn, Blair Campbell (AUS)	Fellow
De Gregorio Monsalvo, Itziar (E)	Fellow
De Silva, Gayandhi Manomala (AUS)	Fellow
Salinas, Alejandro (RCH)	Network Specialist
Treister, Ezequiel (RA)	Fellow

Departures (1 July–30 September 2006)

Europe	
Alberth, Manuela (D)	Purchasing Assistant
Bortolussi, Alessandro (I)	Paid Associate
Chuzel, Olivier (F)	Software Engineer
Duhr, Linda (NL)	Secretary/Assistant
Ostaschek, Iris (A)	Secretary/Assistant

Chile	
Doublier, Vanessa (F)	Operation Staff Astronomer
Preminger, Daisy (RCH)	Data Handling Administrator
Scarpa, Riccardo (I)	Operation Staff Astronomer
Vreeswijk, Paul (NL)	Fellow

ESO is the European Organisation for Astronomical Research in the Southern Hemisphere. Whilst the Headquarters (comprising the scientific, technical and administrative centre of the organisation) are located in Garching near Munich, Germany, ESO operates three observational sites in the Chilean Atacama desert. The Very Large Telescope (VLT), is located on Paranal, a 2 600 m high mountain south of Antofagasta. At La Silla, 600 km north of Santiago de Chile at 2 400 m altitude, ESO operates several medium-sized optical telescopes. The third site is the 5 000 m high Llano de Chajnantor, near San Pedro de Atacama. Here a new submillimetre telescope (APEX) is in operation, and a giant array of 12-m submillimetre antennas (ALMA) is under development. Over 1600 proposals are made each year for the use of the ESO telescopes.

The ESO Messenger is published four times a year: normally in March, June, September and December. ESO also publishes Conference Proceedings and other material connected to its activities. Press Releases inform the media about particular events. For further information, contact the ESO Public Affairs Department at the following address:

ESO Headquarters
Karl-Schwarzschild-Straße 2
85748 Garching bei München
Germany
Phone +49 89 320 06-0
Fax +49 89 320 23 62
information@eso.org
www.eso.org

The ESO Messenger:
Editor: Peter Shaver
Technical editor: Jutta Boxheimer
www.eso.org/messenger/

Printed by
Peschke Druck
Schatzbogen 35
81805 München
Germany

ISSN 0722-6691

Contents

Front Cover Picture: Globular Cluster 47 Tucanae
See page 10 for details.